Processing and properties of multifunctional bio-based poly(lactic acid) composites

SUBMITTED IN PARTIAL FULFILLMENT OF THE REQUIREMENTS

OF THE DEGREE OF DOCTOR OF PHILOSOPHY

June 2015

Fang Mai

School of Engineering and Materials Science

Queen Mary University of London

Mile End Road, London, E1 4NS

Declaration

I declare that the work performed is entirely by myself during the course of my Ph.D studies at the Queen Mary University of London and has not been submitted for a degree at this or any other University.

Fang Mai

Acknowledgements

Researchers are like Sherlock Holmes. We are searching for hidden clues and then reasoning them. This dissertation is not only a personal accomplishment; it is also a product of many people. It took more than determination and hard work for the completion of this thesis.

I would like to acknowledge first the China Scholarship Council (CSC) for the financial support, as well as offering me the opportunity for further study and this great international experience.

Especially, I give my supervisors Dr. Ton Peijs and Dr. Emiliano Bilotti all my gratefulness for giving me the opportunity to work on the HIGHBIOPOL project, and for all the support and guidance during my PhD. Ton's sense of humour, easily understood explanations and open mind allowed me to grow. Emiliano's patience and kindness guided me through the process.

I gratefully acknowledge the support of Mr. Kaloyan Palatov for the teamwork and early development of the project during the first year. I would like to thank Dr. Wei Tu for his constant help and his invaluable inputs through the project. I also want to thank the technical staff Mr. Vince Ford for designing and manufacturing some of the experimental equipments.

Many thanks to my collaborator, Dr. Alexandre Clerbaux, Mr. Fang-Yue Chan, Mr. Michael Mainil, Dr. Michael Claes, and Mr. Julien Amadou in Nanocyl S.A. (Belgium); Dr. Youssef Habibi, Dr. Jean-Marie Raquez, and Dr. Philippe Dubois in University of Mons (Belgium).

Thanks are given to my wise and lovely colleagues at Queen Mary University of London and Nanoforce Technology Limited who helped me in any shape or form.

A huge thank to my soul mate and husband Dong Dong for his love and understanding during my good and bad times. He always stands by my side, and there is no word to convey how much I love him.

I would also like to thank my friends and family for their continual support and encouragement during my stressful stages.

I looked back these years and want to say, doing a PhD was tough, but great, and I would totally do it again.

Abstract

Following the eco-design concepts, this thesis investigated the manufacturing and properties of multifunctional bioplastic poly(lactic acid) (PLA) based composites. The main advantages of using bio-based polymer are to create performance products from sustainable resources, competing with fossil hydrocarbon sourced polymers, at the same time leaving open the possibility of composting as an alternative end-of-life option in addition to recycling.

In Part I, self-reinforced PLA (SR-PLA) composites were produced based on oriented PLA tapes and a thin layer of PLA matrix, which were combined using a film-stacking technique into a 'brick-and-mortar' laminated structure. The optimization of the uniaxial drawing and structure of these tapes, together with a study of the interfacial, tensile, impact and thermal properties of the obtained SR-PLA composites were investigated. In order to be successful in more demanding engineering applications the important issue regarding biodegradation during the PLA-based product's lifetime needs to be addressed. Therefore, monitoring of degradation levels during usage is of a vital interest. This is the subject of study of the 2nd part of the thesis.

In Part II the aim is to develop multifunctional engineering bioplastics with improved performances (mechanical and electrical) and added functionalities (sensing properties). An in-situ degradation monitoring system for biodegradable polymers was successfully developed through the incorporation of carbon nanotubes (CNTs) in PLA. Changes in electrical resistivity of the PLA/CNT nanocomposites were successfully correlated with degradation levels of this bioplastic. PLA/CNT nanocomposites demonstrated excellent degradation sensing abilities at CNT concentrations around the percolation threshold,

with resistivity changes of about four orders of magnitude with biodegradation. The exceptional mechanical, electrical properties and 1D anisotropic geometry of CNTs also make them ideal reinforcing fillers for polymeric fibres. Therefore, the influence of CNT content and solid-state drawing on microstructure and the resulting mechanical and electrical properties of these nanocomposites were investigated.

Table of Contents

List of Tables

List of Figures

Chapter 1.

Introduction

1.1 End of life options for composite waste: Recycle, reuse or dispose?

A growing public awareness and new environmental legislations have created a substantial driving force for manufacturing of materials and end-products that consider their environmental impact at all stages of the life cycle. At this moment, 'eco-design' or 'designing for recycling' must be an important part of our daily lives if we are to preserve the natural resources of our planet. The automotive industry, in particular, is now trying to make every component recyclable because of an European Union (EU) directive on the end-of-life of vehicles (ELV). This regulation states that by 2015 all vehicles must be made of 95% recyclable materials, of which 85% can be recovered through reuse or mechanical recycling and 10% through energy recovery or thermal recycling [1].

For this reason, bio-based and biodegradable polymers and composites have been the subject of many studies over the last two decades. Poly(lactic acid) (PLA) is one of the most promising thermoplastic bio-based polymers because of its attractive mechanical properties, low emission of greenhouse gases, low amount of energy used for production, potential biodegradability and high industrial production capacity. However, due to its high brittleness (a typical tensile strain at break of less than 6% [2]) and low heat deflection temperature (HDT), PLA has not yet gained full market acceptance as an

engineering resin.

One possible strategy to improve the mechanical and thermal properties of PLA has been through the addition of natural fibres to make so-called ‘green composites’ [3, 4]. To date, a number of composite manufacturers have introduced in their product range PLA composites reinforced with natural fibres. The main driving force in pursuing the use of natural fibres is their environmental impact over the entire life cycle.

The concept of recycling polymer based products gained momentum towards the end of the 1970’s fuelled by the oil crises in 1973 and 1978-1979, which resulted in a significant increase in raw material costs. Recycling of polymer composites is an even more recent occurrence with significant work generally not starting until the latter half of the 1980’s. However, with the increasing use of composite products, particularly in the automotive industry which consumes up to 25% of all composites manufactured, the issue of composite recycling is becoming ever more important [5].

The waste hierarchy as shown in Figure 1.1 is to extract the maximum practical benefits from products and to generate the minimum amount of waste. From the point of view of material utilization it is generally preferable to succeed with highest possible level of recycling. Landfill and incineration have always been the simplest but least desirable strategies of disposal accounting for 98% of composites waste, while other routes such as reuse and mechanical recycling account for the remaining 2% [5]. One composite example on disposal level is glass fibre reinforced polymer composites (GRP). During thermal recycling, there is a huge mechanical performance loss of recycled glass fibre compared to its original state [6]. As a result, these recycled fibres cannot be reprocessed or reused as reinforcement of composite due to their poor cost-performance

ratio. The group of Thomason in the University of Strathclyde has been working on the cost effective recycling of GRP. S áez-Rodr íguez *et al.* [7] investigated the regeneration of mechanical performance of thermally recycled glass fibres by using different chemical treatments. The results showed that strength loss of heat treated fibres (0.7 GPa) can be recovered (2.1 GPa). Green composites have clear advantages with respect to energy recovery. Most green composites can be burned without problematic residues as in the case of glass fibre composites. Although the use of natural fibres seems at first to be an environmentally sound approach as they are renewable, there are some issues with respect to end-of-life scenarios for these composites. In the case of mechanical recycling their relatively poor thermal stability may lead to severe additional thermal degradation of the composites during subsequent reprocessing steps.

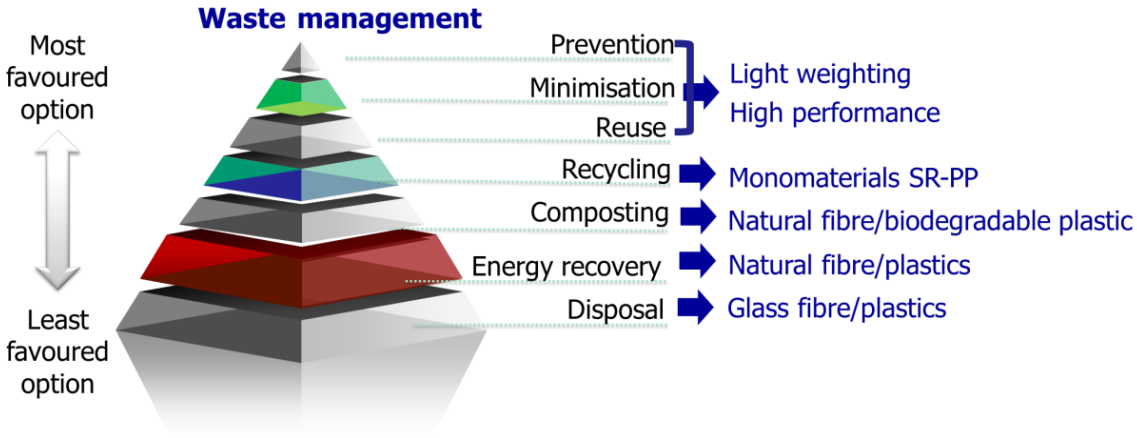

Figure 1.1 The waste hierarchy and examples on each level.

To assist in the transition from disposal of composite waste in landfill to recycling, industry needs to consider designing components for easier disassembly, reuse and recycling at the end of the products' life. One of the basic rules in 'designing for recycling' is a reduction of the variety of materials. In the case of plastics, compatible

polymers should be selected, which in practice means use of monomaterials. An example of monomaterial composites is called self-reinforced polymer composites (SRPs) or ‘all-polymer’ composites, in which a polymer matrix is reinforced with oriented fibres or tapes of the same polymer. The absence of ‘foreign’ reinforcements means enhanced fibre-matrix interfacial adhesion and more importantly, full recyclability without the need for separation of fibre and matrix. After initial conception in the mid-1970s, numerous groups have investigated methods for scaling these concepts up into commercial products. To date, the most commercially applied technology is marketed as Curv®, with examples of loud speaker cones, protective sports equipment, automotive panels, and a major commercial range of luggage. Additionally, the use of PP coextrusion-based SRPs based on PURE® has been prototyped in application such as automotive undertray panel and is reported to be applied to luggage, kayaks, skates and other recreational equipment as well as in motorsports applications [8].

1.2 Objectives

Following eco-design concepts, in the first part of this thesis, another family of SRPs is being presented based on the bioplastic PLA. The main advantages of using bioplastic are to create performance products from sustainable resources, competing with fossil hydrocarbon sourced polymers, at the same time leaving open the possibility of composting as an alternative end-of-life option in addition to recycling. A flow diagram summarizing the possible life cycle of SR-PLA composites is shown in Figure 1.2. PLA pellets can be synthesized from corn through a series of chemical routes. From these pellets, oriented PLA tapes can be processed by extrusion and solid-state drawing.

These tapes can be woven into fabric and subsequently consolidated into sheets. Finally, finished articles can be produced by thermoforming of these sheets. At the end of the products' life, they can be collected and mechanically recycled into other PLA based products such as packaging or even new SR-PLA composites. The bioplastics specialist Purac has sponsored a project called 'Perpetual Plastics Project' to highlight how easily PLA resins can be recycled with a small-scale demonstration machine. A new article can be remade using a 3D printer after the steps of cleaning, drying, shredding, melting and extrusion [9].

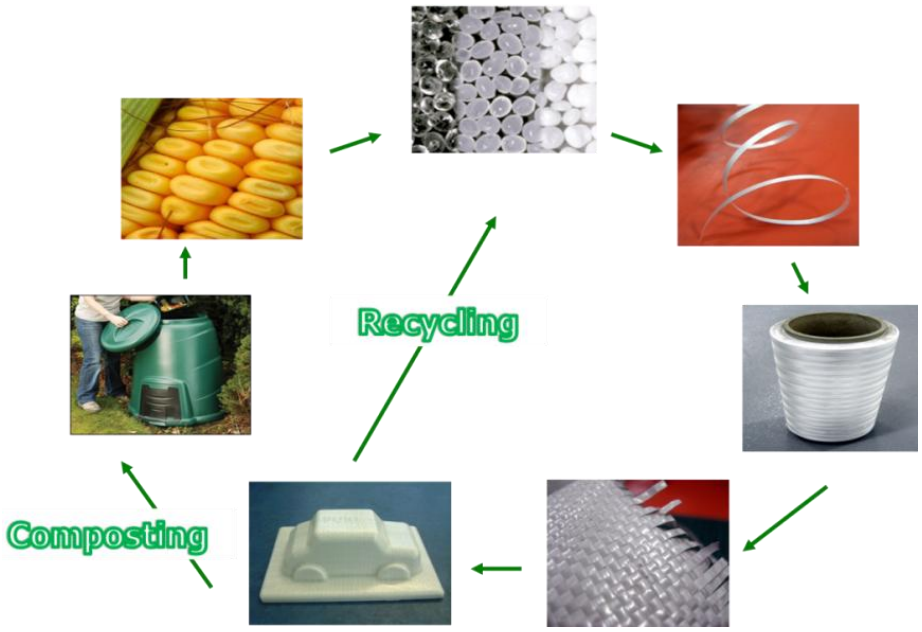

Figure 1.2 Life cycle of SR-PLA composites.

For SR-PLA composites, when these materials can no longer be recycled, these PLA materials can finally be composted in a commercial composting facility. Alternatively, of course they can also be incinerated with energy recovery. Chemical recycling or depolymerisation of PLA to recover the monomer lactic acid could also be an end-of-life solution. Piemonte *et al.* [10] reported that the production of lactic acid from

chemical depolymerisation of PLA is preferable compared to glucose fermentation in terms of energy saving. In brief, the multiple end-of-life options offered by SR-PLA composites empowers them to reduce the environmental impact of plastic products, and gives the end-user maximum flexibility in environmentally sound waste disposal schemes.

The SRP concept applied in this thesis follows earlier work on PP and PET and is based on highly oriented PLA tapes and thin layers of isotropic PLA films, which are combined using a film-stacking technique into a 'brick-and-mortar' structure (see Figure 1.3). The reinforcing tape is solid-state drawn under tension at temperatures just below the melting point of the polymer to orient the polymer chains along the tape's axis to improve strength and stiffness. This layer is then sandwiched between two thin outer layers of a PLA matrix with a lower melting point (154 ^{o}C) than the reinforcing tape (169 ^{o}C). During hot-pressing, the matrix layers are selectively melted to weld the tapes together to form a composite structure, while retaining the mechanical properties of the tape.

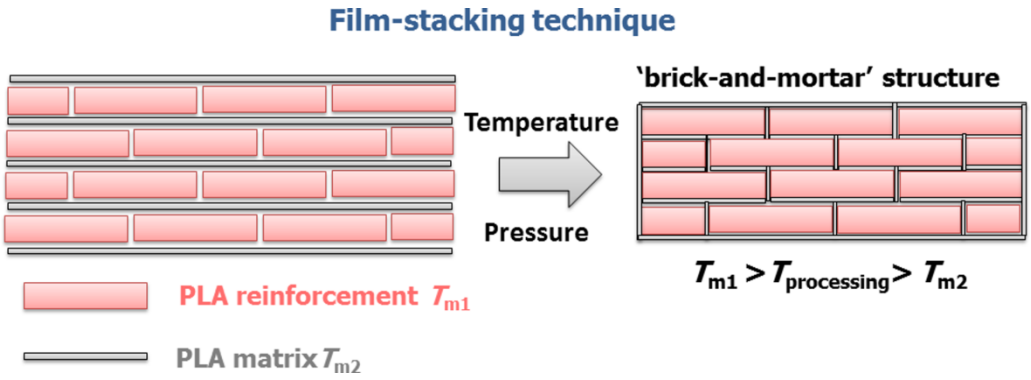

Figure 1.3 Schematic of the hot compaction process.

As will be shown in Chapter 4, these materials hold strong future promise for potential

applications as a high performance bio-based engineering plastic. However, in order to be successful in more demanding applications the important issue regarding degradation during the product's lifetime needs to be addressed. It is for this reason that monitoring of degradation levels during usage could prove to be of a vital interest for this type of materials.

In the second part of the thesis, the aim is therefore to develop a range of multifunctional engineering bioplastic systems with improved performances (mechanical and electrical), functionalities (sensing properties), and processability. Carbon nanotubes (CNTs) have gained considerable attention with their outstanding properties. The combination of high Young's modulus and tensile strength, excellent thermal and electrical conductivity in combination with their low density and high aspect ratio has made them ideal candidate fillers for a whole new range of multifunctional nanocomposites. These opportunities include the use of CNTs as conductive filler in insulating polymer matrices and as reinforcement in structural materials [11-13]. Interestingly, it has been shown that the electrical conductivity of CNT networks in polymer matrices are affected by stimuli such as temperature [14], gases [15], vapour [16], mechanical stress and strain [17,18], pH [19], and liquids [20]. Generally, the underlying mechanism is that the introduced external stimuli results in a deformation of the CNT percolation network, thus leading to a change in electrical conductivity of the composites. Hence, measuring changes in the electrical resistivity of a compound can be used to 'sense' or monitor its structural status. Here we will attempt to use such conductive CNT networks to monitor biodegradation in the PLA matrix, as it is expected that polymer degradation will change the mobility of the CNTs in the polymer matrix, leading to changes in the network and through this changes in electrical

properties.

It is worth mentioning that in order to keep the environmental impact and carbon footprint as low as possible, Nanocyl (Belgium) has been working on the production of CNTs using biosourced hydrocarbon, methane, ethanol and camphor in another work package of the project HiBioPol. However, the CNTs used in the present work are a non-biosourced commercial available product.

Based on the above facts, the main goals of the thesis are:

- To understand the structure-property relationships of PLA during solid-state drawing and to optimize their mechanical properties via processing
- To tackle the high brittleness, low heat resistance and unsatisfactory tensile properties of neat PLA through the development of SR-PLA composites
- To produce conductive PLA/CNT tapes with high strength and modulus
- To provide real-time information of the degree of degradation of PLA through the use of CNT as sensors
- To investigate the market potential of SR-PLA composites

1.3 Scope of the thesis

This project describes the processing and properties of multifunctional bio-based PLA composites. The thesis is divided into two parts. Part I focuses on the manufacturing and properties of SR-PLA composites. Chapter 2 gives a comprehensive overview of the literatures of PLA composites and SRP's. The development of a high performance PLA tape as reinforcement is essential in imparting superior mechanical properties into resulting SR-PLA composites. Therefore, the influence of the applied draw ratio and

drawing temperature on the morphology and mechanical properties are presented in Chapter 3. Then, an investigation of interfacial, mechanical and thermal properties of resulting SR-PLA composites are carried out in Chapter 4. In Part II, the discussion focuses on the development and functionalization of PLA/CNT nanocomposites. After a literature review in Chapter 5, Chapter 6 describes an attempt of reinforcing PLA using CNTs through a melt-compounding process followed by solid-state drawing. The draw ratio dependency of mechanical and electrical properties in these nanocomposites is studied. Chapter 7 successfully explores a novel in-situ degradation monitoring system based on PLA/CNT films. Finally, Chapter 8 summarizes the findings of this project together with some ideas for future research, which could lead on from this project. A marketing study is also performed to determine whether commercial exploitation opportunities exist for the SR-PLA technology developed.

1.4 References

1. E. Commission, *Directive 2000/53/EC of the European Parliament and of the Council of 18 September 2000 on end-of-life vehicles.* Official Journal of the European Communities, L, 2000. **269**: p. 34-269.
2. S. Ebnesajjad, *Handbook of biopolymers and biodegradable plastics: properties, processing and applications.* William Andrew, 2012.
3. T. Mukherjee, and N. Kao, *PLA based biopolymer reinforced with natural fibre: a review.* Journal of Polymers and the Environment, 2011. **19**(3): p. 714-725.
4. P. K. Bajpai, I. Singh, and J. Madaan, *Development and characterization of PLA-based green composites: A review.* Journal of Thermoplastic Composite Materials, 2012: p. 0892705712439571.
5. S. Halliwell, *End of life options for composite waste-recycle, reuse or dispose.* National Composites Network report, 2006.
6. J. L. Thomason, L. Yang, C. C. Kao, and P. Jenkins, *Regeneration of the performance of glass fibre recycled from end-of-life composites or glass fibre waster.* International Glass Fiber Symposia, 2012.
7. E. Sáez-Rodríguez, L. Yang, and J. L. Thomason, *Regeneration of thermally recycled glass fibre for cost-effective composites recycling: Increasing the strength of thermally conditioned glass fibres using cost effective ReCoVeR treatments.*16th European Conference on Composites Materials, 2014.
8. B. Alcock, and T. Peijs, *Technology and development of self-reinforced plymer composites,*

in *Polymer composites-polyolefin fractionation-polymeric peptidomimetics-collagens*. 2013, Springer. p. 1-76.

9. C. Purac, *PLA lifecycle closing the loop with PLA*. 14 October 2014; Available from: http://www.corbion.com/bioplastics/about-bioplastics/pla-lifecycle.
10. V. Piemonte, S. Sabatini, and F. Gironi, *Chemical recycling of PLA: A great opportunity towards the sustainable development?* Journal of Polymers and the Environment, 2013. **21**(3): p. 640-647.
11. H. Deng, R. Zhang, C. T. Reynolds, E. Bilotti, and T. Peijs, *A novel concept for highly oriented carbon nanotube composite tapes or fibres with high strength and electrical conductivity.* Macromolecular Materials and Engineering, 2009. **294**(11): p. 749-755.
12. Q. Zhang, S. Rastogi, D. Chen, D. Lippits, and P. J. Lemstra, *Low percolation threshold in single-walled carbon nanotube/high density polyethylene composites prepared by melt processing technique*. Carbon, 2006. **44**(4): p. 778-785.
13. Q. Wang, J. Dai, W. Li, Z. Wei, and J. Jiang, *The effects of CNT alignment on electrical conductivity and mechanical properties of SWNT/epoxy nanocomposites.* Composites Science and Technology, 2008. **68**(7): p. 1644-1648.
14. J. R. Wood, Q. Zhao, M. D. Frogley, E. R. Meurs, A. D. Prins, T. Peijs, D. J. Dunstan, and H. D. Wagner, *Carbon nanotubes: from molecular to macroscopic sensors.* Physical Review B, 2000. **62**(11): p. 7571-7575.
15. J. K. Abraham, B. Philip, A. Witchurch, V. K. Varadan, and C. C. Reddy, *A compact wireless gas sensor using a carbon nanotube/PMMA thin film chemiresistor*. Smart Materials and Structures, 2004. **13**(5): p. 1045-1049.
16. B. Kumar, M. Castro, and J-F. Feller, *Poly(lactic acid)–multi-wall carbon nanotube conductive biopolymer nanocomposite vapour sensors.* Sensors and Actuators B: Chemical, 2012. **161**(1): p. 621-628.
17. R. Zhang, M. Baxendale, and T. Peijs, *Universal resistivity-strain dependence of carbon nanotube/polymer composites.* Physical Review B, 2007. **76**(19): p. 195433.
18. E. Bilotti, R. Zhang, H. Deng, M. Baxendale, and T. Peijs, *Fabrication and property prediction of conductive and strain sensing TPU/CNT nanocomposite fibres.* Journal of Materials Chemistry, 2010. **20**(42): p. 9449-9455.
19. N. Ferrer-Anglada, M. Kaempgen, and S. Roth, *Transparent and flexible carbon nanotube/polypyrrole and carbon nanotube/polyaniline pH sensors.* Physica Status Solidi (b), 2006. **243**(13): p. 3519-3523.
20. P. Pötschke, T. Andres, T. Villmow, S. Pegel, H. Brünig, K. Kobashi, D. Fischer, and L. Häussler, *Liquid sensing properties of fibres prepared by melt spinning from poly(lactic acid) containing multi-walled carbon nanotubes.* Composites Science and Technology, 2010. **70**(2): p. 343-349.

Part I. Bio-based self-reinforced polymer composites

Chapter 2.

Literature review

2.1 Poly(lactic acid) (PLA): A sustainable bioplastic

Polymers derived from renewable resources are now considered as promising alternatives to traditional petro-based polymers as they fulfil current environmental concerns. Poly(lactic acid) (PLA) is one of the most promising bioplastic because of its attractive mechanical properties, low emission of greenhouse gases, low amount of energy used for production, potential biodegradability and high industrial production capacity.

The first attempt to prepare PLA was ascribed to Carothers (at DuPont) in 1932 as a low molecular weight product by heating lactic acid under vacuum [1]. However, the initial uses were limited to medical and pharmaceutical applications due to its limited capacity, high manufacturing cost, and low molecular weight. There is a sharp rise in the development and commercial marketing of PLA in the last two decades, since the advancement in the fermentation of dextrose obtained from corn dramatically reduced the cost to make monomer lactic acid [2]. During the last years of 20^{th} century several companies have made attempts to produce PLA in industrial scale. NatureWorks Llc. (USA) announced a production capacity of about 140,000 ton/year of PLA under the name Ingeo^{TM}, mainly for the commodity market, such as film and fibres for packaging, housewares, and clothing.

PLA belongs to the family of aliphatic polyesters with the basic building block of lactic acid. The monomer lactic acid has two optically active stereoisomers: dextro- ($_D$-) and levo- ($_L$-) (Figure 2.1). Natural fermentation generally yields a mixture of 99.5% of the $_L$-isomer and 0.5% of the $_D$-isomer. The two isomers have identical physical properties, with the exception that of the $_L$-isomer rotates the plane of polarized right clockwise while the $_D$-isomer rotates it anti-clockwise.

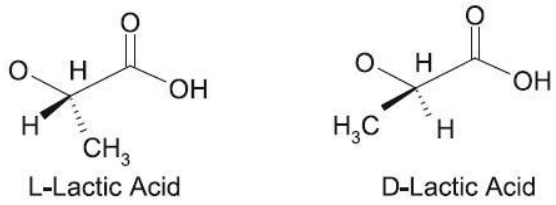

Figure 2.1 Two stereoisomers of lactic acid.

There are two major routes to produce PLA from the monomer lactic acid (Figure 2.2). The conventional process is by the polycondensation of lactic acid. This process is carried out under high vacuum and high temperature. Solvent is used to extract by-products. This method leads to low molecular weight PLA due to difficulties of removing water and impurities [3]. The second method is ring-opening polymerization through the lactide intermediate. This method results in a higher molecular weight polymer and uses milder conditions [4].

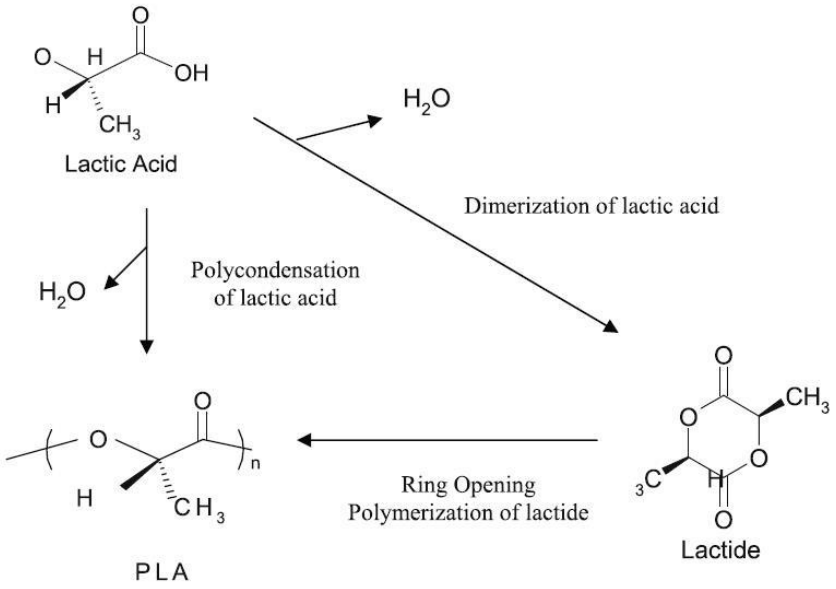

Figure 2.2 Polymerization routes to PLA [3].

Production of PLA via the lactide route allows the possibility of modifying the physical properties by controlling the stereochemical structure of the polymer [5]. The ratio of $_D$- and $_L$-isomers and their distribution along the polymer backbone can influence the molecular weight, crystallinity, and melting temperature of the end product [3]. Since the $_D$-form is normally considered as defects in fermented lactic acid, fully amorphous materials can be produced by the inclusion of relatively high $_D$-lactide content (> 15%) [6], whereas highly crystalline materials can be achieved when the $_D$ content is low (< 2%) [7]. The crystallinity and melting temperatures of both pure poly-$_L$-lactide (PLLA) and poly-$_D$-lactide (PDLA) are about 37% and 175-178 ℃, respectively.

Representations of PLA polymer chains having different ratios and distributions of the $_D$- and $_L$- isomers are shown in Figure 2.3. Different melting temperatures of PLA, varying from 130 ^{o}C to 220 ^{o}C, can be obtained [6]. PLLA having only $_L$-lactic units has a melting temperature of 180 ℃ and is shown in the upper row of Figure 2.3. A blend of PLLA and PDLA can lead to a polymeric stereocomplex with melting temperature as

high as 220 ^{o}C (See the bottom row of Figure 2.3).

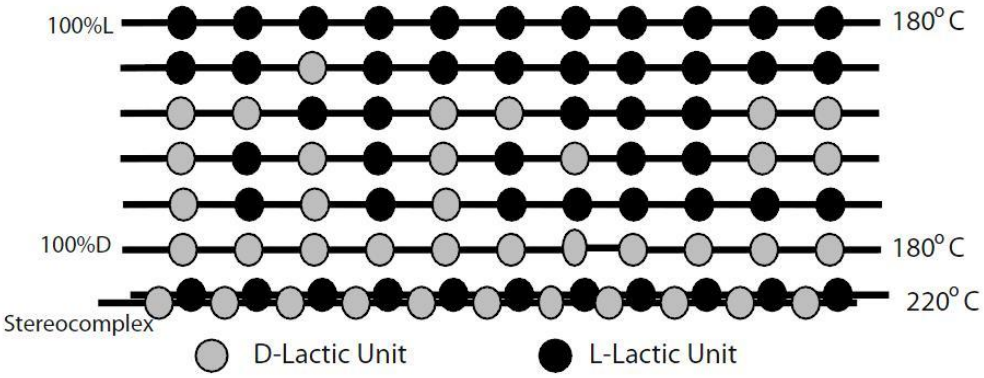

Figure 2.3 Examples of molecular configurations of PLA obtained through combining the two lactic acid isomers in varying proportions [3].

The mechanical properties of lactic acid based polymers can be varied to a large extent depending on not only stereochemical structures, but also crystallinity, molecular weight, crystalline orientation, the processing history, and so on. Generally, semi-crystalline PLA is preferred to the amorphous PLA when high mechanical properties are desired. Semi-crystalline PLA has an approximate tensile modulus of 3 GPa, tensile strength of 50-70 MPa, flexural strength of 100 MPa, and strain at break of about 4% [8]. It has been shown that tensile strength and modulus of PLA increases by a factor of two when the molecular weight increases from 50 to 100 kDa [9]. A further increase in molecular weight to 300 kDa seemed not to influence the properties of the polymers significantly. Grijpma and Pennings [10] investigated the importance of the crystalline fraction in the toughness of PLA. They varied crystallinity of PLA copolymers by introducing 0-15 mol.% $_{D}$-lactide. The impact strength (37 kJ m^{-2}) reached maximum at $_{D}$-lactide content of 0.5 mol.% and a heat of fusion of 60 J g^{-1}. They explained that this optimum in mechanical properties is reached at a point where the entanglement density is relatively

high and the crystallinity is large enough to make the effect of physical cross-linking on the brittle tensile strength. Superior mechanical properties have also been achieved by stereocomplexation of enantiomeric PLAs, which was ascribed to formation of stereocomplex crystallites giving intermolecular cross-linking [11]. There is no significant differences in mechanical properties of polymers of similar molar masses, but prepared by different polymerization processes [12].

2.2 Natural fibre reinforced PLA composites

In comparison with commodity polymers such as polyethylene (PE), polypropylene (PP), polystyrene (PS) and poly(ethylene terephthalate) (PET), the mechanical properties of semi-crystalline PLA are attractive, particularly its high Young's modulus, making it as an excellent substitute for commodity polymers in short-time packaging. However, due to its high brittleness and low heat deflection temperature (HDT), PLA has not yet gained full market acceptance as an engineering resin.

One possible strategy to improve the mechanical and thermal properties of PLA has been through the addition of natural fibres (NFs) to make so-called 'green composites' [13]. NFs have advantages such as low cost, high specific strength and modulus, biodegradability and renewability compared to glass fibres (GFs).

Dicker *et al.* [14] used Ashby plots for a comparative evaluation of the mechanical properties of various fibres and their composites as shown in Figure 2.4. It can be seen that NFs and GFs are comparable in terms of specific stiffness and specific strength. However, a wide gap appears when comparing the mechanical properties of composite materials constructed from each of these fibres. There are several reasons for this

disparity between the properties of the raw fibres and their composites. One reason is the poor thermal stability of NFs. Wielage *et al.* [15] showed that the tensile properties of NFs can decrease by as much as 60% when the fibres were processed for 60 min at 220 ^{o}C. Moreover, the poor compatibility between hydrophilic natural fibre and hydrophobic polymer matrix is also responsible. Numerous attempts have been made to overcome this issue, which will be discussed in details in the following paragraphs.

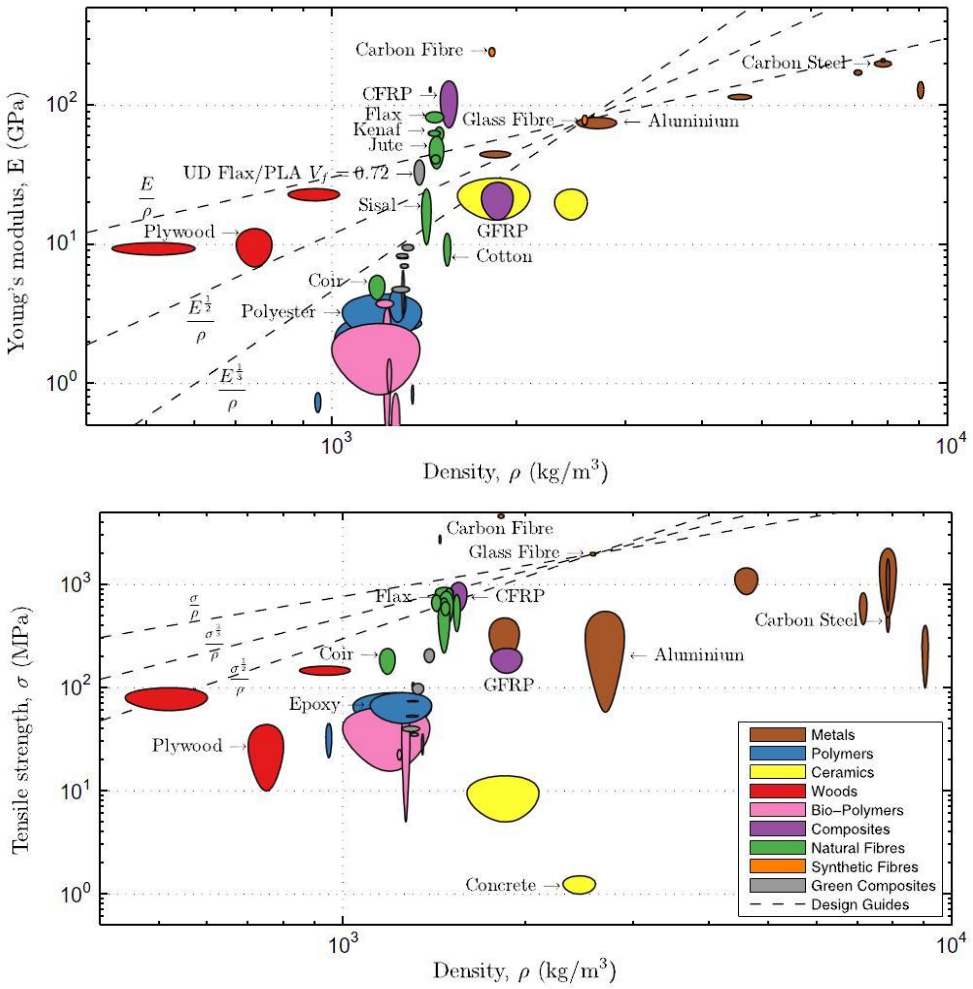

Figure 2.4 Density specific mechanical properties [14].

Table 2.1 Comparison of the mechanical properties of PLA-based green composites.

Author (year)	**Fibre type (proportion)**	**Tensile strength [MPa]**	**Young's modulus [GPa]**	**Impact strength increase in %** *
Oksman *et al.* [18] (2003)	Flax (30 wt.%)	53	8.3	-27%
Nishino *et al.* [19] (2003)	Kenaf (70 vol.%)	62	6.3	-
Plackett *et al.* [20] (2003)	Jute fibre (40 wt.%)	93.5	8.7	-7%
Huda *et al.* [21] (2005)	Recycled newspaper cellulose fibre (30 wt.%)	47.7	6.3	-49%
Li *et al.* [22] (2006)	Bamboo fibre (30 wt.%)	45	3	-
Bax *et al.* [23] (2008)	Cordenka rayon fibre (30 wt.%)	58	4.9	350
Bax *et al.* [23] (2008)	Flax (30 wt.%)	54	6.3	-45%
Cheng *et al.* [24] (2009)	Chicken feather fibre (5 wt.%)	55	4.2	-
Bledzki *et al.* [16] (2009)	Man-made cellulose (30 wt.%)	91	5.8	260
Bledzki *et al.* [16] (2009)	Abaca fibre (30 wt.%)	74	8.2	140
Bledzki *et al.* [17] (2010)	Jute fibre (30 wt.%)	82	9.6	20

** Because the test methods presented in different papers differ from each other, percentage change values compared to the value for pure matrix given in every particular work are presented. Values are calculated by using information which was not given in numeric values but in figures.*

A comparative study on the mechanical properties of various NFs reinforced PLA composites is given in Table 2.1. The different extent of reinforcement accounts for the type of fibre used and its homogenization to the matrix. The composites with flax show higher strength and modulus within the NFs group, since the flax is characterized by higher mechanical properties than for example bamboo. The other factors that affect the mechanical strength include fibre diameter, length and aspect ratio. The diameters of NF bundles range considerably more than 50 μm. Man-made cellulose occurs in most cases as elementary fibres with a diameter of only 12 μm. Increasing fibre diameter affects the aspect ratio and thus decreases the mechanical performance of the composites. Bledzki and Jaskiewicz [16] pointed out that the highest aspect ratio of the man-made cellulose fibre is the main cause for its enhanced mechanical properties. Similarly, jute fibre bundles undergo separation during processing, allowing a better distribution and a favourable diameter for improved mechanical properties [17].

With regards to tensile strength, it is very sensitive to the fibre/matrix interfacial adhesion. When an external load is applied to composites, the load is transferred from the matrix at the surface of composites to the fibres nearest the surface and continues from fibre to fibre via matrix and interface. Therefore, a weak interface induces an ineffective load distribution and the mechanical properties of the composites are impaired. On the contrary, a strong interface can assure an efficient load transfer to fibres even after several fibres are broken, with a consequent improvement of composite mechanical behaviour. It is therefore clear that optimization of interfacial adhesion is necessary in order to improve the overall mechanical properties.

Both PLA and NFs are hydrophilic in nature and apparently is assumed that this

property will facilitate a better adhesion. Nevertheless, long fibre pull-outs and clean fibre surface of the PLA/flax composites as observed by Oksman *et al.* [18] proves a poor adhesion between the fibre and the matrix. Modifications of fibres were extensively reported in literatures. Mukherjee and Kao [25] reviewed the effect of fibre surface treatment on the fibre-matrix adhesion and mechanical properties of NFs reinforced PLA composites. Huda *et al.* [21] examined the effect of the addition of silane coupling agent and talc on the thermal and mechanical properties of PLA/recycled newspaper composites. The silane treated talc reinforced PLA/recycled newspaper hybrid composites flexural and impact strength was found to be significantly higher than that of those made without silane coupling agent. The silane treated hybrid composites showed improved properties such as a flexural strength of 132 MPa and a flexural modulus of 15.3 GPa, while the untreated composites exhibited flexural strength and modulus values of only 77 MPa and 6.7 GPa, respectively.

Interestingly, Juntaro *et al.* [26] successfully attached nano-sized bacterial cellulose (BC) onto sisal fibres and then incorporated them into PLA. The presence of nanofibres led to a rise in interfacial adhesion with PLA, thus significantly improved both fibre-dominated and interface-dominated properties of these hierarchical composites.

The impact strength of a composite depends on the type of fibre and is often inversely proportional to its interfacial adhesion with the matrix. Bax *et al.* [23] prepared Cordenka reinforced PLA composite and reported a maximum impact strength of 72 kJ m^{-2} with the addition of 30 wt.% fibres, which is approximately 4.5 times that of pure PLA. This value is also higher than the impact strength of PP/flax composite (32 kJ m^{-2}) as reported in the literature [27]. Bledzki *et al.* [16] also obtained a 260% increase in

impact strength for man-made cellulose reinforced PLA composites. On the other hand, a decrease in impact strength was observed in case of jute fibres by Plackett *et al.* [20]. Similar results were observed by Oksman *et al.* [18] and Bax *et al.* [23] for PLA/flax composites. This can be explained by the relatively strong fibre-matrix adhesion leading to a more brittle failure behaviour in PLA/flax composites as compared to PLA/Cordenka composites.

Improved HDTs are also observed in NFs reinforced PLA composites mainly due to increased crystallinity, modulus and/or the improved adhesion between matrix and fibre. Huda *et al.* [28] reported that surface-treated kenaf fibre reinforced laminated composites possessed higher storage moduli, impact strength and HDT than pure PLA resin but at the expense of tensile strength.

To date, a number of composite manufacturers have introduced NFs reinforced PLA composites in their product range. FKuR (Germany) has developed wood reinforced PLA compounds (FIBROLON), which can be extruded or injection moulded into complex profiles, panels, and hollow profiles and/or into components for automotive interiors. Products of wood and biodegradable polyesters are also developed by FuturaMat (France) under the trade name BioFibra® in grades suitable for injection moulding, extrusion, or thermoforming. Large scale use of PLA/NFs composites in automotive applications have been reported as well. Toyota, for example, uses kenaf fibre reinforced PLA composites for its Prius hybrid car interior parts [29].

However, there are some major drawbacks which could limit the commercial adoption of these fibres as reinforcements in composites.

First challenge comes to the fibre dispersion and its interfacial adhesion with the

polymer matrix. Although chemical modification of fibres can potentially solve this issue, large amounts of hazardous chemicals are typically involved and chemical waste must be disposed appropriately.

Variability in fibre properties is another major issue to be resolved if these materials are used in structural applications where durability must be accurately predicted. Due to NFs being obtained from natural sources, crop variety, factors including seed density, soil quality, fertilization, field location, fibre location on the plant, climate and harvest timing could all induce variability in properties, such as fibre shape, length and chemical composition.

Furthermore, Summerscales *et al.* [30] compiled the results of quantitative life cycle assessment (QLCA) from Dissanayake *et al.*'s work. They found that the total energy required for flax using low energy agricultural processes was even greater than glass fibres. Therefore, the 'green' claim for NFs composites may only be appropriate when the best practice is adopted in the growth, separation and processing of NFs, at the same time the durability of NFs composites is comparable to GFs composites.

Although the use of NFs to reinforce PLA seems at first to be an environmentally sound approach as they are renewable, there are some issues with respect to end-of-life scenarios for these composites. In the case of mechanical recycling their relatively poor thermal stability may lead to severe additional thermal degradation of the composites during subsequent reprocessing steps. Furthermore, the recycling process of a traditional composite usually requires high technology and high cost due to the difficult separation of the fibre from polymer matrix [31]. Actually, the introduction of any 'foreign' filler is in conflict with the basic idea behind recycling and monomaterial

products.

2.3 Self-reinforced polymer composites

2.3.1 Self-reinforced polymer composites

A promising approach to composite recycling is the concept of 'self-reinforced polymer' composites (SRPs) or 'all-polymer' composites, in which a polymer matrix is reinforced with oriented fibres or tapes of the same polymer. The absence of 'foreign' reinforcements means enhanced fibre-matrix interfacial adhesion and more importantly, full recyclability without the need for separation of fibre and matrix. The concept was first presented by Capiati and Porter [32] using oriented PE reinforcement and PE matrix with different melting temperatures. In following several decades, it has been successfully transferred to a range of polymers using various consolidation technologies.

The most frequently used technology to manufacture SRPs is film-stacking, where similar polymers with different melting temperatures are used to achieve melting of one phase to yield matrix, while retention of another phase to yield reinforcement. Examples of this method include the work of Capiati and Porter [32], Kazanci *et al.* [33], Barany *et al.* [34], Houshyar *et al.* [35], and more recently Gong and Yang [36]. This method has many advantages, such as ease of production, good matrix distribution, can be applied to commercial polymer fibres or fabrics and films. The processing window can be large by selecting similar polymers but with very different melting temperatures. A wide variety of thin polymer films means that fibre volume fractions can be fairly well controlled. Other approaches for introduction of a polymer matrix phase amongst

polymer fibres include melt impregnation [37], powder impregnation [38], and solution impregnation [39, 40]. A low viscosity of the polymer matrix is crucial for good impregnation, where reinforcement fibres/tapes should be surrounded by matrix without voids. However, compared to non-crosslinked thermosets, the melt viscosities of thermoplastics are usually 3-6 orders higher, which means it is more difficult for thermoplastics to achieve a good matrix distribution by melt-impregnation.

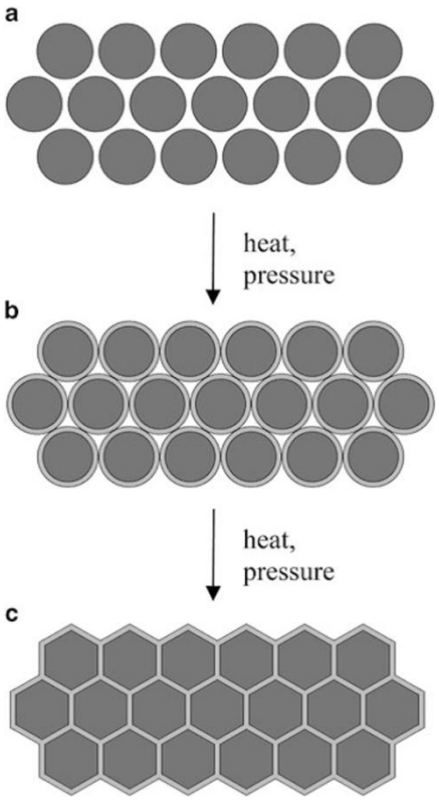

Figure 2.5 Consolidation of a SRPs from homogenous fibres by a hot compaction technology [41].

In 1993, Ward and others at the University of Leeds described a simple but innovative processing method, called 'hot-compaction' [42], which has been investigated for a range of polymers [43-46]. Here an assembly of oriented polymer fibres or tapes is heated to a critical temperature, while held under pressure, such that a thin skin on the

surface of each oriented element is 'selectively melted', creating a matrix phase. On subsequent fast cooling, the molten material recrystallises to form the matrix of the composite, with the remaining fraction of the original oriented phase acting as the reinforcement. This process is shown schematically in Figure 2.5. The first hot-compaction studies were carried out on unidirectional aligned melt-spun PE fibres [42]. They found that a maximum modulus of 36 GPa was obtained at the optimum compaction temperature of 136 ^{o}C with a processing window of ± 2 ^{o}C. DSC results showed that the optimum sample had around 15% of the molten and recrystallized

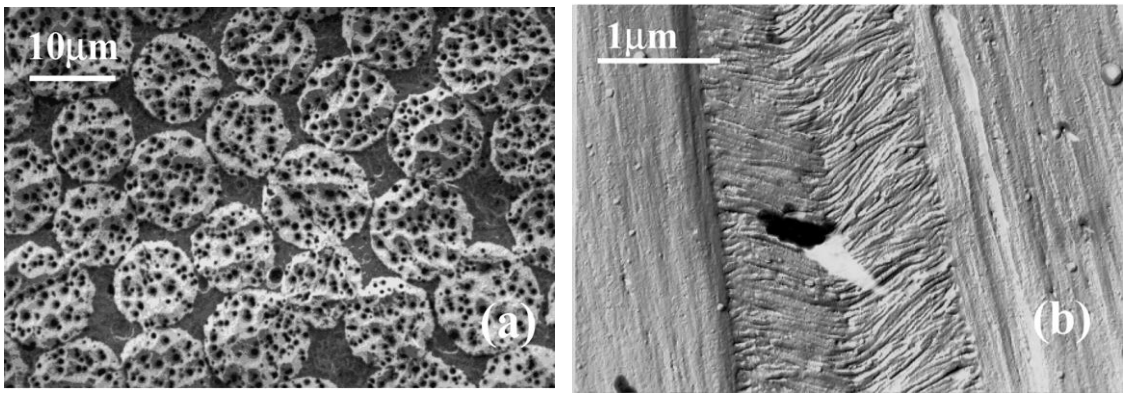

Figure 2.6 Etched micrographs from unidirectional melt-spun CERTRAN PE fibres. (a) SEM picture of a transverse section of compacted fibres. (b) TEM picture of an interstitial lamellar region and its junction with adjacent fibres.

matrix phase. In a later study [47], SEM and TEM of etched compacted samples showed how the recrystallized material fills the interstices in the close packed fibres. The molten skins recrystallized epitaxially on the surfaces of the un-molten portion of the fibres, as shown in Figure 2.6. Conditions were found for the successful compaction of a wide range of polymer fibres and tapes, including gel-spun PE fibres [41, 48], PET fibres [44], liquid crystalline polymer fibres [49] and fibrillated PP tapes [50]. Recent efforts have mainly focused on PP and this material is now commercially available under the

trade name Curv®. While it is a very elegant concept, the hot compaction process is clearly temperature sensitive. The need for unique and well-controlled composite processing routes may mean that these composites are more expensive to manufacture and more sensitive to manufacturing parameters than conventional composites.

In the early 2000s, Peijs and coworkers developed a co-extrusion technique based on PP [31]. The key development is the concept of co-extruding multilayered tapes consisting of a PP homopolymer core covered by a thin PP copolymer skin with a lower melting temperature (see Figure 2.7). Subsequent solid-state drawing of these co-extruded tapes leads to a large increase in mechanical properties. These tapes can be woven into fabrics, and then further consolidated into sheets. An example of SRPs produced by using coextruded tape technology is shown in Figure 2.8.

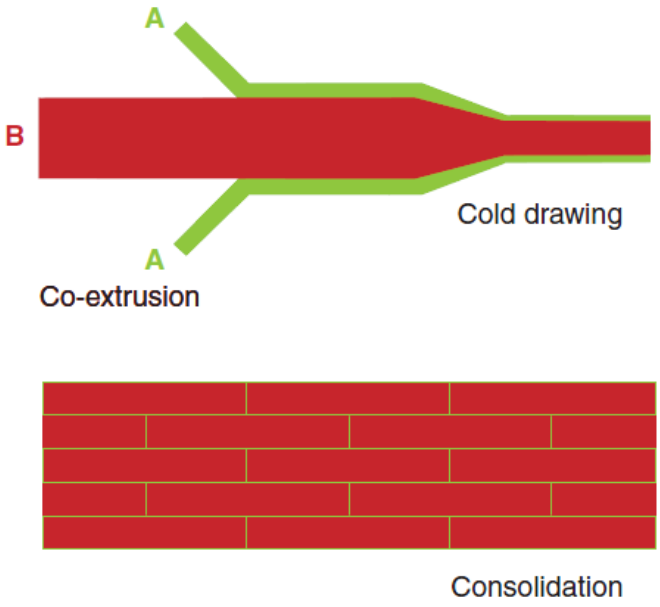

Figure 2.7 Co-extrusion technology is used for the development of high-performance PP tapes. These tapes consist of a highly oriented core (B) and a thin polymer skin (A) to weld the tapes together in a subsequent consolidation process.

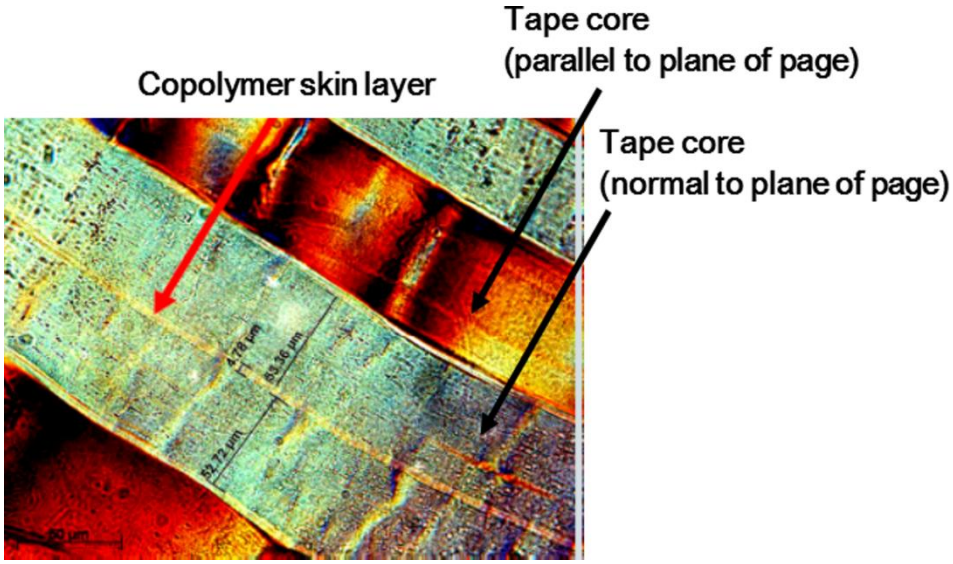

Figure 2.8 Optical micrograph of a cross-section of a co-extruded PP woven tape-based SRP [51].

In this way, the reinforcement and matrix phase of the composite are produced at the same time; hence there is no need for a separate impregnation step when manufacturing the composites. The bonding between fibre or tape and matrix is achieved during co-extrusion. The processing temperature window could be widened to as much as 30 ^{o}C. Cabrera *et al.* [52] studied the effect of consolidation temperature on the flexural stiffness of unidirectional SR-PP produced by using co-extruded tape. They found that over the range of consolidation temperatures studied (140-170 ^{o}C), there was no significant effect of consolidation temperature on the flexural stiffness of the laminates, indicating that this wide temperature window would make composites based on co-extruded tapes less sensitive to thermal relaxation during hot-consolidation than mono-extruded tapes with a much narrower processing temperature window. The other main advantage of using co-extruded tapes is that the matrix material can be evenly distributed during composite consolidation. The volume fractions of reinforcement in these composites was extremely high (~ 90% or greater), while various parameters

could be used to adjust mechanical [53, 54] and interfacial properties [55].

Because of the large processing window, a wide range of composite fabrication techniques were demonstrated by Cabrera *et al.*, including filament winding [56], non-isothermal stamping [57] and the creation of sandwich panels [58]. Although the temperature processing window is quite wide, the characteristics of the final composite, such as static and dynamic mechanical properties [59, 60], fatigue resistance [61], impact resistance [62] and porosity [63], are very dependent on these processing parameters. This allows the composite properties to be tailored to the final application. Following the commercialization of SR-PP composites using co-extruded tape technology as the product PURE®, this idea was later also applied to create composites based on PET. Zhang and Peijs reported the use of co-extruded PET yarns with a copolyester skin layer to facilitate easier processing, resulting in composites with a fibre volume fraction of ~ 70% [64].

2.3.2 Self-reinforced poly(lactic acid) composites

The creation of SRPs comprising various bioabsorbable precursor polymer fibres was also investigated mainly for medical applications, including polyglycolide (PGA), polyglycolide-lactide copolymer and PLA. This section will review the production and properties of the precursor PLA fibres first, followed by the development of SR-PLA composites to date.

2.3.2.1 PLA fibre

The development of high-stiffness and high-strength PLA fibres is essential in imparting superior mechanical properties onto the resulting SR-PLA composite. The mechanical

properties of fibres can be increased via molecular orientation during spinning and drawing, and the most commonly used methods of producing PLA fibres are melt spinning and solution spinning. The following paragraphs will review on the production of PLA fibres by both methods, along with correlations between structure and properties of the fibres. Comprehensive data on PLA fibre spinning are presented in Table 2.2.

In general, solution-spun fibres are superior to melt-spun fibres from the standpoint of mechanical properties. This is attributed to the lower chain entanglement of polymer molecules in the solution state as compared to the melt state. For instance, Penning *et al.* [65] reported that dry spinning followed by hot drawing resulted in low crystallinity fibres having a tensile strength of 1 GPa, whereas fibres prepared from melt spinning followed by hot drawing had considerably lower strengths, ranging from 0.19 GPa for completely amorphous copolymers to 0.53 GPa for PLA homopolymer. Fambri *et al.* [66] were able to obtain fibres with tensile strengths and modulus of 1.1 GPa and 10 GPa, respectively, with a PURAC brand biomedical material having M_v = 660,000. Similarly, Leenslag *et al.* [67] produced fibres with tensile strengths and modulus of 2.1 GPa and 16 GPa from PLA with M_v = 900,000. The main drawbacks are that solvents such as chloroform and toluene are necessary, and the production speed is rather low.

Table 2.2 Properties of oriented PLA fibre/tape.

Author (year)	**Method**	**Material**	**Strength/ modulus [GPa]**	**Comment**
Eling *et al.* [68] (1982)	Melt spinning and drawing	PLA	0.50 / 7.0	Initial $M_v < 3\times10^5$
Fambri *et al.*	Melt spinning	PLA	0.87 / 9.2	DR=10; Initial $M_v=3.3\times10^5$

[69] (1997)	and hot drawing			Drawing at 160 ^{o}C; Crystallinity ~ 59.2%
Mezghani *et al.* [70] (1998)	High speed melt spinning	PLA	0.38 / 6.0	Take-up velocity ~2000 m/min; Initial M_n=105,300 Daltons Extrusion temperature ~233 ^{o}C; Crystallinity ~ 42%
Yuan *et al.* [71] (2001)	Melt spinning and hot drawing	PLA	0.53 / 5.2	DR=4.71; Initial M_v=4.95×10^5 Drawing at 120 ^{o}C; Crystallinity ~61.9%
Cicero *et al.* [72] (2002)	Melt spinning and hot drawing	PLA	0.38 / 3.2	DR=6; Initial M_n=47,600 Radiant heating levels ~75%; Crystallinity ~ 47%
Sawai *et al.* [73] (2006)	Solid-state coextrusion	PLA	0.50 / 8.0	DR=14; Initial M_v=4.6×10^5 Drawing at 170 ^{o}C; Crystallinity ~49%
Leenslag *et al.* [67] (1987)	Solution spinning and hot drawing	PLA	2.1 / 16	DR=20; Initial M_v=9×10^5 Chloroform/toluene mixtures as solvent Solution temperature 60 ^{o}C; Drawing at 204 ^{o}C Crystallinity ~53%
Fambri *et al.* [66] (1994)	Solution spinning and hot drawing	PLA	1.1 / 10	Initial M_v=6.2×10^5 Chloroform as solvent Drawing temperature 150-210 ^{o}C

Table 2.2 (Continued)

Commercial PLA fibres are mainly produced by melt spinning. Generally, PLA fibres are produced by a two-stage process: first melt extrusion, and then solid-state hot drawing. Eling *et al.* [68] reported melt extrusion of PLA at 185 ^{o}C through a capillary, followed by hot drawing in an electric tube furnace. The obtained fibres had a modulus

of 7 GPa and tensile strength of 0.5 GPa. The investigation of Cicero *et al.* [72] illustrates the two-step melt spinning of textile grade PLA. A maximum modulus and tensile strength of 3.2 GPa and 0.38 GPa were obtained respectively. Later, Cicero *et al.* [74] investigated the crystalline morphology of PLA by small-angle X-ray scattering and atomic force microscopy. They proposed a representation of the molecular structure of PLA (Figure 2.9) where the alignment of microfibres along the fibre axis is determined by the draw ratio. The crystalline and amorphous regions form stacks within the microfibrils and the interfibrillar region is populated by amorphous chains. Fambri *et al.* [69] reported melt-spun PLA fibres with tensile modulus of 9.2 GPa and tensile strength of 0.87 GPa. Yuan *et al.* [71] prepared PLA fibres by a two-step melt spinning process. Results showed that M_v dropped sharply by 13-20% during pulverization and by 39-69% during melt extrusion. The hot-drawing process had little effect on M_v of PLA.

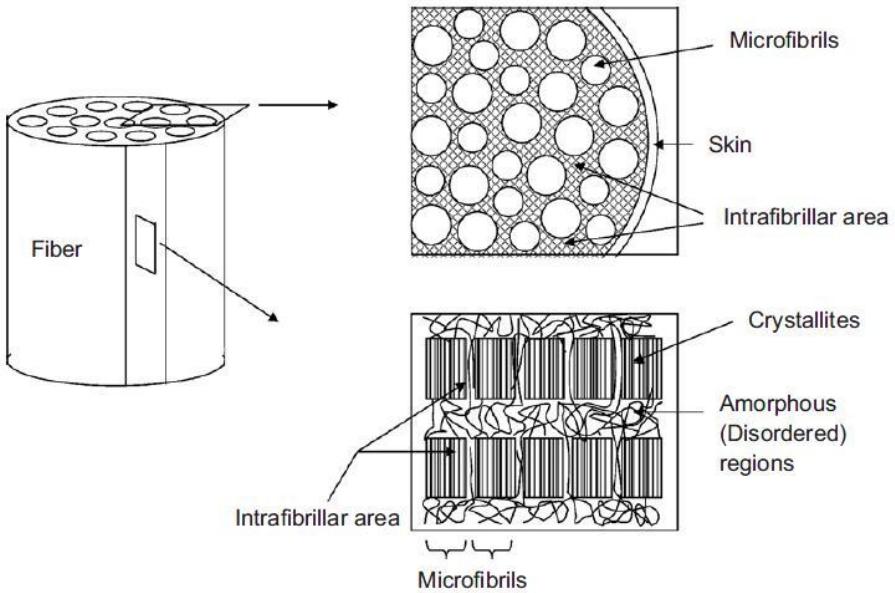

Figure 2.9 Supra-morphological model for two-step, melt-spun PLA [74].

PLA filaments can be spun at high speed take-up velocities of up to 5000 m min^{-1} [70]. The crystallinity, birefringence, tensile strength, Young's modulus and yield strength, all exhibit maxima at take-up velocities between 2000 and 3000 m min^{-1}. The boiling water shrinkage exhibits a minimum in this range, indicating that a stable morphology is developed through stress induced crystallization. The maximum tensile strength of these as-spun filaments was 385 MPa with a maximum modulus of 6 GPa.

2.3.2.2 Self-reinforced PLA composites

SR-PLA composites have been intensively studied since 1984, mainly for clinical use such as sutures, rods, screws and plates. Although few details regarding the exact processing routes were published in academic literature at that time, these bioresorbable composites were considered attractive as they possessed mechanical properties that exceeded most isotropic bioplastic, and could be naturally absorbed by the body over time, thus removing the need for surgical removal.

In 1988, Törmälä *et al.* successfully manufactured an SR-PLA composite with higher strength than non-reinforced PLA for use in osteosynthesis devices [75]. The composite was produced by subjecting the fibres to elevated temperature and pressure. This process leads to more melting of the inner fibres but still allowed for the retention of some fibre orientation.

Improved strength and rigidity were widely reported in literature. Table 2.3 compares the mechanical properties of SR-PLA reported in literatures. Majola *et al.* [76] successfully produced SR-PLA composite using sintering techniques at temperatures of 130-135 ^{o}C for (PDLLA/PLLA rods) and 162-174 ^{o}C (PLLA rods). The fibres were

Table 2.3 Mechanical properties of SR-PLA composite as reported in literature.

Authors (year)	Materials	Method	Elastic modulus [GPa]	Tensile strength [MPa]	Flexural modulus [GPa]	Flexural strength [MPa]	Shear strength [MPa]
Törmälä (1992) [77]	PLLA	Hot drawing	-	-	10	300	220
Törmälä (1992) [77]	PLLA	Sintering	-	-	-	250	96
Majola *et al.* (1992) [76]	PLLA	Sintering	-	-	-	250-271	94-98
Majola *et al.* (1992) [76]	PLLA/PDLA	Sintering	-	-	-	209	102
Haltia *et al.* (2002) [78]	PLLA	Hot drawing	-	-	5.6	210	-
Wright *et al.* (2005) [79]	PLLA	Hot compaction	5.4	-	5.6	-	143
Wright *et al.* (2006) [80]	PLLA	Hot compaction	-	-	5.6	150	-
Li and Yao (2007) [81]	PLLA	Film stacking	2.3	43.6	-	-	-

initially produced by hot drawing and melt spinning techniques. They reported that the composite had initial bending and shear strengths of 250-271 MPa and 94-98 MPa respectively, which are significantly higher than of those non-reinforced PLLA (145 MPa and 53 MPa respectively).

Some studies also incorporated hydroxyapatite (HA) or tricalcium phosphate (TCP) into SR-PLA composites. The concept of combining bioceramics with SRPs in order to produce not only high strength and biocompatibility but also bioactivity had been tried earlier by Kellomaki *et al.* [82].

Since these composites are used in clinical applications, many reports quantified the mechanical properties of SR-PLA composites as a function of time of *in vitro* conditioning and others have data from animal experiments. Majola *et al.* [76] evaluated the strength and strength retention of SR-PLA composite rods after intramedullary and subcutaneous implantation in rabbits. They found that strength retention of SR-PLLA intramedullary rods is sufficient for fixation of experimental cortical bone osteotomies.

Kellomaki *et al.* [83] designed several different bioresorbable scaffolds and found that SR-PLA rods were successfully used as scaffolds for bone formation in muscle by free tibial periosteal grafts in animal experiments. Wright-Charlesworth *et al.* [80] presented results of a nanoindentation study carried out with SR-PLA composites. The mechanical properties near the edge were lower than the interior of the sample after *in vitro* degradation, and changes were seen earlier for nanoindentation than for traditional flexural or tensile tests.

Self-reinforced bone fracture fixation pins and screws based on PLLA and PGA have

been available in the market under trade names such as the Smartpin™ and Smartscrew™ by ConMed Linvatec. Nowadays, bioresorbable self-reinforced bone fracture fixation devices are in clinical use or in clinical research in more than 20 countries [84]. The surgeon can select materials with tailored *in vivo* strength retention that suits individual needs in fracture fixation applications.

Few studies on SR-PLA have focused on engineering rather than biomedical applications. One group studied various physical and thermal treatments and their effects on widening the processing window [81]. Jia *et al.* [85] reported SR-PLA composites and PLA reinforced polybutylene succinate (PBS) (PLA-PBS) composites based on commercial textile grade Ingeo™ PLA yarns from NatureWorks®. Despite the fact that these Ingeo™ have rather limited mechanical performance, improved tensile strength and modulus were observed for both types of SRPs, with the highest improvements reported for SR-PLA. They explained this by the better properties of the PLA matrix compared to PBS and better interfacial adhesion in the case of SR-PLA.

In conclusion, PLA is considered as a very promising bioplastic but exhibits rather poor heat stability and high brittleness in its pristine state. Although natural fibres reinforced PLA composites do have some ecological advantages since they are renewable, there are some major drawbacks, such as poor interfacial adhesion with PLA, variability in fibre properties, and poor thermal stability during recycling process. The multiple end-of-life options offered by SR-PLA composites, including recycling and compositing, empowers them to reduce the environmental impact of materials, and gives the end-user maximum flexibility in selecting environmentally sound waste disposal schemes. To date, most studies on SR-PLA have focused on biomedical rather than engineering

applications. It will be very interesting to overcome the disadvantages of PLA by developing SR-PLA composites, thus converting high cost raw materials to value adding products.

2.4 References

1. W. H. Carothers, and J. Arvin, *Studies on polymerization and ring formation. II. Polyesters.* Journal of the American Chemical Society, 1929. **51**(8): p. 2560-2570.
2. J. Lunt, and A. L. Shafer, *Polylactic acid polymers from corn. Applications in the textiles industry.* Journal of Industrial Textiles, 2000. **29**(3): p. 191-205.
3. O. Avinc, and A. Khoddami, *Overview of poly(lactic acid) (PLA) fibre.* Fibre Chemistry, 2009. **41**(6): p. 391-401.
4. R. D. Benson, R. L. Borchardt, P. R. Gruber, E. S. Hall, M. L. Iwen, and J. J. Kolstad, *Continuous process for manufacture of lactide polymers with controlled optical purity*, 1992, US Patents 5142023.
5. D. J. Sawyer, *Bioprocessing-no longer a field of dreams*. in *Macromolecular Symposia*. 2003. Wiley Online Library.
6. R. S. Blackburn, *Biodegradable and sustainable fibres*. 2005: Elsevier.
7. M. Hartmann, and D. Kaplan, *Biopolymers from renewable resources.* D. L. Kaplan, Ed, 1998: p. 367.
8. J. F. Mano, R. A. Sousa, L. F. Boesel, N. M. Neves, and R. L. Reis, *Bioinert, biodegradable and injectable polymeric matrix composites for hard tissue replacement: state of the art and recent developments.* Composites Science and Technology, 2004. **64**(6): p. 798-817.
9. I. Engelberg, and J. Kohn, *Physico-mechanical properties of degradable polymers used in medical applications: a comparative study.* Biomaterials, 1991. **12**(3): p. 292-304.
10. D. W. Grijpma, and A.J. Pennings, *(Co) polymers of L‐lactide, 2. Mechanical properties.* Macromolecular Chemistry and Physics, 1994. **195**(5): p. 1649-1663.
11. H. Tsuji, and Y. Ikada, *Stereocomplex formation between enantiomeric poly (lactic acid) s. XI. Mechanical properties and morphology of solution-cast films.* Polymer, 1999. **40**(24): p. 6699-6708.
12. M. Ajioka, K. Enomoto, K. Suzuki, and A. Yamaguchi, *The basic properties of poly (lactic acid) produced by the direct condensation polymerization of lactic acid.* Journal of Environmental Polymer Degradation, 1995. **3**(4): p. 225-234.
13. L. A. Berglund, and T. Peijs, *Cellulose biocomposites-from bulk moldings to nanostructured systems.* MRS Bulletin, 2010. **35**(03): p. 201-207.
14. M. P. Dicker, P. F. Duckworth, A. B. Baker, G. Francois, M. K. Hazzard, and P. M. Weaver, *Green composites: A review of material attributes and complementary applications.* Composites Part A: Applied Science and Manufacturing, 2014. **56**: p. 280-289.
15. B. Wielage, T. Lampke, G. Marx, K. Nestler, and D. Starke, *Thermogravimetric and differential scanning calorimetric analysis of natural fibres and polypropylene.* Thermochimica Acta, 1999. **337**(1): p. 169-177.
16. A. K. Bledzki, A. Jaszkiewicz, and D. Scherzer, *Mechanical properties of PLA composites*

with man-made cellulose and abaca fibres. Composites Part A: Applied Science and Manufacturing, 2009. **40**(4): p. 404-412.

17. A. Bledzki, and A. Jaszkiewicz, *Mechanical performance of biocomposites based on PLA and PHBV reinforced with natural fibres-A comparative study to PP.* Composites Science and Technology, 2010. **70**(12): p. 1687-1696.
18. K. Oksman, M. Skrifvars, and J. F. Selin, *Natural fibres as reinforcement in polylactic acid (PLA) composites.* Composites Science and Technology, 2003. **63**(9): p. 1317-1324.
19. T. Nishino, K. Hirao, M. Kotera, K. Nakamae, and H. Inagaki, *Kenaf reinforced biodegradable composite.* Composites Science and Technology, 2003. **63**(9): p. 1281-1286.
20. D. Plackett, A. T. Løgstrup, P. W. Batsberg, and L. Nielsen, *Biodegradable composites based on L-polylactide and jute fibres.* Composites Science and Technology, 2003. **63**(9): p. 1287-1296.
21. M. S. Huda, L. T. Drzal, M. Misra, A. K. Mohanty, K. Williams, and D. F. Mielewski, *A study on biocomposites from recycled newspaper fibre and poly (lactic acid).* Industrial & Engineering Chemistry Research, 2005. **44**(15): p. 5593-5601.
22. S. H. Lee, and S. Wang, *Biodegradable polymers/bamboo fibre biocomposite with bio-based coupling agent.* Composites Part A: Applied Science and Manufacturing, 2006. **37**(1): p. 80-91.
23. B. Bax, and J. Müssig, *Impact and tensile properties of PLA/Cordenka and PLA/flax composites.* Composites Science and Technology, 2008. **68**(7): p. 1601-1607.
24. S. Cheng, K. T. Lau, T. Liu, Y. Zhao, P. M. Lam, and Y. Yin, *Mechanical and thermal properties of chicken feather fibre/PLA green composites.* Composites Part B: Engineering, 2009. **40**(7): p. 650-654.
25. T. Mukherjee, and N. Kao, *PLA based biopolymer reinforced with natural fibre: a review.* Journal of Polymers and the Environment, 2011. **19**(3): p. 714-725.
26. J. Juntaro, M. Pommet, G. Kalinka, A. Mantalaris, M. S. Shaffer, and A. Bismarck, *Creating hierarchical structures in renewable composites by attaching bacterial cellulose onto sisal fibres.* Advanced Materials, 2008. **20**(16): p. 3122-3126.
27. H. L. Bos, J. Müssig, and M. J. van den Oever, *Mechanical properties of short-flax-fibre reinforced compounds.* Composites Part A: Applied Science and Manufacturing, 2006. **37**(10): p. 1591-1604.
28. M. S. Huda, L. T. Drzal, A. K. Mohanty, and M. Misra, *Effect of fibre surface-treatments on the properties of laminated biocomposites from poly (lactic acid)(PLA) and kenaf fibres.* Composites Science and Technology, 2008. **68**(2): p. 424-432.
29. P. Mapleston, *Automakers work on sustainable platforms (biopolymers).* Modern Plastics, 2003. **80**(3): p. 45.
30. J. Summerscales, N. Dissanayake, A. Virk, and W. Hall, *A review of bast fibres and their composites. Part 2-Composites.* Composites Part A: Applied Science and Manufacturing, 2010. **41**(10): p. 1336-1344.
31. T. Peijs, *Composites for recyclability.* Materials Today, 2003. **6**(4): p. 30-35.
32. N. J. Capiati, and R. S. Porter, *The concept of one polymer composites modelled with high density polyethylene.* Journal of Materials Science, 1975. **10**(10): p. 1671-1677.
32. M. Kazanci, D. Cohn, G. Marom, C. Migliaresi, and A. Pegoretti, *Fatigue characterization of polyethylene fibre reinforced polyolefin biomedical composites.* Composites Part A: Applied Science and Manufacturing, 2002. **33**(4): p. 453-458.
34. T. Bárány, J. Karger−Kocsis, and T. Czigány, *Development and characterization of*

self–reinforced poly (propylene) composites: carded mat reinforcement. Polymers for Advanced Technologies, 2006. **17**(9‐10): p. 818-824.

35. S. Houshyar, R. A. Shanks, and A. Hodzic, *Influence of different woven geometry in poly (propylene) woven composites.* Macromolecular Materials and Engineering, 2005. **290**(1): p. 45-52.

36. Y. Gong, and G. Yang, *All-polyamide composites prepared by resin transfer molding.* Journal of Materials Science, 2010. **45**(19): p. 5237-5243.

37. A. Ajji, A. Ait-Kadi, and A. Rochette, *Polyethylene-ultra high modulus polyethylene short fibres composites.* Journal of Composite Materials, 1992. **26**(1): p. 121-131.

38. G. Hinrichsen, S. Kreuzberger, Q. Pan, and M. Rath, *Production and characterization of UHMWPE fibres/LDPE composites.* Mechanics of Composite Materials, 1996. **32**(6): p. 497-503.

39. Y. Cohen, D. M. Rein, and L. Vaykhansky, *A novel composite based on ultra-high-molecular-weight polyethylene.* Composites Science and Technology, 1997. **57**(8): p. 1149-1154.

40. F. Lacroix, M. Werwer, and K. Schulte, *Solution impregnation of polyethylene fibre/polyethylene matrix composites.* Composites Part A: Applied Science and Manufacturing, 1998. **29**(4): p. 371-376.

41. P. Hine, I. Ward, N. Jordan, R. Olley, and D. Bassett, *A comparison of the hot-compaction behaviour of oriented, high-modulus, polyethylene fibres and tapes.* Journal of Macromolecular Science, Part B, 2001. **40**(5): p. 959-989.

42. P. Hine, I. Ward, R. Olley, and D. Bassett, *The hot compaction of high modulus melt-spun polyethylene fibres.* Journal of Materials Science, 1993. **28**(2): p. 316-324.

43. I. Ward, and P. Hine, *The science and technology of hot compaction.* Polymer, 2004. **45**(5): p. 1413-1427.

44. J. Rasburn, P. Hine, I. Ward, R. Olley, D. Bassett, and M. Kabeel, *The hot compaction of polyethylene terephthalate.* Journal of Materials Science, 1995. **30**(3): p. 615-622.

45. D. Wright, J. Gilbert, and E. Lautenschlager, *The effect of processing temperature and time on the structure and fracture characteristics of self-reinforced composite poly (methyl methacrylate).* Journal of Materials Science: Materials in Medicine, 1999. **10**(8): p. 503-512.

46. P. Hine, I. Ward, N. Jordan, R. Olley, and D. Bassett, *The hot compaction behaviour of woven oriented polypropylene fibres and tapes. I. Mechanical properties.* Polymer, 2003. **44**(4): p. 1117-1131.

47. M. Kabeel, D. Bassett, R. Olley, P. Hine, and I. Ward, *Differential melting in compacted high-modulus melt-spun polyethylene fibres.* Journal of Materials Science, 1995. **30**(3): p. 601-606.

48. R. Yan, P. Hine, I. Ward, R. Olley, and D. Bassett, *The hot compaction of SPECTRA gel-spun polyethylene fibre.* Journal of Materials Science, 1997. **32**(18): p. 4821-4832.

49. I. Ward, and P. Hine, *Novel composites by hot compaction of fibres.* Polymer Engineering & Science, 1997. **37**(11): p. 1809-1814.

50. P. Hine, I. Ward, and J. Teckoe, *The hot compaction of woven polypropylene tapes.* Journal of Materials Science, 1998. **33**(11): p. 2725-2733.

51. B. Alcock, and T. Peijs, *Technology and development of self-reinforced polymer composites,* in *Polymer composites–polyolefin fractionation–polymeric peptidomimetics–collagens.* 2013, Springer. p. 1-76.

52. N. Cabrera, B. Alcock B, J. Loos, and T. Peijs, *Processing of all-polypropylene composites for ultimate recyclability.* Proceedings of the Institution of Mechanical Engineers, Part L: Journal of Materials Design and Applications, 2004. **218**(2): p. 145-155.

53. B. Alcock, N. O. Cabrera, N. M. Barkoula, and T. Peijs, *The effect of processing conditions on the mechanical properties and thermal stability of highly oriented PP tapes.* European Polymer Journal, 2009. **45**(10): p. 2878-2894.

54. T. Schimanski, J. Loos, T. Peijs, B. Alcock, and P. J. Lemstra, *On the overdrawing of melt‐spun isotactic polypropylene tapes.* Journal of Applied Polymer Science, 2007. **103**(5): p. 2920-2931.

55. B. Alcock, N. O. Cabrera, N. M. Barkoula, J. Loos, and T. Peijs, *Interfacial properties of highly oriented coextruded polypropylene tapes for the creation of recyclable all-polypropylene composites.* Journal of Applied Polymer Science, 2007. **104**(1): p. 118-129.

56. Cabrera, N.O., et al., *Filament winding of co-extruded polypropylene tapes for fully recyclable all-polypropylene composite products.* Applied Composite Materials, 2008. **15**(1): p. 27-45.

57. N. O. Cabrera, B. Alcock, E. T. J. Klompen, and T. Peijs, *Non-isothermal stamp forming of continuous tape reinforced all-polypropylene composite sheet.* Composites Part A-Applied Science and Manufacturing, 2008. **39**(9): p. 1455-1466.

58. N. O. Cabrera, B. Alcock, and T. Peijs, *Design and manufacture of all-PP sandwich panels based on co-extruded polypropylene tapes.* Composites Part B-Engineering, 2008. **39**(7-8): p. 1183-1195.

59. B. Alcock, N. O. Cabrera, N. M. Barkoula, J. Loos, and T. Peijs, *The mechanical properties of unidirectional all-polypropylene composites.* Composites Part A: Applied Science and Manufacturing, 2006. **37**(5): p. 716-726.

60. B. Alcock, N. O. Cabrera, N. M. Barkoula, A. Spoelstra, J. Loos, and T. Peijs, *The mechanical properties of woven tape all-polypropylene composites.* Composites Part A: Applied Science and Manufacturing, 2007. **38**(1): p. 147-161.

61. N. M. Barkoula, B. Alcock, N. O. Cabrera, and T. Peijs, *Fatigue properties of highly oriented polypropylene tapes and all-polypropylene composites.* ECCM13, 2008. **50**: p. 100.

62. B. Alcock, N. O. Cabrera, N. M. Barkoula, and T. Peijs, *Low velocity impact performance of recyclable all-polypropylene composites.* Composites Science and Technology, 2006. **66**(11): p. 1724-1737.

63. H. Deng, C. Reynolds, N. O. Cabrera, N. M. Barkoula, B. Alcock, and T. Peijs *The water absorption behaviour of all-polypropylene composites and its effect on mechanical properties.* Composites Part B: Engineering, 2010. **41**(4): p. 268-275.

64. J. M. Zhang, and T. Peijs, *Self-reinforced poly (ethylene terephthalate) composites by hot consolidation of bi-component PET yarns.* Composites Part A: Applied Science and Manufacturing, 2010. **41**(8): p. 964-972.

65. J. Penning, H. Dijkstra, and A. Pennings, *Preparation and properties of absorbable fibres from L-lactide copolymers.* Polymer, 1993. **34**(5): p. 942-951.

66. L. Fambri, A. Pegoretti, M. Mazzurana, and C. Migliaresi, *Biodegradable fibres.* Journal of Materials Science: Materials in Medicine, 1994. **5**(9-10): p. 679-683.

67. J. Leenslag, and A. Pennings, *High-strength poly(l-lactide) fibres by a dry-spinning/hot-drawing process.* Polymer, 1987. **28**(10): p. 1695-1702.

68. B. Eling, S. Gogolewski, and A. Pennings, *Biodegradable materials of poly (l-lactic acid): 1. Melt-spun and solution-spun fibres.* Polymer, 1982. **23**(11): p. 1587-1593.

69. L. Fambri, A. Pegoretti, R. Fenner, S. Incardona, and C. Migliaresi, *Biodegradable fibres of poly (L-lactic acid) produced by melt spinning.* Polymer, 1997. **38**(1): p. 79-85.

70. K. Mezghani, and J. Spruiell, *High speed melt spinning of poly (L‐lactic acid) filaments.* Journal of Polymer Science Part B: Polymer Physics, 1998. **36**(6): p. 1005-1012.

71. X. Yuan, A. F. Mak, K. Kwok, B. K. Yung, and K. Yao, *Characterization of poly(L-lactic acid) fibres produced by melt spinning.* Journal of Applied Polymer Science, 2001. **81**(1): p. 251-260.

72. J. A. Cicero, and J. R. Dorgan, *Physical properties and fibre morphology of poly (lactic acid) obtained from continuous two-step melt spinning.* Journal of Polymers and the Environment, 2001. **9**(1): p. 1-10.

73. D. Sawai, T. Yokoyama, T. Kanamoto, M. Sungil, S. H. Hyon, and L. P. Myasnikova, *Crystal transformation and development of tensile properties upon drawing of poly(L-lactic acid) by solid‐state coextrusion: effects of molecular weight*. in *Macromolecular Symposia*. 2006. Wiley Online Library.

74. J. A. Cicero, J. R. Dorgan, J. Janzen, J. Garrett, J. Runt, and J. Lin, *Supramolecular morphology of two‐step, melt‐spun poly(lactic acid) fibres.* Journal of Applied Polymer Science, 2002. **86**(11): p. 2828-2838.

75. J. Laiho, P. Rokkanen, M. Tamminmaki, P. Törmälä, and S. Vainionpää, *Material for Osteosynthesis Devices*, 1988, Google Patents.

76. A. Majola, S. Vainionpää, P. Rokkanen, H. M. Mikkola, and P. Törmälä, *Absorbable self-reinforced polylactide (SR-PLA) composite rods for fracture fixation: strength and strength retention in the bone and subcutaneous tissue of rabbits.* Journal of Materials Science: Materials in Medicine, 1992. **3**(1): p. 43-47.

77. P. Törmälä, *Biodegradable self-reinforced composite materials; manufacturing structure and mechanical properties.* Clinical Materials, 1992. **10**(1): p. 29-34.

78. A-M. Haltia, K. Lähteenkorva, P. Törmälä, A. Helminen, J. Tuominen, J. Seppälä, S. Veittola, and J. Ahvenalmmi, *Self-reinforcement and hydrolytic degradation of amorphous lactic acid based poly (ester-amide), and of its composite with sol-gel derived fibres.* Journal of Materials Science: Materials in Medicine, 2002. **13**(10): p. 903-909.

79. D. D. Wright‐Charlesworth, D. M. Miller, I. Miskioglu, and J. A. King, *Nanoindentation of injection molded PLA and self‐reinforced composite PLA after in vitro conditioning for three months.* Journal of Biomedical Materials Research Part A, 2005. **74**(3): p. 388-396.

80. D. D. Wright‐Charlesworth, J. A. King, D. M. Miller, and C. H. Lim, *In vitro flexural properties of hydroxyapatite and self‐reinforced poly(L‐lactic acid).* Journal of Biomedical Materials Research Part A, 2006. **78**(3): p. 541-549.

81. R. Li, and D. Yao, *Preparation of single poly(lactic acid) composites.* Journal of Applied Polymer Science, 2008. **107**(5): p. 2909-2916.

82. M. Kellomäki, K. Tanner, W. Bonfield, and P. Törmälä, *Reinforced polylactide-hydroxyapatite composites*. in *13th European Conference on Biomaterials. Göteborg, Sweden*. 1997.

83. M. Kellomäki, H. Niiranen, K. Puumanen, N. Ashammakhi, T. Waris, and P. Törmälä, *Bioabsorbable scaffolds for guided bone regeneration and generation.* Biomaterials, 2000. **21**(24): p. 2495-2505.

84. P. Törmälä, *Bioabsorbable surgical composite materials.* Advanced Materials, 1992. **4**(9): p. 589-591.

85. W. Jia, R. H. Gong, and P. J. Hogg, *Poly(lactic acid) fibre reinforced biodegradable*

composites. Composites Part B: Engineering, 2014. **62**: p. 104-112.

Chapter 3.

The influence of solid-state drawing on morphology and properties of melt-spun PLA tapes

3.1 Introduction

For the creation of self-reinforced poly(lactic acid) (SR-PLA) composites, first a tape-manufacturing route needs to be developed and optimized to ensure superior mechanical properties. Such a process will be based on solid-state deformation of PLA tapes rather than circular fibres as these allow for higher maximum 'fibre' volume fraction because of a closer packing in subsequent consolidation processes.

This chapter is concerned with the understanding of structure-property relationships of PLA films and tapes during stretching to optimize its use properties via processing. Since PLA is a semi-crystalline polymer, its mechanical properties depend strongly on its crystallinity, crystal orientation and morphology. Hence, the influence of draw ratio and drawing temperature on the superstructure (orientation and crystallization etc.) and morphology evolution of PLA, and the accompanying changes in mechanical and degradation properties will be discussed.

3.2 Experimental

3.2.1. Materials

PLA (NatureWorks® Ingeo™ 4032D), containing 2.2% of $_D$-isomer units, was purchased from Resinex (UK). Gel permeation chromatograph (GPC) in chloroform showed that the number average molecular weight (M_n) of the as received polymer is 133,500 g mol^{-1}. The melting temperature (T_m) is approximately 169 ℃ as measured by differential scanning calorimetry (DSC).

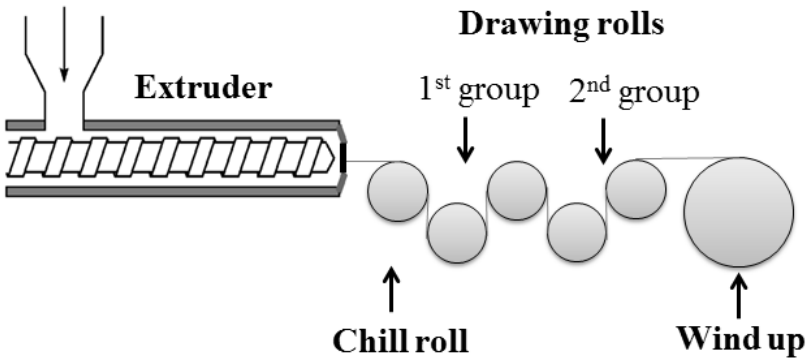

Figure 3.1 Schematic of extrusion and solid-state drawing pilot-production line.

3.2.2. Manufacture of PLA tapes

Figure 3.1 shows the tape production line schematically. A single screw extruder (Dr. Collin GmbH, TEACH-LINE® E 20T) with a length to diameter screw ratio (L/D) of 25:1 and a compression ratio of 2.85:1 was employed to obtain PLA extruded films. Default extrusion settings are described in Table 3.1. Molten polymers were extruded through a 50 mm slit die. These extruded films were quenched on a chill roll, followed by post-drawing on heated rollers (Dr. Collin GmbH, TEACH-LINE® MDO) to create oriented tapes. These tapes were drawn in a two-step solid-state drawing process below

the melting temperature. The first drawing step provided some initial orientation, but ultimate drawing was performed in the second step. The total draw ratio (DR) is defined as the ratio of drawn tape length to original tape length. The DR of as-extruded films is 1.

Table 3.1 Default extrusion parameters.

	Temperature [^{o}C]							**Screw speed**
	Zone 1	Zone 2	Zone 3	Zone 4	Zone 5	Zone 6	Tube	**[rpm]**
Extruder	170	165	210	215	210	200	205	20

The temperature of first set of rollers and initial draw ratio were fixed, while the second drawing conditions were varied for this investigation. The drawing parameters are listed in Table 3.2.

Table 3.2 Solid-state drawing parameters (to give different DR)

	Temperature [^{o}C]	**Roller speed (1^{st} group)**	**Roller speed (2^{nd} group)**
1^{st} drawing	80	0.5 m min^{-1}	2 m min^{-1}
2^{nd} drawing	70/90/110/130	0.2 m min^{-1}	0.8 m min^{-1}

3.2.3. Characterization

Number average molecular weight (M_n) was determined by gel permeation chromatography (GPC). Measurements were performed at 30 ^{o}C in chloroform with an AGILENT Technologies 1200 series, equipped with 2 x Agilent PLgel Mixed D column

and a pre-column. 200 ml of polymer solution with a concentration of 5 mg ml^{-1} was injected at 1 ml min^{-1}. The molecular masses were calculated using a polystyrene standard.

Morphological studies were carried out on gold-coated samples using scanning electron microscopy (SEM) (FEI Inspector-F, The Netherlands).

Differential scanning calorimetry (DSC) was conducted on Mettler-Toledo 822e. All samples were heated to 200 ^{o}C at 10 ^{o}C min^{-1} under a N_2 atmosphere. The degree of crystallization (X_c) was obtained using the following expression:

$$X_C = \frac{\Delta H_m - \Delta H_{cc}}{\Delta H_m^o} \times 100\% \qquad \textit{Equation 3.1}$$

where ΔH_m and ΔH_{cc} are the melting enthalpy and the cold crystallization enthalpy of test sample, ΔH_m^o is the melting enthalpy of the 100% crystalline PLA (93.6 J g^{-1}) [1].

Fourier transform infrared (FT-IR) spectra of various samples were measured with a Bruker Tensor 27 spectrometer. Attenuated total reflectance (ATR) mode was taken for the IR measurement. The spectra were obtained by collecting 16 scans at 4 cm^{-1} resolution.

Wide angle X-ray scattering (WAXS) were carried out at BM26 beamline of European Synchrotron Radiation Facility (ESRF). The energy of the X-ray beam was 1.033 Å. The sample-to-detector distance was 138.6 mm. All the 2D patterns were corrected for background scattering, and then integrated into 1D intensity profiles using fit2d software.

To quantify the degrees of orientation of the lattice plane (200)/(110), Herman's

orientation factor (f) was determined from the azimuthal intensity distribution by equation:

$$f = \frac{3\cos^2\phi - 1}{2} \qquad \textit{Equation 3.2}$$

Where ϕ is the angle between the chain axis and the tape axis, and $\cos^2\phi$ is defined as:

$$\cos^2\phi = \frac{\int_0^{\frac{\pi}{2}} I(\phi)\cos^2\phi\sin\phi d\phi}{\int_0^{\frac{\pi}{2}} I(\phi)\sin\phi d\phi} \qquad \textit{Equation 3.3}$$

Where $I(\phi)$ is the scattering intensity at the angle ϕ. The value of *f* ranges from -0.5 to 1. f = 1 indicates perfect alignments of polymer chains along drawing direction, whereas f = -0.5 means all the chains align perpendicularly to the drawing direction. When f = 0, it means that the chains are randomly aligned.

In addition to the Herman's orientation factor, the full width at half maximum (FWHM) of the (200)/(110) diffraction peaks generated from the fitted azimuthal intensity distribution was also used to gain a qualitative estimate of the orientation. Smaller FWHM values correspond to a higher degree of orientation.

Tensile tests were performed using an Instron 5586 at room temperature, equipped with a 1 kN load cell. Since the strain at break of as-extruded PLA film was less than 20%, a lower testing crosshead speed (8 mm/min) was used. Rectangle-shaped specimens were used for testing. The reported values were calculated as averages over six specimens.

The dynamic mechanical analysis (DMA) Q800 from TA Instruments was performed on PLA tapes with different draw ratios. Specimens were tested in tension mode. A gauge length of 15 mm was used. The system was cooled to -10 ^{o}C, and then heated to 150 ^{o}C at a rate of 3 ^{o}C min^{-1}. A static force of 0.01 N was applied to ensure the tape was taut between the grips.

3.3 Results and discussion

3.3.1 The influence of drawing on mechanical properties of PLA tape

It is expected that the mechanical properties will improve with increasing DR because of increasing strain-induced crystallization and orientation. Figure 3.2(a) shows typical stress-strain curves of the PLA tape prepared at 90 ℃ upon different draw ratios. It should be noted that a yielding point is observed in the stress-strain curve of as-extruded film, while the strain at break exceeds 6%. This slightly more ductile behaviour could be possibly explained by plane stress conditions being present in these thin specimens [2]. Besides, the tightness of the clamps was also found to promote more ductile behaviour [2]. For drawn PLA tape, the strain hardening is observed after yielding. This slope of the strain hardening is strongly related to the DR. As DR increases to 4, the slope of the strain hardening actually jumps. The higher the DR, the greater the strain hardening of the tapes. This can be explained by the strain-induced crystallization and orientation of PLA. The strain-hardening behaviour is advantageous to industrial thermoforming processes because it assists in the production of higher quality films with uniform thickness, named self-level [3]. As expected, drawing has a positive effect on the Young's modulus and tensile strength of the tapes. As shown in Figure 3.3(a),

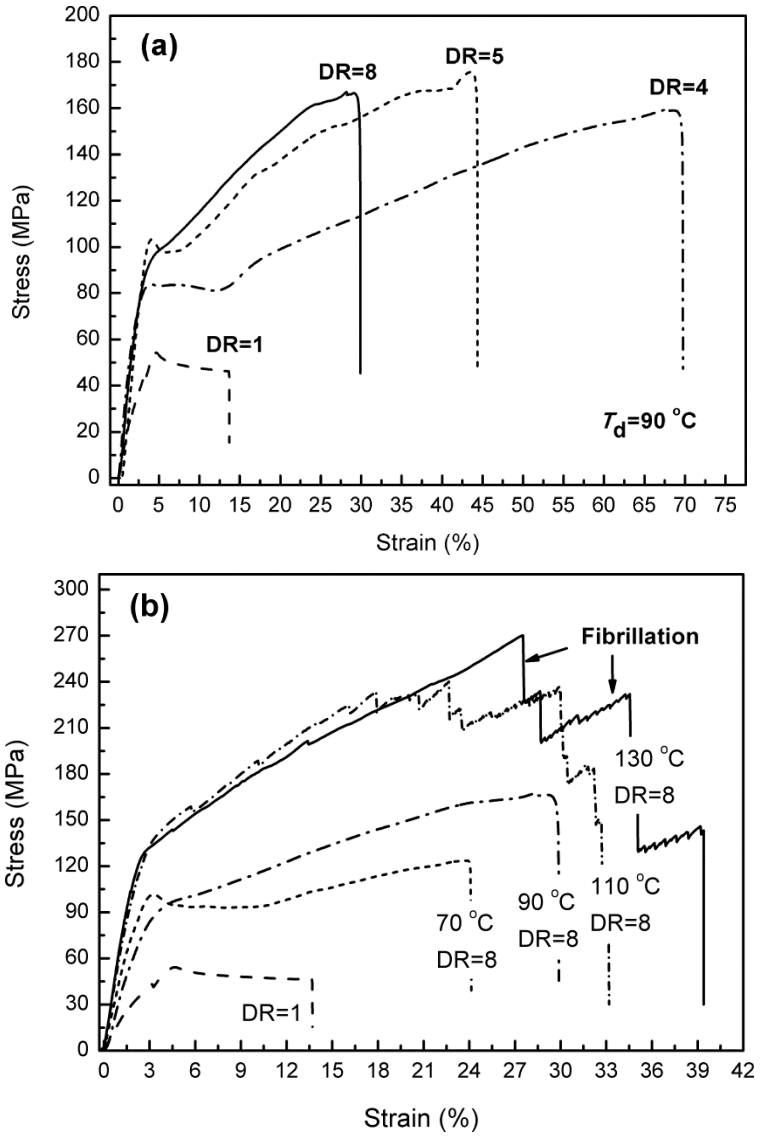

Figure 3.2 Stress-strain curves of PLA films and tapes subjected to (a) various draw ratios (T_d=90 °C), and (b) different drawing temperatures (DR=8).

compared to as-extruded PLA film (1.8 GPa in modulus and 53 MPa in tensile strength), a 128% and 227% increase in Young's modulus and tensile strength were achieved for oriented tapes of DR=8 drawn at 90 °C (4.1 GPa in modulus and 174 MPa in tensile strength), respectively. Interestingly, compared to as-extruded films, there is a significant increase in strain at break and ductility of the tapes with DR=4, leading to a much improved toughness. Further increase in DR results in a reduction of the strain at

break. This behaviour is similar as hot drawn PLA fibres reported in [4]. It is worth noting that tapes with DR=8 still have a strain at break of 30%.

It was reported that for a fixed draw ratio, the 2nd drawing temperature can have a dramatic effect on mechanical properties [5]. For this set of experiments, tapes were produced at a constant take-up speed and increasing drawing temperature (T_d) in the second step from 70 to 130 ℃ in 20 ℃ increments. From the tensile test data presented in Figure 3.2(b) and Figure 3.3(b), a significant influence of T_d on the overall mechanical behaviour can be seen. Young's modulus and tensile strength of the post drawn tapes increases with T_d, with maximum values obtained for tapes drawn at 130 °C. The Young's modulus and tensile strength for tapes drawn at 130 ℃ are 6.7 GPa and 280 MPa, respectively. These values are 1.6 times and 1.5 times higher than for tapes drawn at 70 ℃. Compared to isotropic PLA films, a 3.7 and 5.2 times increase in Young's modulus and tensile strength is achieved.

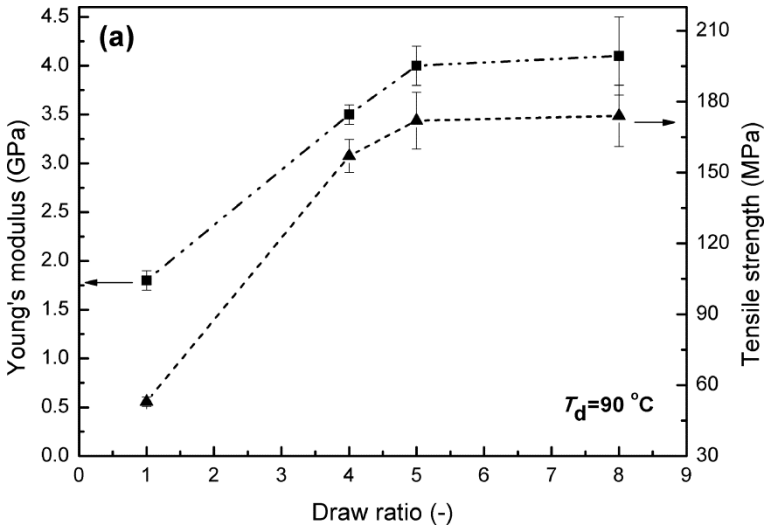

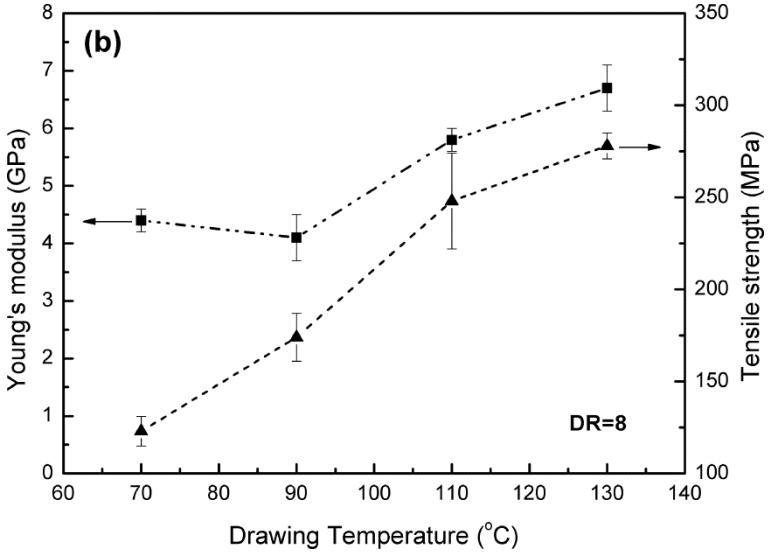

Figure 3.3 Young's modulus and tensile strength as a function of (a) draw ratio and (b) drawing temperature in the specimen.

Interestingly, in comparison to the small strain at break of as-extruded films, a much more ductile behaviour is observed after drawing. Compared to isotropic PLA, a 3.2 and 12.7 times increase in strain at break and toughness is obtained for tapes drawn at 130 ℃ (see Table 3.3). In contrast to the relatively smooth fracture surface of isotropic PLA, fibrillation takes place during the fracture process of these drawn tapes due to their highly anisotropic structures. As seen in Figure 3.2b, each drop in stress is accompanied by breakage along the axial direction in the tapes. In these oriented specimens, growing cracks are arrested by the anisotropic microstructure and catastrophic failure is postponed [6]. As a result, not only modulus and tensile strength but also ductility is greatly enhanced for tapes drawn at 130 ℃.

Table 3.3 Tensile properties of various PLA tapes.

T_d [°C]	DR	Young's modulus [GPa]	Tensile strength [MPa]	Strain at break [-]	Work of fracture* [J m^{-3}]
As-extruded	1	1.8±0.1	53±2	0.12±0.02	5.9×10^{6}
90	4	3.5±0.1	157±7	0.66±0.09	8.3×10^{7}
90	5	4.0±0.2	172±12	0.42±0.06	5.9×10^{7}
90	8	4.1±0.4	174±13	0.29±0.03	3.8×10^{7}
110	8	5.8±0.2	248±26	0.33±0.03	6.3×10^{7}
130	8	6.7±0.4	278±7	0.38±0.03	7.5×10^{7}

* *Work of fracture* = $\int_0^{\varepsilon_f} \sigma d\varepsilon$, *where* σ *is stress,* ε *is strain, and* ε_f *is the failure strain.*

The maximum tensile modulus and strength that could be achieved in this work were 6.7 GPa and 0.28 GPa, respectively. These tensile properties are comparable to the maximum moduli and strengths previously reported for melt-spun drawn PLA fibres (see Table 2.2), but are well below those of melt-spun polyethylene (PE), polypropylene (PP) and poly(ethylene terephthalate) (PET) with moduli ranging from 15 to 70 GPa [7]. The reason for this is the low intrinsic modulus of a PLA crystal. Nishino *et al.* reported the crystal modulus of an *α*-form crystal of PLA by using X-ray diffraction [8]. They reported 12 GPa for the crystal modulus of the *α*-form along the chain axis, meaning that the theoretically maximum achievable Young's modulus of a PLA fibre is well below the experimentally reported moduli for PE (235 GPa), PP (40 GPa) and PET (108 GPa), which all have much higher crystal moduli [9].

Overall, it can be concluded that drawing at 130 ℃ on the pilot line lead to good quality tapes as moduli of 6.7 GPa for these melt-crystallized PLA tapes compares well with a theoretical modulus of 12 GPa. Because of this, the highly oriented PLA tapes drawn at

130 ℃ were used as the reinforcement phase for SR-PLA composites.

3.3.2 The influence of drawing on thermal properties of PLA tapes

DSC was performed to find the development in crystallinity after drawing. As seen in Figure 3.4(a), the as-extruded films were almost amorphous (4% crystallinity content). The melting peaks observed are related to the crystallization developed during the DSC scan. It should be noted that for as-extruded films a glass transition with an enthalpy relaxation rather than a typical step change is observed. For samples that have been stored for a long time below the T_g, the 1st heating curve often exhibits an endothermic relaxation peak rather than a step change. This peak can no longer be observed in the cooling curve. Preparing amorphous film is very important, because a too high initial crystallinity will reduce the maximum attainable draw ratio and consequently lower the final tape's mechanical properties. In agreement, Hyon and co-workers [10] started from as-spun fibres with crystallinity not greater than 5%, to draw them six times.

For tapes drawn at 90 ^{o}C, the crystallinity increased dramatically to 53% and then reached a plateau at DR=4. The T_g and cold crystallization peaks were not detected in the DSC thermograms of drawn tapes. The melting peaks of all the samples appeared at 166 ^{o}C.

Furthermore, it is clear that increasing the drawing temperature results in a higher degree of crystallinity. The value for tapes drawn at 70 ^{o}C is 55% and rises to 67% for tapes drawn at 130 ^{o}C. Two different melting peaks can be distinguished for tapes drawn at 130 ^{o}C, at about 160 and 169 ^{o}C, respectively. The observed secondary peaks at lower temperatures are most likely due to varying lamellae thicknesses being present in the respective tapes.

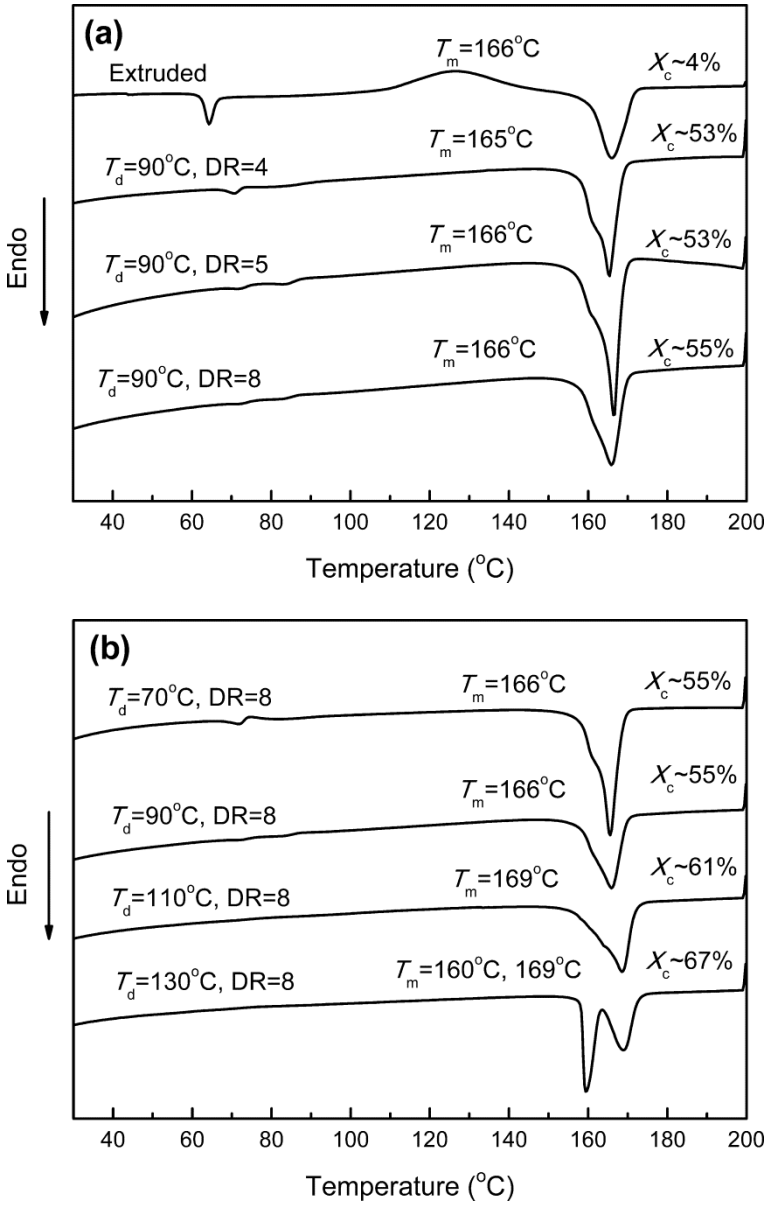

Figure 3.4 DSC thermograms of (a) samples drawn at 90 °C with various draw ratios, and (b) samples drawn at different temperatures with draw ratio of 8.

Since the mechanical properties of polymers are dependent on intermolecular interactions, the performance of polymers depends on the applied strain rate and temperature. The typical DMA plots, displaying the storage modulus (*E'*) and tan δ (*E''/E'*) as a function of temperature, are shown in Figure 3.5. The mechanical glass transition is taken as the temperature of the maximum in tan δ. As seen in Figure 3.5(a),

all the tapes show a similarly shaped curve. Below T_g, E' does not change much with temperature because the amorphous molecules are still essentially glassy. As soon as T_g is approached, however, the polymer chains in the amorphous phase begin to move, resulting in a reduced stiffness.

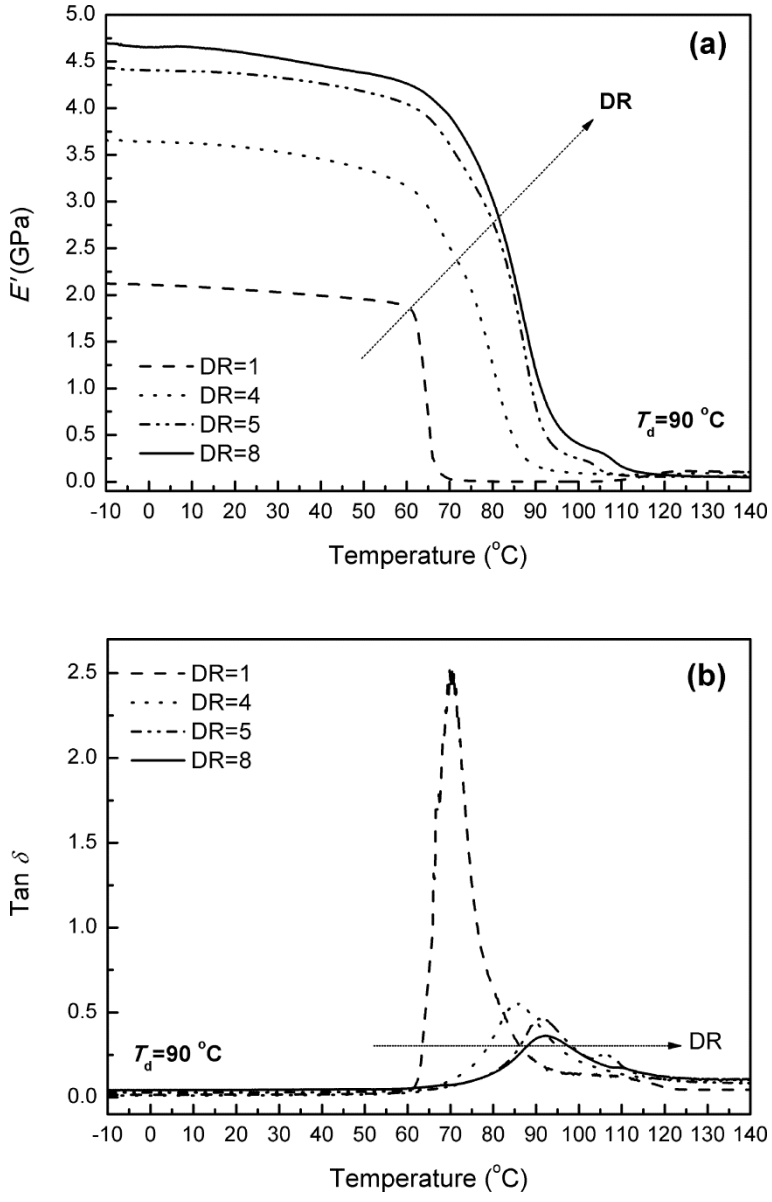

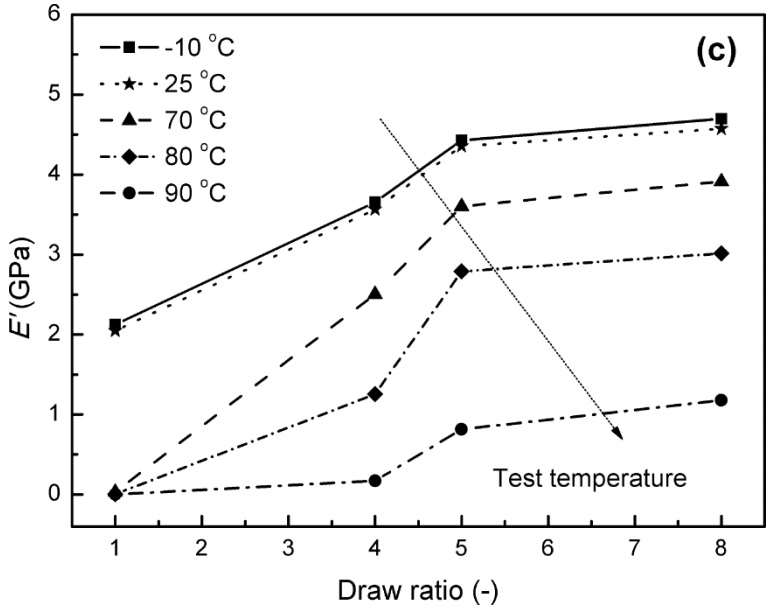

Figure 3.5 (a) Storage modulus and (b) loss factor against temperature for a range of PLA tapes with increasing draw ratio; (c) Storage modulus vs. draw ratio for a range of PLA tapes with increasing test temperature

Figure 3.5(b) shows how the solid-state drawing influenced the tan δ peak position of PLA. As we can see, the tan δ peak is shifted to higher temperature with increased draw ratio. The peak position for PLA was at 70.0 ℃ and increased to 92.2 ℃ for the drawn tapes with DR=8. It was reported that T_g is influenced by the degree of crystallinity in PLA [11]. Moreover, it was reported earlier that orientation leads to a lower entropy in tapes, thus resulting in a higher T_m [12]. Similarly, upon heating, the highly ordered oriented PLA chains in the amorphous phase will try to re-establish their preferential isotropic state. However, the chains in constrained tapes have less mobility and as a result a higher T_g. Therefore, this positive shift in tan δ peak position can be attributed to strain-induced crystallization and a constrained oriented amorphous phase. Additionally, the intensity of the tan δ peak decreased with draw ratio compared to as-extruded film. This indicates that fewer polymer chains are participating in this transition. It should be

noted that the T_g values obtained from DMA are typically higher than those from DSC. This is because the oriented tapes studied with DSC are unconstrained and can relax before reaching T_g. Sub-T_g relaxation is inhibited for the DMA experiment because the oriented tapes are always slightly stressed. The confinement of the pre-strain prevents, or at least slows down, relaxation [12].

Moreover, *E'* increases with draw ratio within the temperature range studied. As seen in Figure 3.5(c), below T_g (70-92 ℃), there is no significant change in *E'* for all tapes when increasing the test temperature from -10 ℃ to 25 ℃. At 80 ℃, drawn tapes with DR=4 possess a low storage modulus, approximately 1.3 GPa, which indicates that the tapes have totally relaxed. The higher stretched tapes with DR=5 and 8, retain a higher modulus at elevated temperatures, possessing storage moduli of 2.8 GPa and 3.0 GPa respectively at 80 ℃. These values shows that these tapes still possesses a greater storage modulus at 80 ℃ than undrawn PLA possesses at room temperature (2 GPa).

3.3.3 Structure development in PLA tapes during solid-state drawing

It was shown that depending on the drawing conditions, PLA is able to crystallize into different forms. When an amorphous film was drawn by a tensile force slightly above the T_g (60 ℃), an oriented film with α crystals was obtained. When a semi-crystalline sample with α crystals was drawn, a part of the α crystals was transformed into oriented β crystals, depending on the draw conditions [13]. Eling *et al.* [14] reported that β crystals were generated upon tensile drawing at a high temperature to a higher DR, whereas drawing at a low temperature and/or low draw ratio produced α crystals. Thus, the drawn products of PLA commonly consist of β crystals or a mixture of β and α crystal. Leenslag *et al.* [15] and Hoogsteen *et al.* [16] prepared high-strength PLA fibres

that consisted of pure β-form crystals by hot drawing of solution-spun fibres at 200-204 ℃, namely 20-25 ℃ above T_m of an α crystal, to a draw ratio of 14-20. They found that the formation of β crystals depended on the sample molecular weight and molecular weight distribution in addition to the drawing temperature and draw ratio.

It is very difficult to distinguish β reflection in WAXD pattern due to the overlap with α reflection. Since only long sequences of the 3_1 helix contribute to the X-ray $(003)_\beta$ reflection and shorter ones do not contribute to the intensity of this reflection, whereas the IR band of 912 cm^{-1} is active to the 3_1 helix independent of the sequence lengths. Thus, IR spectroscopy was more sensitive to detect a small amount of β crystals within a sample [17]. Therefore, the crystal transformation upon drawing was also characterized by IR spectroscopy. Cohn *et al.* [18] reported an absorption band at 921 cm^{-1} characteristic of α crystal. On the other hand, β crystals exhibit an absorption band at 912 cm^{-1} which is assigned to the CH_3 rocking mode of β crystals.

Figure 3.6 shows FT-IR spectra for a DR series prepared by solid-state drawing of PLLA at different drawing temperatures. According to the many FT-IR studies of PLLA, the band at 955 cm^{-1} is ascribed to the amorphous phase. The strong band at 871 cm^{-1} is attributed to the C-C backbone stretching. No absorption peak of either α or β crystal is observed for an original as-extruded film. An absorption band at 923 cm^{-1} characteristic of α-form crystal appeared at a DR of 4. The intensity of this band became gradually stronger with increasing DR. All the samples do not show a new absorption band at 912 cm^{-1} characteristic of β-form crystal, indicating no crystal transformation obtained in this study.

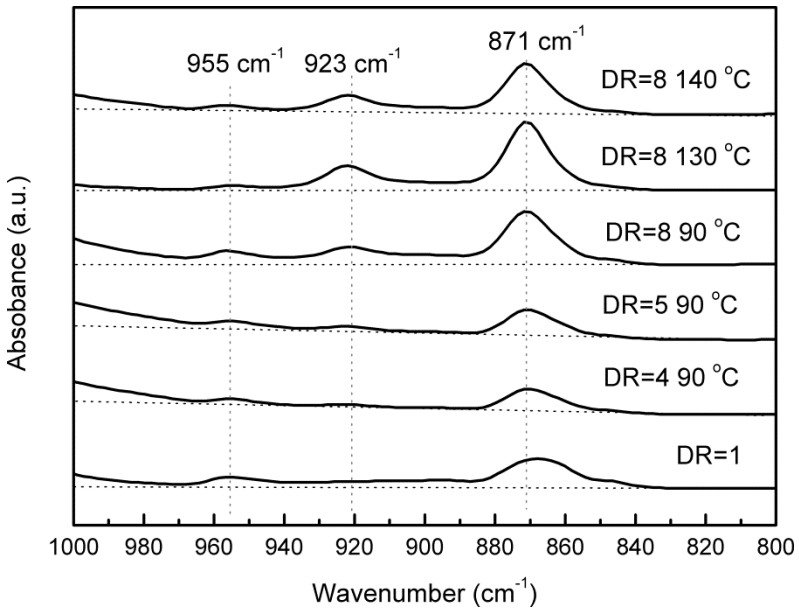

Figure 3.6 Infrared spectra in the 800-1000 cm^{-1} region for a DR series prepared at different drawing temperature.

2D-WAXS was performed to determine the PLA orientation after stretching. Figure 3.7 displays the 2D-WAXS patterns of a DR series of PLA drawn at T_d = 90 °C and also a T_d series of PLA with DR=8. Herman's orientation factor (*f*) calculated from Gaussian function, as well as the full width at half maximum (FWHM) of the (200)/(110) diffraction peaks are used to quantify the orientation of PLA, and the corresponding values for various tapes are listed in Table 3.4.

The PLA as-extruded film shows a diffuse isotropic scatter typical of an amorphous polymer. In the case of uniaxially drawn PLA tape with DR=4, there is a rapid growth of discrete equatorial reflections with low azimuthal spread typical of a well-oriented crystalline phase. The Herman's orientation factors of PLA tapes drawn at 90 °C are 0.99 and 0.98 for DR=4 and 5, respectively. However, upon further drawing to DR=8, Herman's orientation factor decreases to 0.55. This tape displays a wider azimuthal

spread suggesting crystals with poorer orientation, which is quite unusual. This phenomenon occasionally occurs when the sample is 'overdrawn' at low temperature.

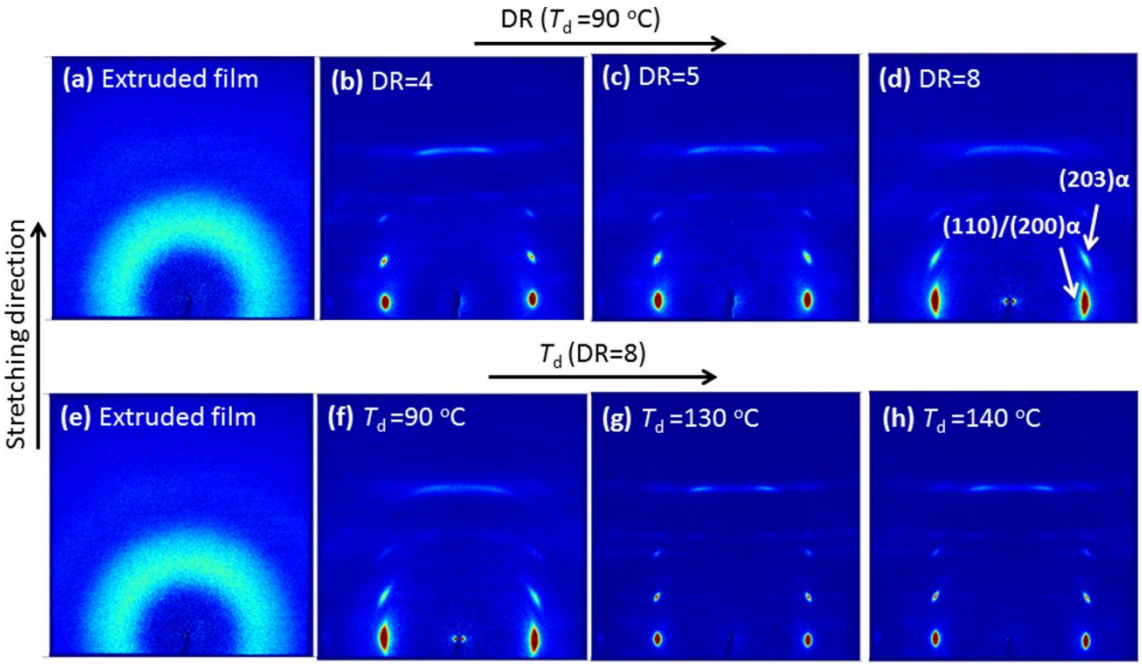

Figure 3.7 2D WAXS patterns of (a, e) as-extruded films, tapes drawn at 90 °C with DR of (b) 4, (c) 5 and (d, f) 8, and PLA tapes drawn at (g) 130 ℃ (DR=8) and (h) 140 ℃ (DR=8).The patterns were recorded with the incident beam perpendicular to the tapes.

Table 3.4 Herman's orientation factors of various PLA tapes obtained by WAXS.

T_d [°C]	**DR**	**Herman's factor (200)/(110)**	**FWHM (200)/(110) [°]**
90	4	0.99	7.4
90	5	0.98	9.4
90	8	0.55	16.3
130	8	0.99	5.3
140	8	0.99	6.2

Figure 3.8 Optical appearance of PLA tapes. From left to right; as-extruded film, tapes drawn at 90 ^{o}C to DR=4, 5 and 8. There is a clear transition from fully transparent to an opaque tape structure at DR > 5.

An 'overdrawing' regime was observed for the tape drawn at 90 ^{o}C to DR=8. It can be seen in Figure 3.8 that tapes drawn at DR=4 and 5 are transparent while the tape drawn at DR=8 is completely opaque due to the development of micro-voids. SEM was also performed in order to explain this phenomenon. As seen in Figure 3.9, the alignment of lamellae stacks can be viewed clearly for tapes drawn at DR=4. Denser packing of lamellae is found in tapes drawn at DR=5. At DR=8, fibrillated structure is observed. Micro-voids align parallel to the drawing direction. Furthermore, wavy striations appear perpendicular to the tape axis. These striations are present not only at the surface of the tape but in the core as well, indicating crystal reassembling. Therefore, the decreased crystalline orientation observed in WAXS may be due to the breakage of the oriented structure in the overdrawing samples. Zhang *et al.* [19] reported that when the drawing temperature is just above T_g (75 ^{o}C), during further stretching of PLA (strain > 100%), voids and cavities appear and develop, together with the breakage of existing crystals.

These wormlike structures have also been observed before in the oriented PP tapes. Schimanski *et al.* [20] found that for PP tapes with DR > 10, an 'overdrawing' regime existed where tapes changed from transparent to opaque. They also observed that the crystal orientation increased rapidly with increasing DR at first, but started to decrease for DR > 10. They explained this phenomenon by the fibrillated structure in the overdrawing regime, in which high density regions are parallel aligned to the drawing direction and separated by low-density regions. Alcock [21] pointed out that the production of overdrawn tapes is not common in industry, since overdrawing is associated with increased fibre breakage during manufacturing.

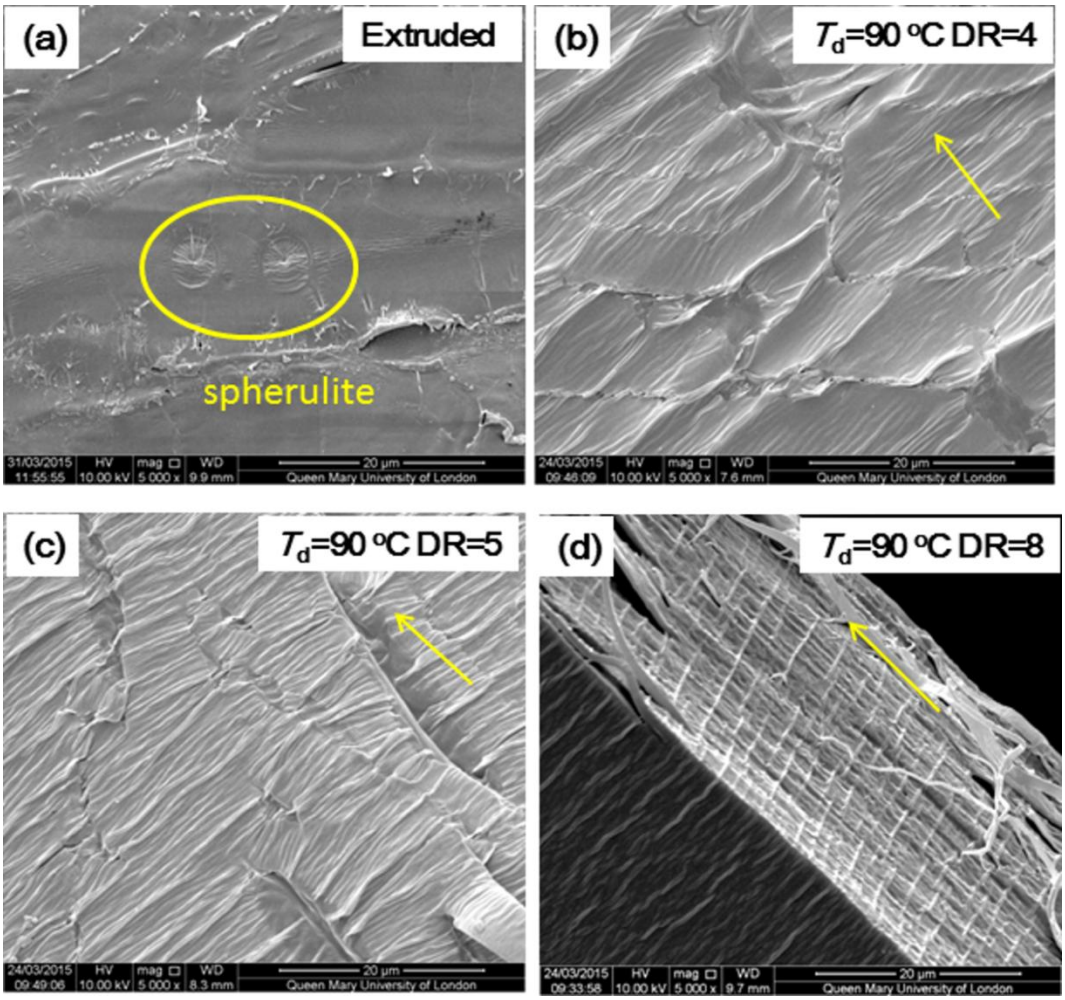

Figure 3.9 SEM cross-section images of (a) as-extruded films and tapes drawn at 90 ^{o}C

with (b) DR=4, (c) DR=5, and (d) DR=8. Arrows indicate the stretching directions.

It should be noted that the arcs transform into spots with increasing T_d, demonstrating an increase in orientation of the crystalline phase. Therefore, the improved modulus and strength with T_d can be attributed to both an increase in crystallinity as well as orientation of the crystalline phase.

3.3.4 Degradation behaviour of oriented PLA tapes

In previous works [11], the authors reported extensively on the thermal degradation of PLA after melt processing. This degradation is attributed to ester group cleavage, as a consequence of the hydrolytic process at the high temperature of melt processing in the presence of residual water. In present work, PLA extruded films produced by melt processing showed a reduction of M_n by about 28%, from 133,500 g mol^{-1} of pellets to about 96,100 g mol^{-1} for as-extruded films. Eling *et al.* [14] produced fibres in which degradation was no higher than 40%. Fambri *et al.* [22] reported a molar mass degradation of more than 60% after melt spinning, but this result can be attributed more to shear stress effects due to long residence time (10 min).

It has been found that the degradability of PLA can be modified significantly by changing the microstructure of the polymer. Figure 3.10 presents the GPC results of undrawn and drawn PLA tapes before and after degradation in two mediums at 50 ^{o}C. The results show that drawing has a significant effect on the hydrolytic degradation. In both medium, the extent of degradation was lower for drawn tapes than for as-extruded films. For example, after degradation for 4 weeks in water, the molecular weight of the tape with DR=8 is about twice that of isotropic films. It is well-known that the degradation of semi-crystalline polymers first occurs in the amorphous phase and then

in the crystalline regions, and therefore, our observation should be expected. This is also consistent with results reported by others [1].

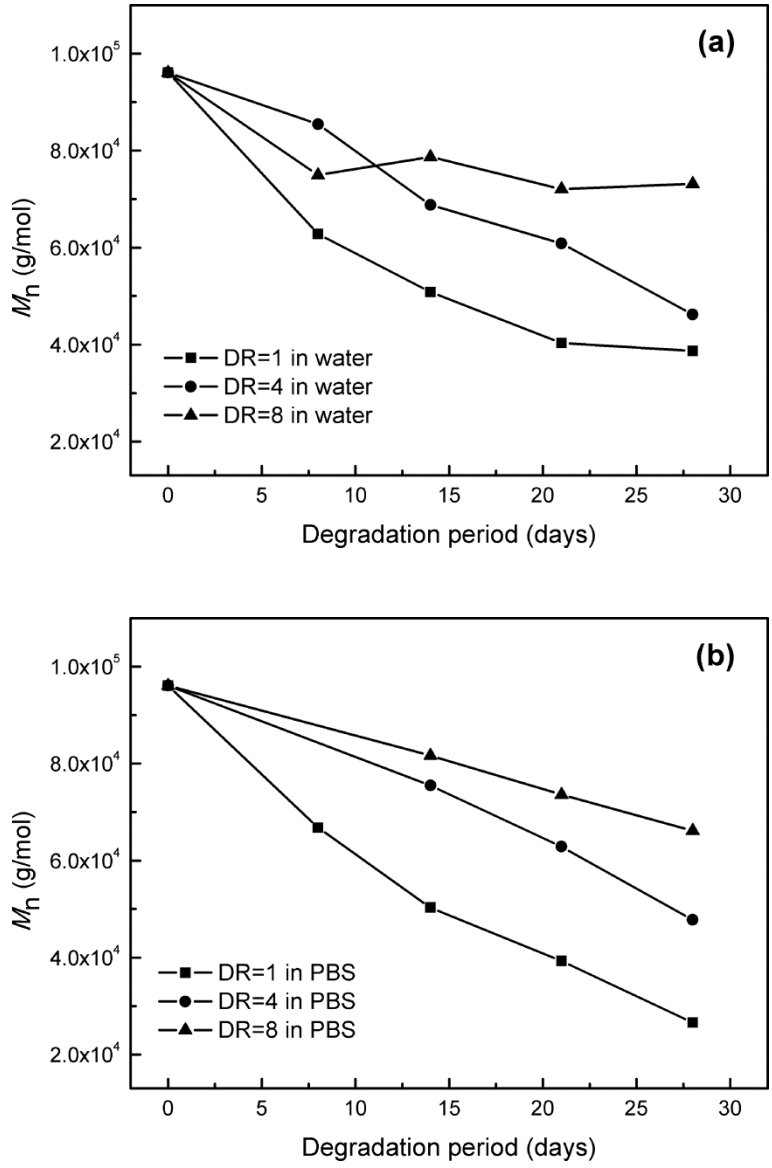

Figure 3.10 Residual molecular weights of PLA as-extruded and drawn tapes before and after degradation in (a) water and (b) PBS.

It is not easy to completely analyse how the microstructure affects the hydrolytic degradation of PLA because the crystallinity as well as the molecular orientation changes with the draw ratio. Rangari and Vasanthan [1] suggest that the crystallinity

plays a dominant role in determining the extent of degradation relative to the molecular orientation. The study of PLA degradation will be discussed in details in Chapter 7.

In summary, solid-state drawing has a significant effect on the hydrolytic degradation behaviour of PLA due to the morphological changes. Therefore, it can be useful for tailoring the degradability of PLA products.

3.4. Conclusions

The drawing conditions of PLA determine the morphology of the polymer, and through this control their mechanical properties and degradation profile. Both draw ratio and drawing temperature play an important role in the polymer morphology and resulting properties. An increase in modulus and strength is seen with increasing draw ratio, due to the strain-induced crystallization and orientation. Drawing at higher temperatures increases the modulus and strength further, which accounts for the improved orientation and crystallinity. More importantly, a large increase in toughness was observed with drawing, which is highly relevant for numerous PLA applications. α-form crystal were observed in all tapes.

3.5 References

1. D. Rangari, and N. Vasanthan, *Study of strain-induced crystallization and enzymatic degradation of drawn poly(l-lactic acid)(PLLA) Films.* Macromolecules, 2012. **45**(18): p. 7397-7403.
2. D. W. Grijpma, and A. J. Pennings, *(Co)polymers of L-lactide, 2 Mechanical properties.* Macromolecular Chemistry and Physics, 2003. **195**(5): p. 1649-1663.
3. M. O. Oh, and S. H. Kim, *Conformational development of polylactide films induced by uniaxial drawing.* Polymer International, 2014. **63**(7): p. 1247-1253.
4. B. Gupta, N. Revagade, N. Anjum, B. Atthoff, and J. Hilborn, *Preparation of poly(lactic acid) fibre by dry-jet-wet-spinning. I. Influence of draw ratio on fibre properties.* Journal of Applied Polymer Science, 2006. **100** (2): p. 1239-1246.
5. T. Schimanski, T. Peijs, P. J. Lemstra, and J. Loos, *Influence of postdrawing temperature on*

mechanical properties of melt-spun isotactic polypropylene. Macromolecules, 2004. **37**(5): p. 1810-1815.

6. D. W. Grijpma, H. Altpeter, M. J. Bevis, and J. Feijen, *Improvement of the mechanical properties of poly (D, L ‐ lactide) by orientation.* Polymer International, 2002. **51**(10): p. 845-851.
7. B. Alcock, and T. Peijs, *Technology and development of self-reinforced polymer composites*, in *Polymer composites–polyolefin fractionation–polymeric peptidomimetics–collagens*. 2013, Springer. p. 1-76.
8. T. Nishino, M. Tanaka, and K. Nakamae, *Elastic moduli of the crystalline regions of biodegradable polymers.* Polymer Preprints Japan-English Edition, 2000. **49**(1): p. E 316-E 316.
9. B. Crist, *The ultimate strength and stiffness of polymers.* Annual Review of Materials Science, 1995. **25**(1): p. 295-323.
10. S. H. Hyon, K. Jamshidi, and Y. Ikada, *Melt spinning of poly-L-lactide and hydrolysis of the fibre in vitro*, in *Polymers as biomaterials*. 1984, Springer. p. 51-65.
11. B. Gupta, N. Revagade, and J. Hilborn, *Poly(lactic acid) fibre: an overview.* Progress in Polymer Science, 2007. **32**(4): p. 455-482.
12. N. M. Barkoula, T. Peijs, T. Schimanski, and J. Loos, *Processing of single polymer composites using the concept of constrained fibres.* Polymer Composites, 2005. **26**(1): p. 114-120.
13. B. Kalb, and A. Pennings, *General crystallization behaviour of poly(L-lactic acid).* Polymer, 1980. **21**(6): p. 607-612.
14. B. Eling, S. Gogolewski, and A. Pennings, *Biodegradable materials of poly(l-lactic acid): 1. Melt-spun and solution-spun fibres.* Polymer, 1982. **23**(11): p. 1587-1593.
15. J. Leenslag, and A. Pennings, *High-strength poly(l-lactide) fibres by a dry-spinning/hot-drawing process.* Polymer, 1987. **28**(10): p. 1695-1702.
16. W. Hoogsteen, A. Postema, A. Pennings, G. Ten Brinke, and P. Zugenmaier, *Crystal structure, conformation and morphology of solution-spun poly (L-lactide) fibres.* Macromolecules, 1990. **23**(2): p. 634-642.
17. D. Sawai, K. Takahashi, A. Sasashige, T. Kanamoto, and S. H. Hyon, *Preparation of oriented β-form poly (l-lactic acid) by solid-state coextrusion: effect of extrusion variables.* Macromolecules, 2003. **36**(10): p. 3601-3605.
18. D. Cohn, and H. Younes, *Biodegradable PEO/PLA block copolymers.* Journal of Biomedical Materials Research, 1988. **22**(11): p. 993-1009.
19. X. Zhang, K. Schneider, G. Liu, J. Chen, K. Brüning, D. Wang, and M. Stamm, *Structure variation of tensile-deformed amorphous poly(L-lactic acid): Effects of deformation rate and strain.* Polymer, 2011**. 52**(18)*:* p. 4141-4149.
20. T. Schimanski, J. Loos, T. Peijs, B. Alcock, and P. J. Lemstra, *On the overdrawing of melt-spun isotactic polypropylene tapes.* Journal of Applied Polymer Science, 2007. **103**(5): p. 2920-2931.
21. B. Alcock, *Single polymer composites based on polypropylene: processing and properties*, 2004, Queen Mary, University of London.
22. L. Fambri, A. Pegoretti, R. Fenner, S. Incardona, and C. Migliaresi, *Biodegradable fibres of poly(L-lactic acid) produced by melt spinning.* Polymer, 1997. **38**(1): p. 79-85.

Chapter 4.

Manufacturing and properties of SR-PLA composites

4.1 Introduction

In the previous chapter, highly oriented poly(lactic acid) (PLA) tapes with good mechanical properties have been developed. In order to consolidate these tapes into SR-PLA composite, a PLA matrix with a lower melting point than the PLA oriented tapes, will be used to bond the tapes together using a film-stacking technique into a 'brick-and-mortar' structure. During consolidation, the matrix layers are selectively melted to weld the PLA tapes together to form a composite structure. The optimization of interfacial bonding between tape and matrix film is crucial to the performance of SR-PLA composites. For this, appropriate compaction conditions that ensure sufficient fusion bonding need to be determined. In this chapter, the effect of compaction temperatures, pressure and corona surface treatment on the interfacial properties were investigated first.

Once optimal interfacial properties are defined, an investigation of the basic mechanical properties and heat resistance of SR-PLA composites is carried out. As reviewed in Chapter 2, to date, SR-PLA composites have been studied mainly for clinical use rather than engineering applications. Until now, impact behaviour and HDT of SR-PLA composites, which both limit the majority of applications of PLA, have not been studied. In this chapter, interfacial, mechanical and thermal properties of resulting SR-PLA

composites are reported.

4.2 Experimental

4.2.1 Materials

NatureWorks® Ingeo™ PLA 4032D and 3051D were used for the reinforcing tapes and matrix phase, respectively. Both grades are poly(L-lactic acid) (PLLA). Unless otherwise specified, PLA in this chapter always refer to PLLA. The weight average molecular weight (M_w) of PLA 4032D and 3051D are 133,500 and 72,633 g mol^{-1} respectively, as determined by means of gel permeation chromatograph (GPC) in chloroform with an AGILENT Technologies 1200 series, equipped with 2 x Agilent PLgel Mixed D column and a pre-column. The melting temperature (T_m) of the PLAs used are approximately 169 °C for the oriented tapes and 154 °C for the matrix phase, as measured by differential scanning calorimetry (DSC) (see Figure 4.1).

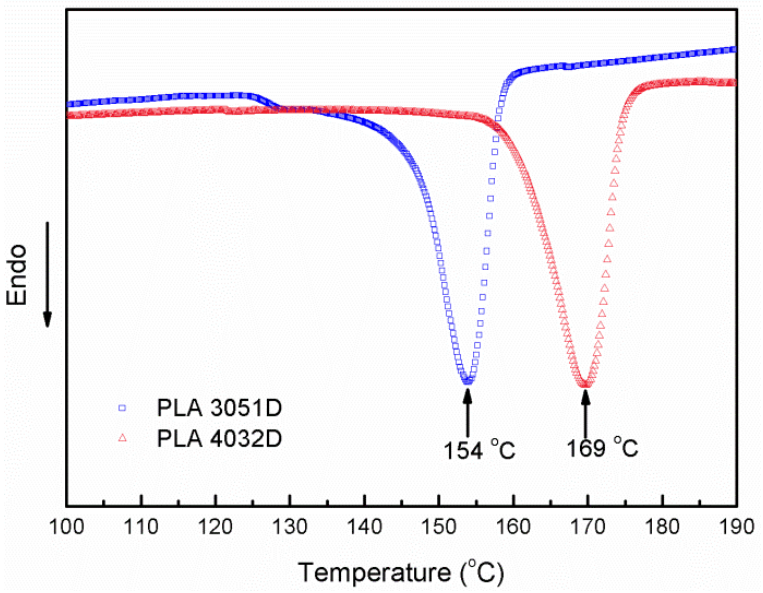

Figure 4.1 DSC melting endotherms of PLA pellets used for tape and matrix.

4.2.2 Manufacture of SR-PLA composites

Since the compaction process requires the heating of tapes, it is crucial to determine how these tapes behave at elevated temperatures. Upon heating there will be significant relaxation of the polymer molecules that have been oriented in the solid-state drawing process, leading to a decrease in mechanical properties. To assess the 'free' shrinkage of PLA tapes with no external pressure applied, sets of five 10 cm long tapes were heated to different temperatures in an oven. Preliminary tests showed that for all temperatures, shrinkage increases with time. For each temperature, a plateau value of shrinkage was reached after 60 min. All free shrinkage measurements were performed by placing tapes in an oven, allowing the oven to equilibrate to required temperature, and then holding for 60 min. Total shrinkage is defined as fraction of initial sample length remaining after exposure to elevated temperature.

Figure 4.2 represents the shrinkage as a function of draw ratio, for various discrete oven temperatures. From this graph, it is clear that there is an increase in free shrinkage with increasing draw ratio and temperature, which is detrimental for mechanical performances. The polymer molecules have been highly oriented by solid-state drawing (see Chapter 3), and upon heating there will be significant relaxation and a decrease in mechanical properties. In order to limit shrinkage during processing at elevated temperature, the tapes are pre-tensioned, and pressure is applied while heating. It was reported that a shift of about 10 ^{o}C in T_m for constrained and unconstrained fibres could be measured in the case of PE, PET and PA6, while shift greater than 20 ^{o}C can be obtained in PP fibres [1]. Therefore, it might be expected that constraining the tapes can also further expand the temperature processing window of hot compacted SR-PLA.

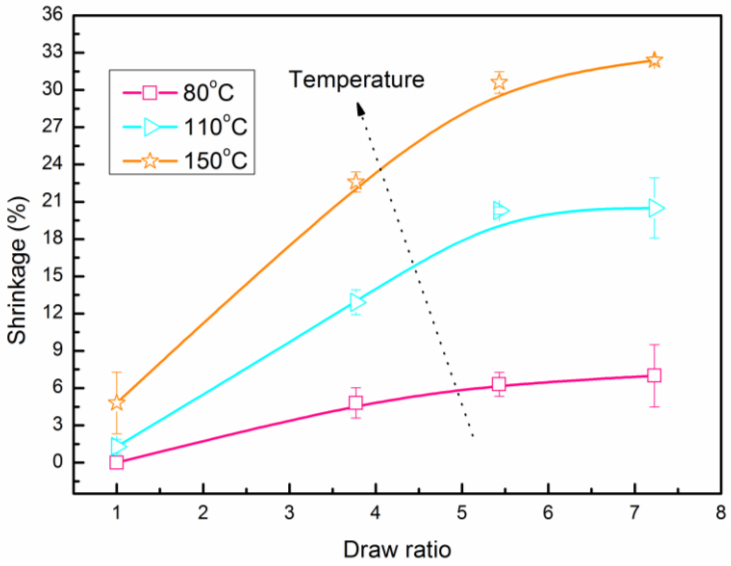

Figure 4.2 Tape free shrinkage vs. draw ratio (tape post-drawn at 90 °C) at elevated temperature.

Unidirectional (UD) and bi-directional (BD) laminates with a thickness of ~ 1.6 mm (67 vol.% of tape) were manufactured by stacking in a $[0]_{20}$ or $[0, 90]_{5s}$ lay-up configuration in a mould. Here the number in between brackets indicates the tape orientation within each layer, while the number layers of repeating groups are indicated by the subscript. To avoid coupling effects, the cross-ply laminate were made symmetric, which means that the laminate is mirrored around the mid-plane. Possible symmetric arrangements for the BD laminates are shown in Figure 4.3a. Laminates were produced at a compaction pressure of 2.5 MPa and a temperature of 150 or 160 °C (Figure 4.3b). The entire cycle from insertion of the mould into the press until removal of the consolidated laminate took approximately 30 min. All test specimens were then cut from the laminates using a band saw to the required dimensions.

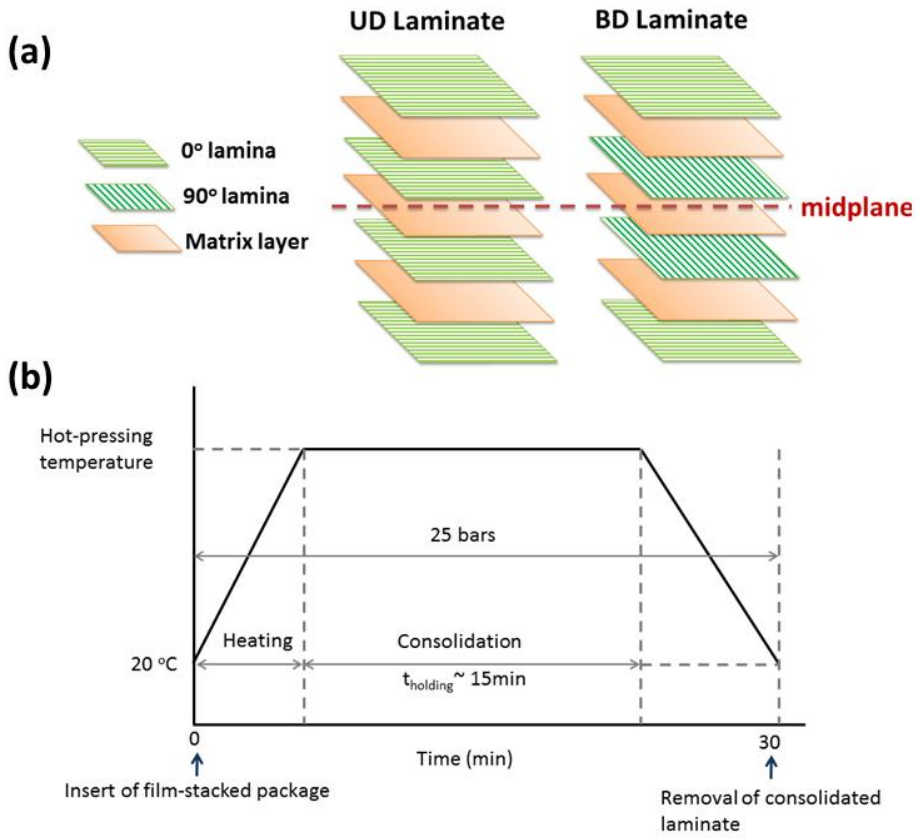

Figure 4.3 (a) Symmetric lay-up of SR-PLA laminates; (b) Time-temperature and time-pressure profiles during consolidation.

4.2.3 Corona treatment of PLA tapes and matrix

Corona treatment is widely used to increase the surface energy, wettability, and adhesion characteristics by introducing polar groups onto polymeric surfaces [2]. In this work, both reinforcing tapes and matrix films were corona treated at ambient temperature in air using a BD-20AC Laboratory Corona Treater. The electrode power was 30 W for a treatment time of 2 min. The surface area of the electrode and the gap distance were 1.4 × 7.0 cm, and approximately 1 cm, respectively.

4.2.4 Characterization

DSC was conducted on Mettler-Toledo 822e. All samples were heated to 200 ^{o}C at 10 ^{o}C min^{-1} under a N_2 atmosphere.

Tensile tests were performed using an Instron 5586 at room temperature, equipped with a 10 kN load cell at a crosshead speed of 8mm/min. UD and BD specimens were loaded at $\theta = 0^{o}$ and $\theta = 0^{o}/90^{o}$, respectively, where θ is defined as the angle between the tape direction and loading direction. Aluminium tabs were adhesively bonded to the specimens to prevent clamp failure. The reported values were calculated as averages over six specimens.

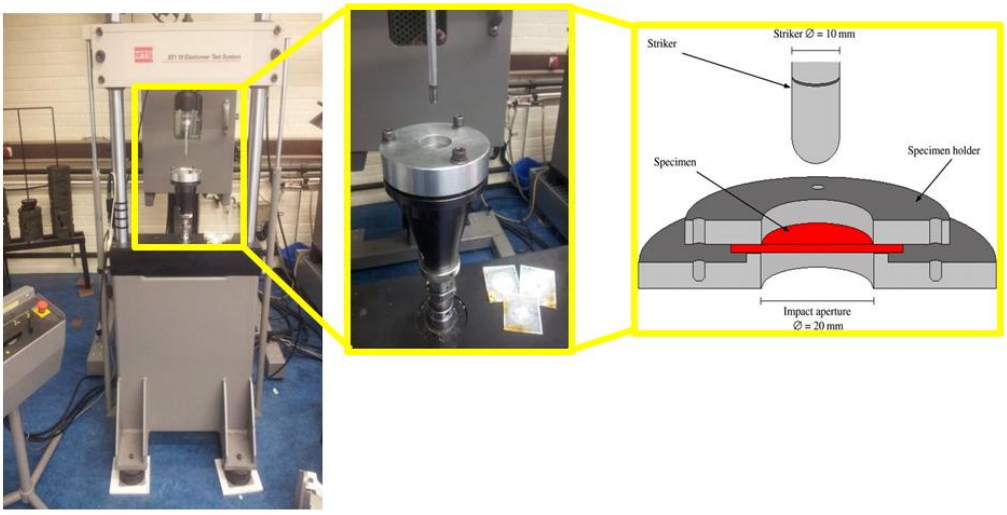

Figure 4.4 Image of dart impact test set-up showing servo-hydraulic tester, impact striker, specimen and specimen holder.

Impact performance of BD laminates was measured using a penetrating dart test on a Zwick Rel tensile machine, as seen in Figure 4.4. Laminates (60 × 60 mm) were clamped between two plates with an internal diameter of 20 mm. A hemispherical dart with a diameter of 10 mm was used and impact energies were obtained by recording the

load-time curve during penetration. The constant speed during penetration was 1 m s^{-1}.

ASTM Standard D648 defines the HDT at which the test bar deflects by 0.25 mm. A constant load of 1.83 MPa was applied at the mid-point of a 3-point bending sample. A Q800 dynamic mechanical analyser (DMA) from TA Instruments was used for determining HDT. For the test to be valid under the ASTM conditions, the smaller DMA sample must deform to the same strain induced in the sample at a load of 1.83 MPa as that in ASTM sample. Therefore, first the sample dimensions as well as applied load for testing on DMA Q800 were calculated as described in [3]. The clamp with 50 mm span was used for 3-point bending test. The sample was heated at the rate of 2 ^{o}C min^{-1} from -10 to 170 ^{o}C. The sample displacement was recorded as a function of temperature.

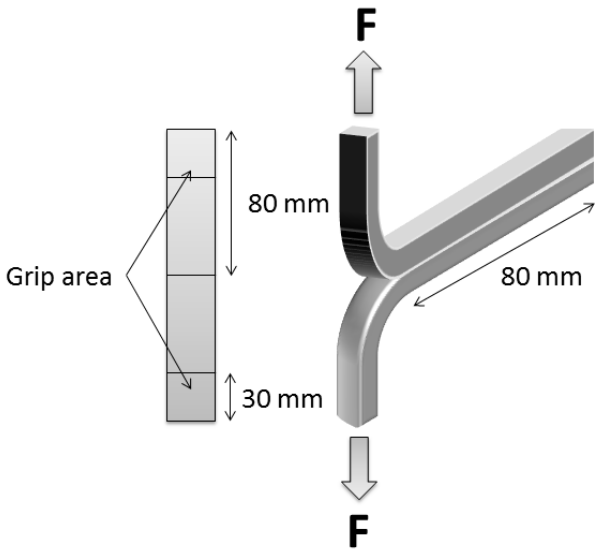

Figure 4.5 Geometry and schematic of the T-peel sample.

To suitably determine the bonding characteristics of a wide range of different tapes, T-peel tests (Mode I failure) was performed (Figure 4.5). Teflon film was used at the mid-plane between tape and matrix film to create an unbounded region. The specimens were peeled along the tape direction in a universal tensile machine equipped with a 100

N load cell at a cross-head speed of 150 mm min^{-1}. The peeling force is defined as a force per unit width.

4.3 Results and discussion

4.3.1 Tailoring the interfacial properties of SR-PLA composites

The optimization of interfacial bonding between tape and matrix film is crucial to the performance of SR-PLA composites. For this, appropriate compaction conditions that ensure good levels of fusion bonding need to be determined. The effect of compaction temperatures, pressure and corona surface treatment on peel strength was investigated and plotted Figure 4.6.

As seen in Figure 4.6b, the peel strength increases with compaction temperature. At 150 ^{o}C, good fusion bonding is not yet achieved, as the compression moulded sample could be easily peeled apart by hands. A dramatic increase in peeling strength is observed for a temperature of 160 ^{o}C or above. A compaction temperature of 170 ^{o}C leads to a peel force of 0.95 N mm^{-1}, 10 times higher than the peel force achieved at 150 ^{o}C. This is because T_m of the matrix is around 155 ^{o}C as measured by DSC and at 170 ^{o}C the matrix is fully melted, which results in strong bonding. Figure 4.6a shows photographs of peel surfaces of samples compacted at different temperatures. For poorly bonded sample, compacted at 150 ^{o}C and 0.3 MPa, the surface is smooth, while for well bonded sample, compacted at 170 ^{o}C and 0.3 MPa, fibrillation is evident, indicating cohesive failure within the oriented tape.

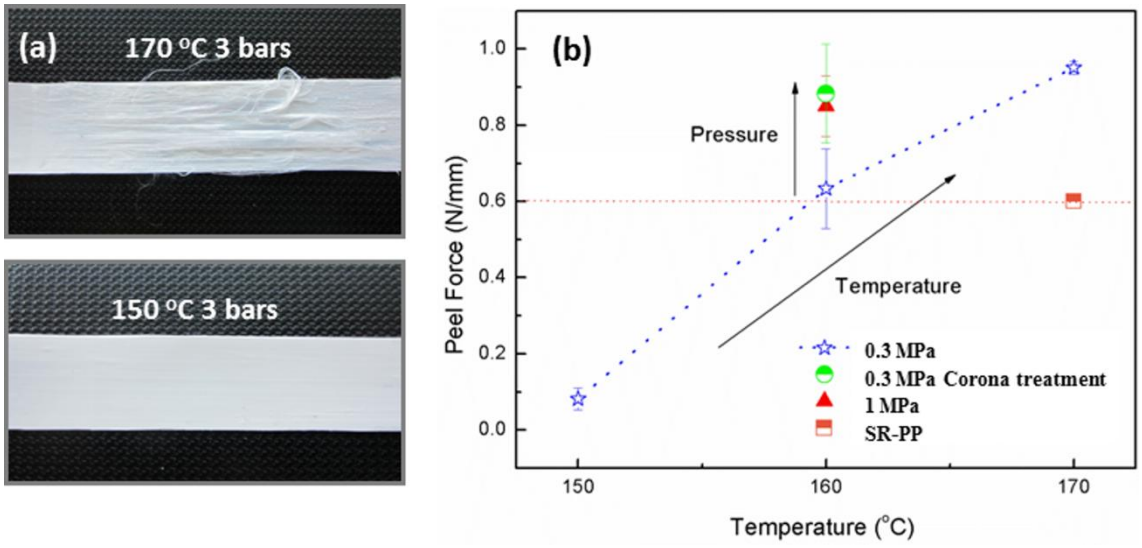

Figure 4.6 (a) Photographs of peel surfaces; (b) Average peel force as a function of compaction temperature for tapes compacted under different conditions.

Apart from temperature, pressure has also a significant effect on the bonding. For a moulding temperature of 160 ^{o}C, the peel force reaches 0.85 N mm^{-1} when the applied pressure is 1 MPa. Corona treatment of both tape and matrix is also used to improve the welding property. At the same compaction temperature of 160 ^{o}C and pressure of 0.3 MPa, peel force increases from 0.63 N mm^{-1} to 0.88 N mm^{-1} with corona treatment. Although the increment is significant, it may not justify the implementation in an industrial environment because it would add cost. Furthermore, equivalent levels of adhesive bonding can be achieved by simply adapting pressure and temperature during hot-pressing.

The sample processed at 160 ^{o}C and 10 bars shows a slightly lower peel force compared to that of 170 ^{o}C and 3 bars, but experience less relaxation during hot-pressing, permitting maximum retention of tape properties. Hence, increasing pressure rather than temperature appears to be favourable for optimizing overall performance of SR-PLA

composites.

4.3.2 Tensile properties of SR-PLA composites

So far PLA tape with good mechanical and interfacial properties have been obtained by optimizing solid-state drawing parameters and consolidation conditions. The mechanical properties of actual SR-PLA composites are investigated in the following section.

Figure 4.7 compares the mechanical properties of PLA tape and unidirectional (UD) and bi-directional (BD) SR-PLA composites obtained in present work with commercial PLA based composites as well as oriented PP and SR-PP composites. Compared to isotropic PLA, the modulus and strength of UD SR-PLA laminate consolidated at 160 ^{o}C increases to 4.4 GPa and 102 MPa, which is an improvement of about 144% and 92%, respectively. Still these values are lower than those of PLA tapes. SR-PLA composites consisting of amorphous sheets as matrix and commercial grade Ingeo^{TM} PLA yarns and fabrics from NatureWorks® were prepared by Li *et al.* [4]. For UD SR-PLA composites with 25 wt.% yarns, a Young's modulus of 3.7 GPa and tensile strength of 58.6 MPa were reported. In our work, the Young's modulus (6.7 GPa) and tensile strength (278 MPa) of the reinforcement tapes are considerably higher than those of the PLA yarns (1.1 GPa and 133 MPa) used in their work. Moreover, higher reinforcement content was achieved due to the tape geometry that allows for a 'brick-and-mortar' composite morphology, leading to higher tensile properties. Particularly the tensile strength of the current SR-PLA composites compares very favourably with other SR-PLA composites, with tensile strength nearly twice than that of SR-PLA based on Ingeo^{TM} yarns [4].

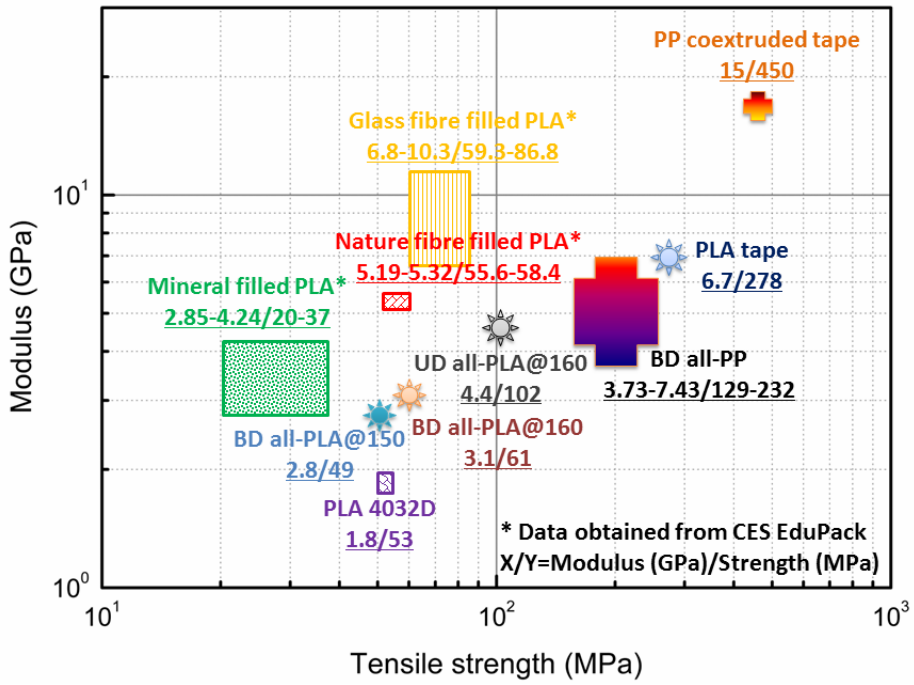

Figure 4.7 Comparison of mechanical property for PLA tape and UD SR-PLA composites, together with commercial thermoplastic composites.

As seen in Figure 4.7, UD SR-PLA composites show better tensile strength and Young's modulus than BD SR-PLA composites compacted at the same temperature. Since an oriented PLA tape will work most effectively when loaded along its axis, composites containing continuous unidirectional tapes show as expected the highest tensile strength and modulus. For a bidirectional laminate, only 50% tapes are effectively loaded due to the cross-ply configuration, with the modulus of the laminate now being the weighted sum of the longitudinal modulus and transverse tape modulus.

Two compaction temperatures were used to prepare BD SR-PLA laminates, but with only little effect on tensile modulus and strength. The slightly increase in tensile properties at high compaction temperatures is due to the increased interfacial bonding and better load transfer.

Compared to glass fibre or natural fibre reinforced PLA composites, although the modulus of UD SR-PLA sheet is lower, the tensile strength is outstanding and exceeds that of the rest PLA-based composites shown in the figure. Therefore, SR-PLA composites could be of particular interest for products where strength is critical.

4.3.3. Impact properties of SR-PLA composites

The relatively poor impact strength of PLA has prevented a broader field of application of these materials. Composite materials generally perform well under impact loadings due to their combination of high strength and high stiffness, and additional energy absorption mechanisms such as delamination.

Figure 4.8 shows the penetration impact energy absorbed by different composite laminates, normalized for specimen thickness. Clearly, isotropic PLA shows very low energy absorption. On the other hand, SR-PLA composites absorbed significantly more energy compared to isotropic PLA. As shown in Chapter 3, the energy required to break a tape is 12.7 times higher than that of isotropic PLA film. Therefore, the tensile failure of PLA tapes in SR-PLA composites is expected to attribute greatly to the total energy absorption. Moreover, during impact, delamination, fibrillation and tape pull-out are additional processes that can potentially absorb significant amounts of energy. The contributions of some of them will be evaluated below. The energy increases from 0.5 J mm^{-1} for isotropic PLA to 6.8 J mm^{-1} for SR-PLA compacted at 150 ^{o}C, which is nearly a 14 times increase. The peak force increases from 205 N mm^{-1} to 819 N mm^{-1}. Although the value of SR-PLA is lower than that of reported for SR-PP laminates, it is still a remarkable improvement. Furthermore, with increasing compaction temperature of SR-PLA, absorbed impact energy is reduced. Similar effects were reported for SR-PP

composites [5, 6] and are related to the fact that weak interfaces can have positive effects on energy absorption by allowing more delamination and less localization of the impact damage, with greater volume of composite being involved in the energy absorption process. As shown in Figure 4.6, an increase in interfacial strength was observed with increasing compaction temperature. Therefore, higher compaction temperature leads to better interfacial bonding, thus resulting in less delamination and less energy absorption.

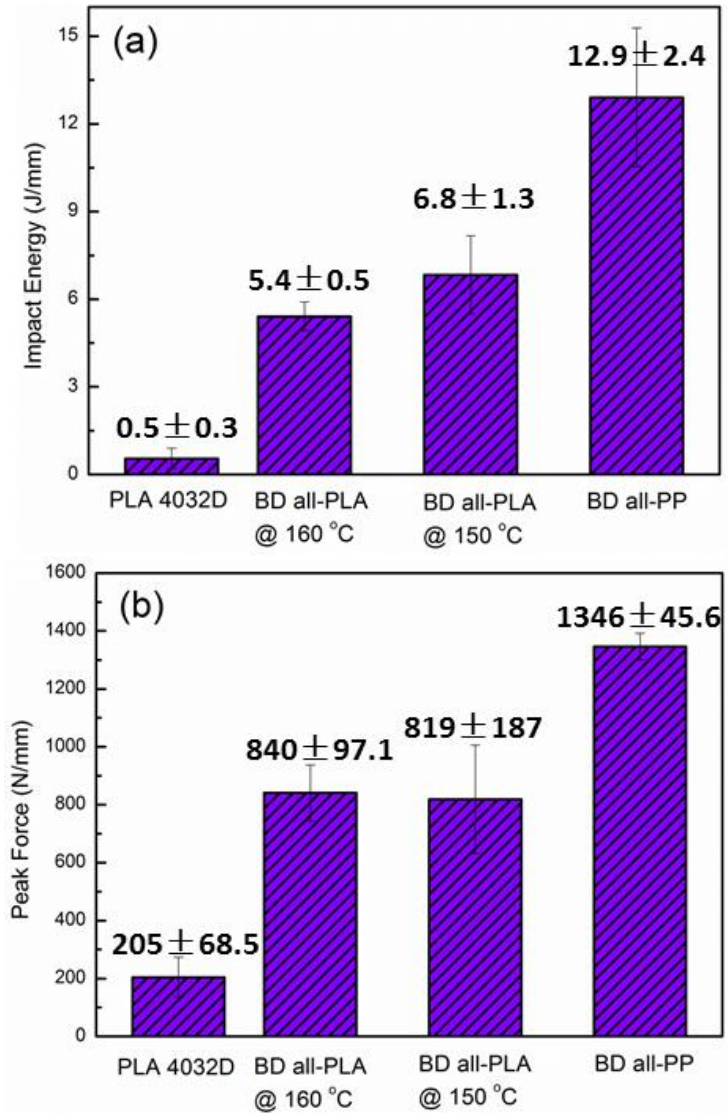

Figure 4.8 Impact energy (a) and peak force (b) normalised for specimen thickness.

By combining the tensile test results with the peel test results on SR-PLA composites, the contribution of the tape failure to the impact resistance of SR-PLA composites can be estimated. Ignoring frictional losses, the energy absorbed upon penetrating impact, E_{total}, can be considered as follows [6]:

$$E_{total} = E_T + E_I \qquad \textit{Equation 4.1}$$

where E_T = energy absorbed by plastic tape deformation, E_I = energy absorbed by interfacial failure. The energy absorbed by tape deformation, E_T, will be dictated by the tensile behaviour of the composite. Since penetration requires tape failure, the energy absorption during impact can be compared to energy absorption during tensile testing of virgin tape and consolidated SR-PLA composites. If the impact load is considered to be solely absorbed by tapes that pass through the impact site, an effective volume of tape which is loaded upon impact can be assumed [7].

The effective tape volume can be modelled by considering the SR-PLA plate as stacked, unconsolidated tapes by ignoring interfacial properties and crimping, and only considering tensile properties of the tape. Alternatively, to account for the effect of tape interactions, crimping, and processing, the tensile properties of bidirectional specimens tested in the 0^o / 90^o direction can be considered [8]. In both cases, the volume loaded in tension can be considered as two rectangular sections running normal to each another with the impact site in the centre (see Figure 4.9). Although the stain rate applied in impact test (6.3×10^{-4} s^{-1}) is smaller than that applied in tensile tests (1.7×10^{-3} s^{-1}), the tensile strength and modulus are relatively consistent over the strain rates [9, 10]. Hence, the absorbed energy is assumed to be similar. Since impact energies are normalized for specimen thickness, the effective tape area, A_{ET}, are considered and given by:

$$A_{ET} = 2abV_f V_f^{'} \qquad \textit{Equation 4.2}$$

where a = striker diameter, 10 mm, b = effective tape length, 60 mm, V_f = volume fraction of tape in composite, and V_f' = volume fraction of effective material in loading direction.

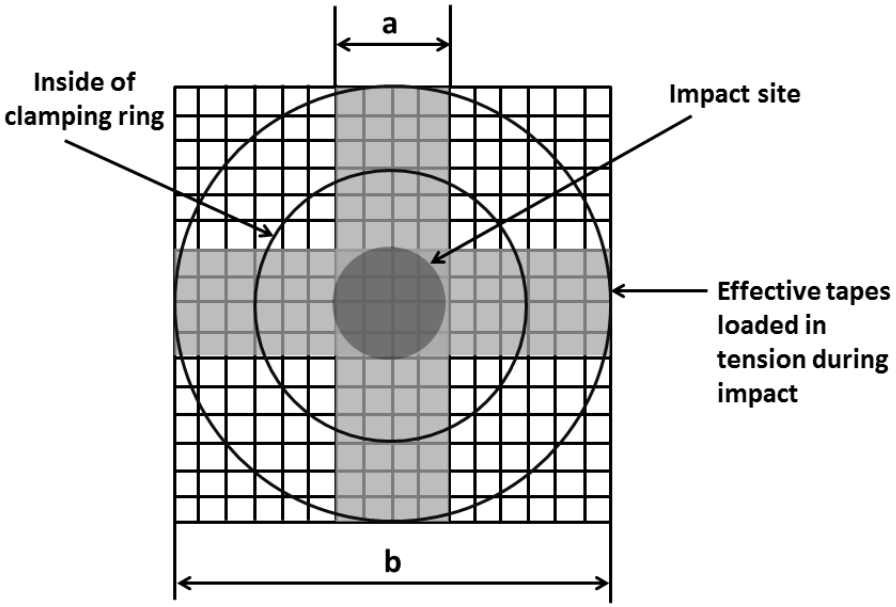

Figure 4.9 Schematic of effective area of tapes loaded in tension during impact (redrawn from [5]).

Table 4.1 lists the energy absorbed by tensile failure of the PLA tape together with the energy absorbed by penetrative impact of BD SR-PLA laminates. It shows that half of the energy absorbed by impact failure of BD SR-PLA compacted at 160 ^{o}C can be attributed to tape failure. On the other hand, the contribution of work of fracture of PLA tape failure decreases to 35% for BD SR-PLA plates compacted at 150 ^{o}C. Since laminates processed at lower temperatures possess lower interfacial strength, more energy is absorbed by other fracture mechanisms such as tape pull-out, debonding, and delamination. Tape pull-out is clearly visible from the out-of-plane deformation of

SR-PLA laminates, as shown in Figure 4.10a.

Table 4.1 Energy absorption mechanism of SR-PLA composites.

Specimen	**Tape**	**BD SR-PLA**	
Compaction temperature [^{o}C]	-	150	160
Absorbed impact energy [J m^{-1}] [1]	-	6.8×10^{3}	5.4×10^{3}
Energy absorbed by tape tensile failure (per unit thickness) [J m^{-3}] [2]	7.5×10^{7}	4.4×10^{6}	5.0×10^{6}
Effective area loaded in tensile [m^{2}] [3]	2.70×10^{-4}	5.39×10^{-4}	5.39×10^{-4}
Effective energy absorbed by tape tensile failure (per unit thickness) [J m^{-1}] [4]	2.03×10^{4}	2.37×10^{3}	2.70×10^{3}
Percentage of energy absorbed by tape failure [5]	-	35%	50%

[1] *Experimentally determined dart impact energy per unit thickness of laminate.*

[2] *Experimentally determined work-to-break from integrated stress-strain curves of tape and laminates.*

[3] *Calculated from Equation 4.2.*

[4] *Calculated by multiplying laminate work-to-break (2) and effective tape area (3).*

[5] *Total impact energy (1) normalized to effective tape work-to-break (4).*

Figure 4.10b shows typical impact penetration damage. Isotropic PLA shows lower, more localized, energy absorption since the deformation is limited to the immediate impact site, unlike the SR-PLA specimen which shows large deformations, large amounts of fibrillation and delamination, and thus high energy absorption.

Only the impact behaviour of BD laminates was studied as dart impact tests in case of UD laminates would lead to failure by transverse splitting and delamination along the

tape direction and subsequent low levels of energy absorption [11].

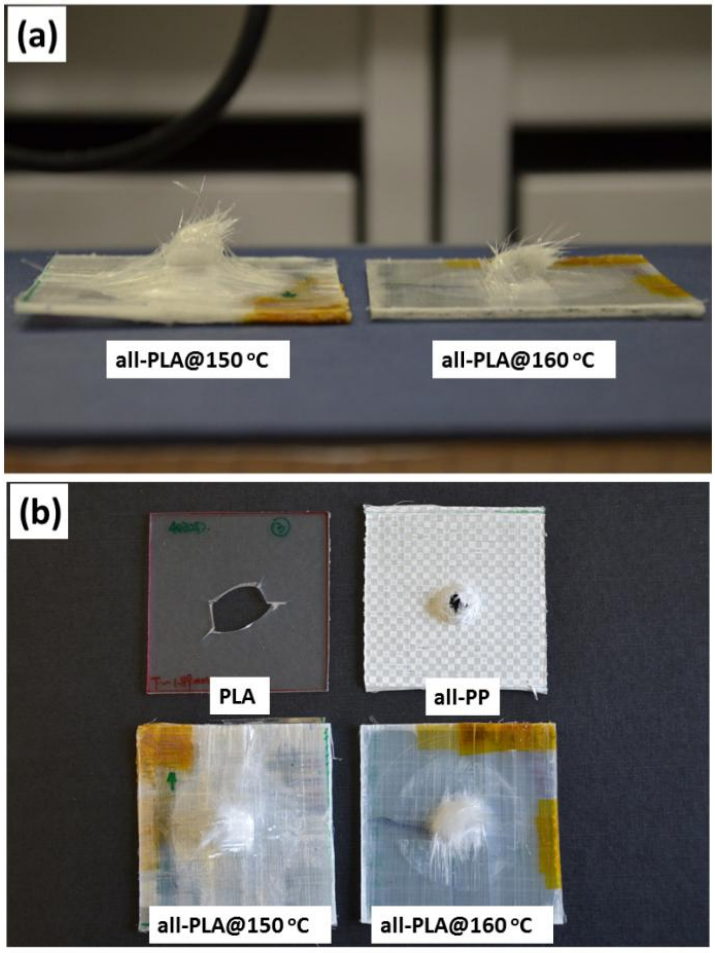

Figure 4.10 (a) Side image of out-of-plane deformation of SR-PLA BD composite laminates. (b) Front image of typical impact penetration damage of different materials.

4.3.4 Heat deflection temperature (HDT)

Apart from its high brittleness, a second limiting property of PLA is its low HDT. One popular strategy is adding plasticising agents or inorganic fillers acting as a nucleating agent. Huda *et al.* [12] reported superior heat-resistance properties of PLA/kenaf fibre composites. The HDT of these natural fibre composites was as high as 174.8 ^{o}C compared to 64.5 ^{o}C of neat PLA. Although the HDT was significantly improved, the

presence of these fibres poses serious concerns with respect to recyclability. Other methods involved heat treatments of samples near the crystallization temperature. Tang *et al.* [13] found a percolation threshold of crystallinity corresponding to HDT. HDT started to increase when the crystallinity exceeds 20%. The neat PLA showed HDT of 52 ^{o}C at 20% crystallinity while 80 ^{o}C at 25% crystallinity after 20 min annealing. It is well known that HDT can also be improved by forming PLA stereocomplex. Nam *et al.* [14] reported that with the addition of 25 wt.% poly($_{D}$-lactic acid) (PDLA), HDT dramatically increased from 56 ^{o}C for PLLA to 110 ^{o}C for stereocomplex PLA.

Table 4.2 The heat deflection temperature (HDT) and corresponding crystallinity (X_c) of the PLA and SR-PLA composites.

Sample	**PLA**	**BD SR-PLA at 150 ^{o}C**	**BD SR-PLA at 160 ^{o}C**	**UD SR-PLA at 160 ^{o}C**
HDT [^{o}C]	57 ±1	67 ±2	66 ±2	83 ±3
$\boldsymbol{X_c}$ **[%]**	8.1	52.3	48.6	48.7

As seen in Table 4.2, the HDT of SR-PLA composites increased compared to that of isotropic PLA. UD SR-PLA compacted at 160 ^{o}C exhibits the highest HDT (~ 83 ^{o}C). This value suggests that the upper service temperature limit for PLA increases with drawing. The improved heat resistance in SR-PLA laminates is mainly derived from the increase in modulus as well as crystallinity. This improvement in HDT for SR-PLA by 26 ^{o}C is useful for many applications and similar to annealed PLA [13], while being slightly below that of stereocomplex PLA [14]. Compared to other plastics, UD SR-PLA composites exhibit a similar HDT as polystyrene (PS) (~ 85 ^{o}C), which is often

used in food packaging, and acrylonitrile butadiene styrene (ABS) (~ 88 ^{o}C). UD SR-PLA composites have a higher HDT than nylon 6 (~ 60 ^{o}C), PP (~ 70 ^{o}C), and PET (~ 65 ^{o}C) [15]. This could open up new markets for PLA bioplastics such as consumer electronics, packaging, vehicle-interior components, and a great deal more.

4.3.5 Prototypes

To illustrate one example of what is possible with SR-PLA composites; Figure 4.11 shows a picture of a football shin pad produced from BD SR-PLA composite. This product shows high impact performance and an attractive textile-like texture. Moreover, combined with its 'green credentials' sports products might be an interesting market. The direct forming route to manufacture the shin pad of SR-PLA composite is to wind the tapes and matrix onto the mould and then place the lay-up into oven, without the need for pre-consolidating. The interfacial strength in the SR-PLA composites is due mainly to the radial forces induced by compressive shrinkage. This is an interesting alternative to stamping of pre-consolidated sheets, as it eliminates an expensive belt-pressing step normally required in the manufacturing of semi-finished sheet products.

Figure 4.11 Football shin pad of Nike Mercurial (left) and the one made of SR-PLA composite (right).

Sandwich panels are a very efficient way of providing high bending stiffness at low weight. The stiff and strong skin facings carry the bending loads, while the core resists shear loads. The principle is the same as a traditional 'I' beam. Since the aim of this research is to produce composite structures in which all phases are PLA, sandwich structures are possible that use SR-PLA composites as a face material and PLA foam as a core material. Again PLA with a lower melting temperature can be used as an adhesive layer to combine the two together. The scheme and a picture of SR-PLA sandwich panel are shown in Figure 4.12. BioFoam® was used as PLA core foam, provided by Synbra Technology bv in Etten-Leur, The Netherlands. The density of PLA foam is 30 kg/m^3. It is isotropic in terms of properties.

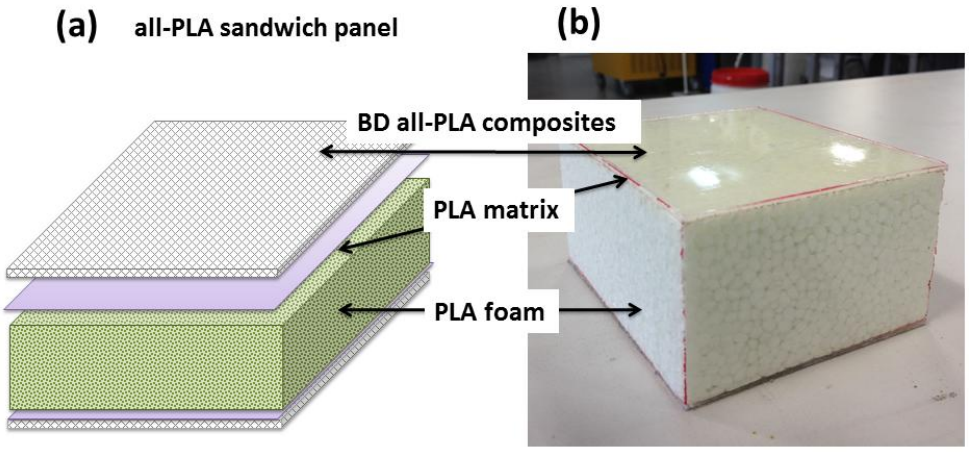

Figure 4.12 (a) Scheme and (b) picture of SR-PLA sandwich panel.

4.4 Conclusions

PLA is considered as one of the most promising bioplastics but exhibits rather limiting heat stability and brittleness in its pristine state. These disadvantages have been overcome by developing SR-PLA composites with enhanced modulus, tensile strength,

impact properties and heat resistance, thus converting high cost raw biobased materials to value adding products. SR-PLA composites exhibit the properties and values to create new market opportunities, together with environmental attributes. It has been shown that it is possible to tailor the mechanical properties of SR-PLA laminates by altering the hot-pressing conditions. Compaction at 160 ^{o}C produced a well bonded structure and SR-PLA composites with good levels of strength and stiffness to make them suitable candidates for semi-structural components. On the other hand, SR-PLA composites consolidated at lower temperature of 150 ^{o}C showed optimal energy absorption, which may find applications that are aimed at protection from low velocity impacts. Moreover, the multiple end-of-life options offered by SR-PLA composites, including recycling and compositing, empowers them to reduce the environmental impact of materials, and gives the end-user maximum flexibility in selecting environmentally sound waste disposal schemes.

4.5 References

1. N. M. Barkoula, T. Peijs, T. Schimanski, and J. Loos, *Processing of single polymer composites using the concept of constrained fibres.* Polymer Composites, 2005. **26**(1): p. 114-120.
2. M. Żenkiewicz, J. Richert, P. Rytlewski, and K. Moraczewski, *Some effects of corona plasma treatment of polylactide/montmorillonite nanocomposite films.* Plasma Processes and Polymers, 2009. **6**(S1): p. S387-S391.
3. S. E. B. Wadud, and R. R. Ullbrich, *Using the DMA Q800 for ASTM International D 648 Deflection Temperature Under Load.*
4. R. Li, and D. Yao, *Preparation of single poly(lactic acid) composites.* Journal of Applied Polymer Science, 2008. **107**(5): p. 2909-2916.
5. B. Alcock, N. O. Cabrera, N. M. Barkoula, and T. Peijs, *Low velocity impact performance of recyclable all-polypropylene composites.* Composites Science and Technology, 2006. **66**(11): p. 1724-1737.
6. B. Alcock, N. O. Cabrera, N. M. Barkoula, Z. Wang, and T. Peijs, *The effect of temperature and strain rate on the impact performance of recyclable all-polypropylene composites.* Composites Part B: Engineering, 2008. **39**(3): p. 537-547.
7. T. Peijs, E. Smets, and L. Govaert, *Strain rate and temperature effects on energy absorption of polyethylene fibres and composites.* Applied Composite Materials, 1994. **1**(1): p. 35-54.

8. B. Alcock, N. O. Cabrera, N. M. Barkoula, A. Spoelstra, J. Loos, and T. Peijs, *The mechanical properties of woven tape all-polypropylene composites.* Composites Part A: Applied Science and Manufacturing, 2007. **38**(1): p. 147-161.

9. B. Alcock, *Single polymer composites based on polypropylene: processing and properties*, 2004, Queen Mary, University of London.

10. C. Norbert, *Recyclable all-polypropylene composites: Concept, properties and manufacturing*, 2004, Technische Universiteit Eindhoven, Netherlands.

11. T. Abraham, S. Wanjale, T. Bárány, J. and Karger-Kocsis, *Tensile mechanical and perforation impact behaviour of all-PP composites containing random PP copolymer as matrix and stretched PP homopolymer as reinforcement: Effect of β nucleation of the matrix.* Composites Part A: Applied Science and Manufacturing, 2009. **40**(5): p. 662-668.

12. M. S. Huda, L. T. Drzal, A. K. Mohanty, and M. Misra, *Effect of fibre surface-treatments on the properties of laminated biocomposites from poly (lactic acid)(PLA) and kenaf fibres.* Composites Science and Technology, 2008. **68**(2): p. 424-432.

13. Z. Tang, C. Zhang, X. Liu, and J. Zhu, *The crystallization behaviour and mechanical properties of polylactic acid in the presence of a crystal nucleating agent.* Journal of Applied Polymer Science, 2012. **125**(2): p. 1108-1115.

14. B. U. Nam, and B. S. Lee, *Toughening of PLA stereocomplex by Impact modifiers.* Journal of the Korea Academia-Industrial Cooperation Society, 2012. **13**(2): p. 919-925.

15. *Heat Deflection Temperature Testing of Plastics*. October 29, 2014; Available from: http://www.matweb.com/reference/deflection-temperature.aspx.

Part II. Multifunctional poly(lactic acid)/carbon nanotube nanocomposites

Chapter 5.

Literature review

In recently years, the increased interest in multifunctional materials is driven by the need for developing new materials that simultaneously perform combined functions. The addition of nanofillers, such as cellulose nanofibrils [1], nanoclays [2], and metallic oxides [3], has received significant interest as a way to improve the properties of PLA. Depending upon the nature and characteristics of the nanoparticles used, the ultimate properties of the resulting nanocomposite can be tailored. Among the various nanofillers, carbon nanotubes (CNTs) have gained great attention and interest as a multifunctional nanomaterial because of their exceptional mechanical, electrical and thermal properties. Also, the high aspect ratio and 1D anisotropic geometry of CNTs makes them especially suitable for polymeric fibre applications.

In this chapter, we first review the structure and fundamental properties of carbon nanotubes. Next, the mechanical reinforcements of various CNT-based composites by different techniques are critically analyzed and compared. Lastly, the electrical percolation behaviour of CNT-based composite and their potential use as macroscopic sensors are highlighted. This review is not intended to be comprehensive, as our focus is on exploiting the exceptional mechanical and electrical properties of carbon nanotubes toward the development of multifunctional materials. More reviews can be found in the literatures. For example, Thostenson *et al.* [4] and Chou *et al.* [5] reviewed recent

advances related to the science and technology of carbon nanotubes and their composites; Breuer and Sundararaj [6] reviewed recent studies on polymer/carbon nanotube composites; Li *et al.* [7] surveyed the recent advances related to the use of carbon nanotubes and their composites as sensors and actuators, while Gibson *et al.* [8] reviewed recent publications dealing with vibrations of carbon nanotubes and their composites.

5.1 Carbon nanotubes

5.1.1 Atomic structure and morphology of carbon nanotube

Nanotube properties are highly dependent on chirality, size, morphology, and nanostructure. The atomic structure of nanotubes can be described in terms of chiral vector: $\vec{c}_h = n\vec{a}_1 + m\vec{a}_2$, as shown in Figure 5.1. Where (*n*, *m*) are integers, and $\vec{a}_1$ and $\vec{a}_2$ are unit vectors. Nanotubes with $n = m$ are called armchair tubes (chiral angle of 30^o), and nanotubes with $m = 0$ are known as zigzag tubes (chiral angles are 0^o). For any other values of *n* and *m* the tubes are chiral tubes.

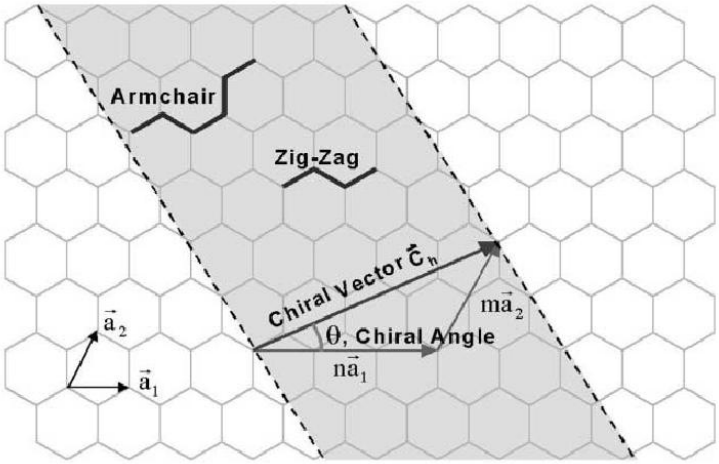

Figure 5.1 Schematic diagram showing how a hexagonal sheet of graphite is 'rolled' to form a carbon nanotube [4].

Depending on chirality, carbon nanotubes can either be conducting or semi-conducting. Wei *et al.* [9] demonstrated that multi-walled carbon nanotubes can carry an electric current density greater than 10^9 A cm^{-2}, which is more than 1,000 times greater than copper; hence these novel electrical properties have generated substantial interest in utilizing carbon nanotubes in nanoelectronics [10]. Investigations on the influence of chirality on the mechanical properties have also been reported. The analytical work of Yakobson *et al.* [11, 12] found that the chirality has a relatively small influence on the elastic stiffness.

CNTs can be broadly classified into two categories: single-walled nanotubes (SWNTs) and multi-walled nanotubes (MWNTs) (see Figure 5.2). A SWNT can be schematically considered as a rolled graphene sheet forming a hollow tube. A MWNT is composed of concentric single-walled tubes, which are held together by van der Waals bonding. SWNTs, in theory, are more desirable for creating high performance nanocomposites as the poor intratube interactions in MWNTs can result in minimal load transfer between the layers through shear. In fact, when nanotubes are embedded in a polymer, effective stress transfer may potentially only be achieved through their outer walls [13]. Furthermore, when considering the effective properties of MWNTs in nanocomposites, the entire cross-sectional area of the nanotubes should be taken into consideration, hence compromising the effective properties for MWNTs [14].

5.1.2 Properties of carbon nanotubes

The general properties of CNTs have been discussed in a number of publications. In this chapter, we will only discuss their mechanical and electrical properties.

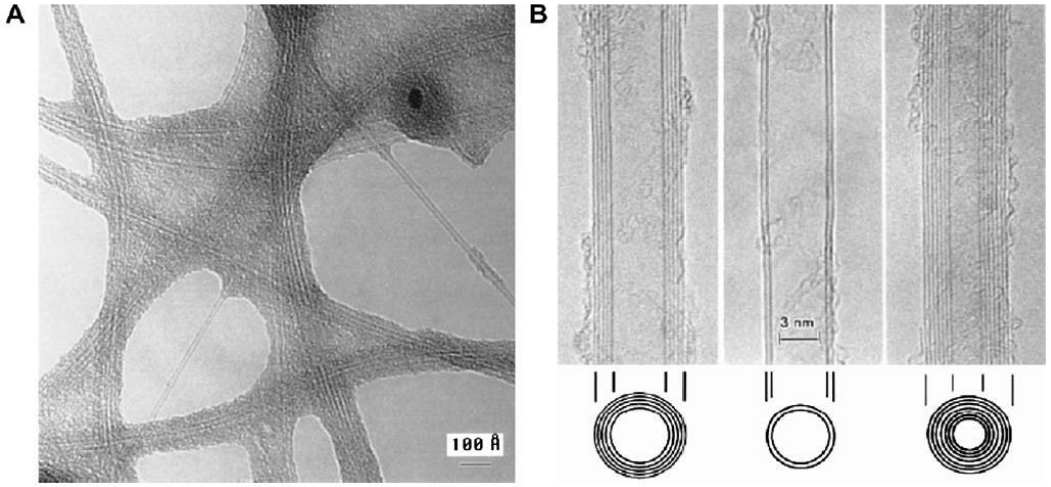

Figure 5.2 TEM images of different CNTs (A: SWCNTs; B: MWCNTs with different layers of 5, 2 and 7) [15].

Mechanical properties of CNTs

Since carbon-carbon covalent bonds are among the strongest atomic bonds in nature, when CNTs were discovered, their structure immediately encouraged speculation about their potential mechanical properties. The mechanical properties of CNTs have been extensively studied both experimentally and theoretically.

The first direct measurement was made by Wong *et al.* in 1997 [16]. They used atomic force microscopy (AFM) to measure the stiffness constant of arc-MWNTs pinned at one end, which gave an average Young's modulus of 1.28 TPa. More importantly, they also made the first strength measurements, obtaining an average bending strength of 14 GPa. Salvetat *et al.* also used AFM to bend an arc-MWNT that had been pinned at each end over a hole [17], obtaining an average modulus of 0.81 TPa (Figure 5.3).

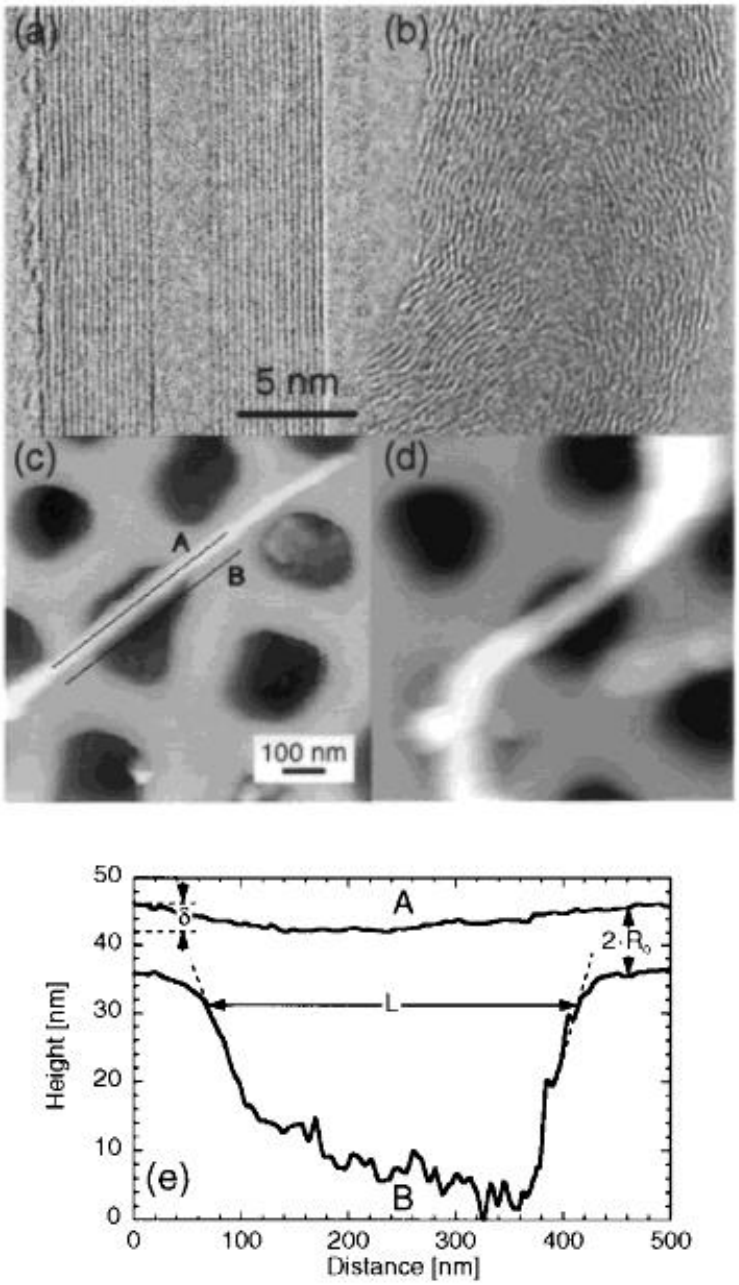

Figure 5.3 (a,b) TEM images of typical nanotubes. (c,d) AFM images of nanotubes adhered on a polished ultrafiltration alumina membrane with a portion bridging a pore of the membrane. (a,c) For an arc-discharge MWNT; (b,d) for a catalytic MWNT. (e) Cross-section profiles of the nanotube (A) and corresponding pore (B) depicted in (c). Reproduced from [17].

Tensile loading of individual arc-MWNTs inside an electron microscope was reported by Yu *et al.* [18]. For a range of tubes, they obtained modulus of 0.27-0.95 TPa and strengths of 11-63 GPa. They also showed MWNT fracture at strains up to 12% in the outermost layer with the inner walls telescoping out in a 'sword-in-sheath' mechanism.

Measurements on SWNTs took longer due to the difficulties in handling them. The first measurement was performed by Salvetat *et al.* [19]. They observed a tensile modulus of 1 TPa for small diameter SWNT bundles. However, the properties of larger diameter bundles were dominated by shear slippage of individual nanotubes within the bundle. Yu *et al.* [20] were able to measure the tensile properties of bundles by a similar approach they used for their MWNT study. They reported moduli in the range 0.32-1.47 TPa and strengths between 10 and 52 GPa. Failure occurred at 5.3%, giving a toughness of about 770 J g^{-1}. Besides, they found that failure occurred for the nanotubes on the perimeter of the bundle only, with the rest of the tubes slipping apart.

It is worth mentioning that in order to have a more accurate idea of the real potential of CNTs as reinforcing fillers for composite materials, a clear definition of the cross-sectional area of CNT needs to be introduced. In fact, the majority of the studies presented in literature assumed that only the external layer of nanotubes carried the load. Hence they used only the area occupied by the external wall as cross-sectional area, ignoring the hollow part of the nanotube. However, this assumption leads to an overestimate of the nanotube's mechanical properties. When nanotubes are used as reinforcing fillers in nanocomposites, the entire volume they occupy needs to be considered in micromechanical models, hence the entire cross-sectional area including the hollow part should be considered. For this reason, Ciselli [22] calculated the

effective Young's modulus and tensile strength for SWNTs, DWNTs and MWNTs. She found that the effective properties of MWNTs reach lower bound values when only the external wall carries the load and upper bound values when all walls carry the load. Calculations are strongly dependent on the structure of the nanotubes and the interaction between the outermost layer and the internal layers.

Electrical properties of CNTs

The unique electrical properties of CNTs are caused by the quantum confinement of electrons normal to the nanotube axis. In the radial direction, electrons are confined by the monolayer thickness of the graphene sheet. Consequently, electrons can propagate only along the nanotube axis, and so to their wave vector points.

The electrical properties of perfect MWNT are rather similar to perfect SWNT. However, due to weak coupling between the concentric cylinders of MWNT, only the outer shell contributes to the electron transport and thus to the final electrical properties [23]. Gojny *et al.* [24] concluded that MWNTs offer the highest potential for enhancement of electrical conductivity, due to the relatively low surface area and high aspect ratio that enables a good dispersion.

5.2 Mechanical properties of polymer/CNT composites

5.2.1 Nanoplatelets vs nanofibres

In general, nanocomposite is a multiphase material where one of the phases is nano-scale. In terms of nanofiller dimensionality, they can be classified as zero-dimensional (nanosphere), one-dimensional (nanofibre), two-dimensional (nanoplatelet), and three-dimensional (interpenetrating network) systems.

An important morphological characteristic for understanding the structure-property relation in nanocomposites is the surface area/volume ratio *(A/V)* of the reinforcement (Figure 5.4). The reduction of particle diameter *(d)*, platelet thickness *(t)*, or fibre diameter *(d)* from micrometer to nanometer changes the ratio by three orders of magnitude. This significant increase in interfacial area for nanofillers means that the properties of the nanocomposites will be dominated by the interface properties. On the other hand, this larger contact surface makes the dispersion of fillers more difficult.

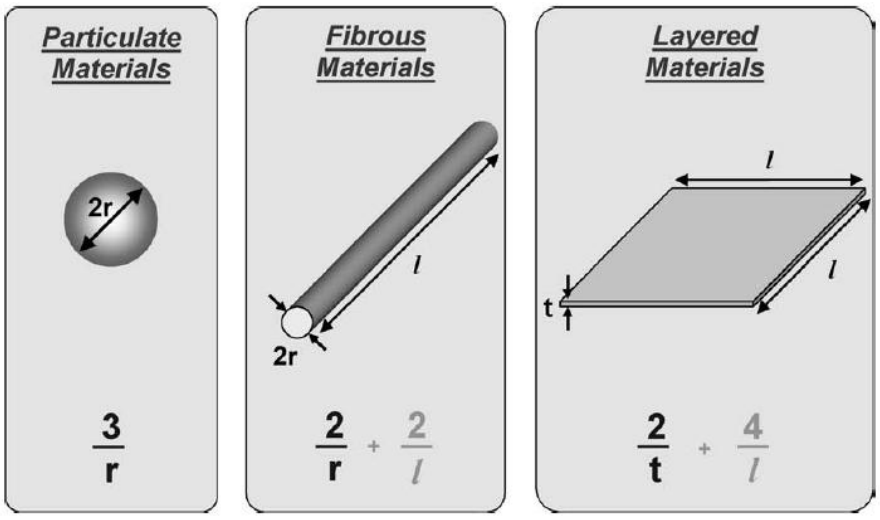

Figure 5.4 Surface area/volume relations for varying reinforcement geometries [25].

In terms of *A/V*, the increase with respect to the aspect ratio is much steeper for platelet compared to fibre, as shown in Figure 5.5. This indicates that the former are more difficult to disperse than the latter, since the contact surface between the platelets is greater compared to fibres. Consequently, homogeneous nanocomposites should be created more easily using nanofibres than nanoplatelets.

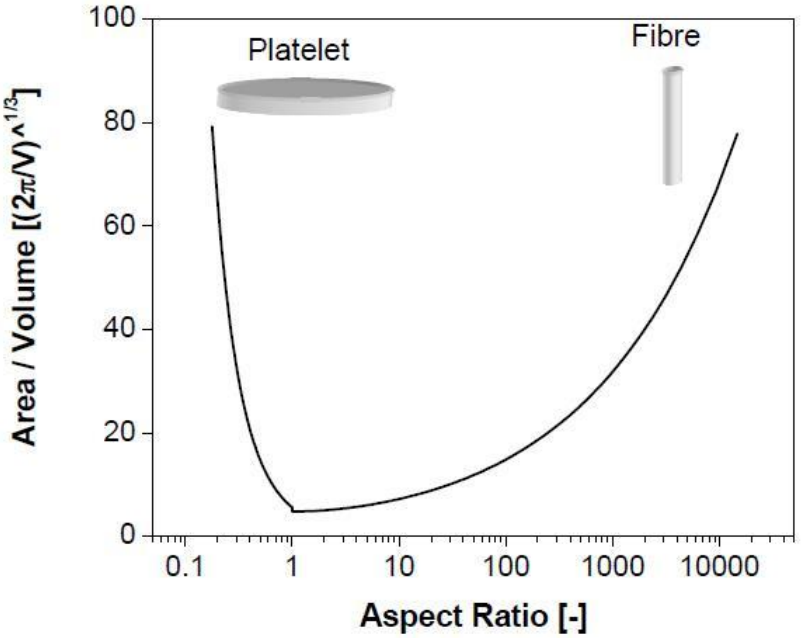

Figure 5.5 Plot of surface area/volume ratio (A/V) vs. aspect ratio for cylindrical particles with a given volume (Redraw from [26]).

Furthermore, theoretical predictions described by van Es [27] show that the shape of the filler has an influence on the mechanical reinforcing potential. Figure 5.6 shows the plot of calculated Young's modulus of unidirectional composites filled by platelets or fibres using the Mori-Tanaka model. It shows that at a given aspect ratio, fibre reinforcement gives a higher reinforcing action than platelet reinforcement. At high aspect ratios, both types of reinforcement approach the upper bound limit given by the rule of mixtures. While fibres with an aspect ratio of 100 already approach optimum reinforcement, platelets need an aspect ratio of 1000. This implies that in the unidirectional composite case, fibres are more effective than platelets. On the other hand, platelets are more effective than fibres in the case of 3D randomly oriented composites, as shown in Figure 5.7.

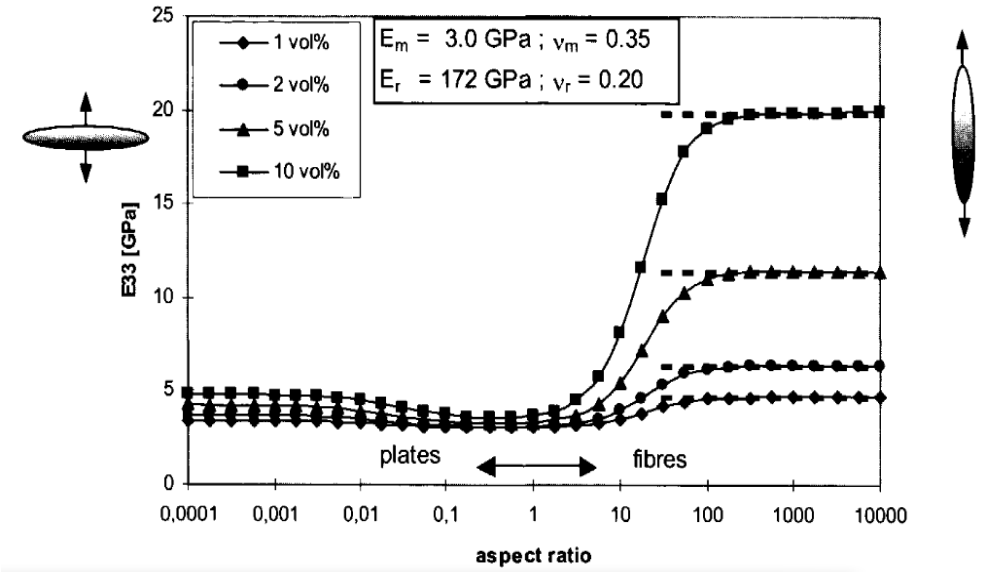

Figure 5.6 Young's modulus E_{33} of a composite with uniaxially oriented fibrous and platelet fillers. Mori-Tanaka's estimates are represented by solid lines. The upper bound reinforcement value, calculated by the rule of mixture, is given by the dotted lines [27].

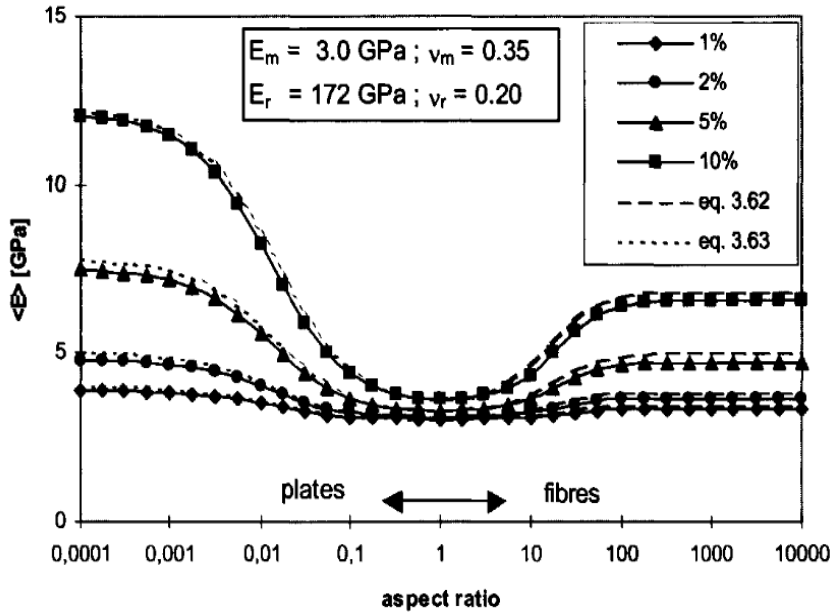

Figure 5.7 Young's modulus of a composite with 3D randomly oriented fibrous and platelet fillers. The solid lines are calculated by using simple approximations, while elaborate Mori-Tanaka's estimates are represented by dotted lines [27].

5.2.2 Mechanical properties of polymer/CNT composites

In this section, we discuss mechanical properties of bulk composites first, followed by fibre composites. In order to compare different studies, we will use the rate of increase of Young's modulus with volume fraction dE_c/dV_f as a measure for reinforcement.

The results for solution processed bulk composites are quite impressive. Cadek *et al.* [28] carried out nanohardness tests on spun-cast films of arc-discharge MWNTs in both polyvinyl acetate (PVA) and polyvinylcarbazole (PVK). They observed increases in moduli from 7 GPa to 12.5 GPa with 0.6 vol.% MWNTs in PVA, and from 2 GPa to 6 GPa with 4.8 vol.% in PVK. These increases are equivalent to the reinforcement values of dY/dV_f = 917 GPa and dY/dV_f =83 GPa for PVA and PVK, respectively. They found that the crystallinity of PVA increased linearly with MWNT content, whereas no such effect was observed for PVK. This indicates that the difference in reinforcement may be related to the presence of a crystalline interface for PVA composites, which may maximize the stress transfer, and an amorphous interface for PVK composites.

It should be noted that Velasco-Santos *et al.* [29] observed reasonably large increases in modulus, from 0.71 GPa for a poly(methyl methacrylate-*co*-ethyl methacrylate) copolymer to 2.34 GPa with 1 wt.% arc-MWNTs (dY/dV_f ~272 GPa). However, in this work no nucleation of crystallinity was observed, suggesting that good stress transfer can be obtained at an amorphous interface depending on the polymer.

Lower reinforcement was observed in the case of melt processing bulk composites. Zhang *et al.* prepared MWNTs reinforced polyamide 6 (PA6) nanocomposites [30, 31]. They observed a three times increase in modulus with the addition of only 2 wt.% MWNTs, corresponding to an impressive dY/dV_f of 64 GPa. Yield strength increased

from 18 to 47 MPa, while no decrease in ductility was observed. These impressive results were attributed to the good dispersion and adhesion, as observed by microscopy measurements.

Many studies reported that similar to polymer molecules, CNTs provide much more effective reinforcement when they are uniaxially aligned compared to randomly distributed in isotropic composites. Kearns and Shambaugh [32] reported very promising mechanical properties in PP/SWNT fibres. A reinforcement value of dY/dV_f ~ 530 GPa and a strength of ~1GPa was observed with the addition of 1 wt.% SWNTs. Moreover, the strain to break actually increased from 19% to 27%, which means SWNTs actually toughened the material.

Coleman *et al.* [33] critically analyzed and compared the mechanical properties of various polymer/CNT composites prepared by different techniques. The results are listed in Table 5.1. It is obvious that composites based on chemically modified CNTs showed the best results. This is not surprising, since functionalization should significantly improve both dispersion and stress transfer. The results for solution processed composites, especially PVA-based composites, are also impressive. However, many of these significant reinforcements are due to crystallinity nucleation, which cannot be relied upon for all polymer matrices. Of all the processing methods, the overall properties are worst for the melt processed composites. However, at an industrial level CNTs reinforced composites are most likely to be produced by melt processing. Therefore, the problems with mechanical reinforcement of melt processed composites must be addressed.

Table 5.1 Summary and comparison of reinforcement of SWNT and MWNT composites fabricated by various methods, where Y is the composite Young's modulus, σ is the composite strength, and V_f is the nanotube volume fraction [33].

	Mean dY/dV_f [GPa]	Median dY/dV_f [GPa]	Max dY/dV_f [GPa]		Max Y [GPa]	Max σ [MPa]
			SWNTs	MWNTs		
Solution	309	128	112	1244	7	348
Melt	23	11	68	64	4.5	80
Melt (fibre)	128	38	530	36	9.8	1032
Epoxy	231	18	94	330	4.5	41
In-situ polymerization	430	60-150	960	150	167	4200
Functionalization	157	115	305	380	29	107

5.3 Electrical conductivity of polymer/CNT composites

Polymer matrices are electrical insulators with extremely low electrical conductivity (10^{-10}-10^{-15} S m^{-1}). Dispersing conductive materials in such insulating matrices can form conductive polymer composites (CPCs). The electrical conductivity of a composite is strongly dependent on the volume fraction of the conductive phase. At low volume fractions, the conductivity remains very close to the conductivity of the pure matrix. When a certain volume fraction is reached, the conductivity of the composite drastically increases by many orders of magnitude. This phenomenon is known as percolation and can be well explained by percolation theory. Because of the high aspect ratio (100-10,000) of CNTs, the electrical percolation threshold of CNT-reinforced polymer nanocomposites is much lower than nanocomposites containing conventional

conducting fillers, such as metallic particles (60 wt.%) or carbon black (3-15 wt.%). Depending on the polymer matrix, the processing conditions and the nanotube type used, percolation thresholds ranging from 0.001 wt.% to more than 10 wt.% have been reported [7]. Sandler *et al.* [34] reported an ultra-low percolation threshold of 0.0025 wt.% for epoxy/MWNT composites, while Bryning *et al.* [35] also reported a very low percolation threshold of 0.0052 vol.% for epoxy/SWNT composites.

There are some traditional thoughts that the electrical conductivity of composites can be significantly improved if CNTs are well dispersed. Liao *et al.* [36] and Kuan *et al.* [37] observed that the electrical resistance decreased as crystallinity of polymer/CNT nanocomposite reduced at the same CNT loading. This phenomenon can be attributed to the better dispersion of CNTs in low crystalline polymer matrices than high crystalline matrixes [36, 37]. The probability of self-aggregation of conductive materials was reduced, and thus more electrical conducting paths were built up in the binary conductive materials system (Figure 5.8).

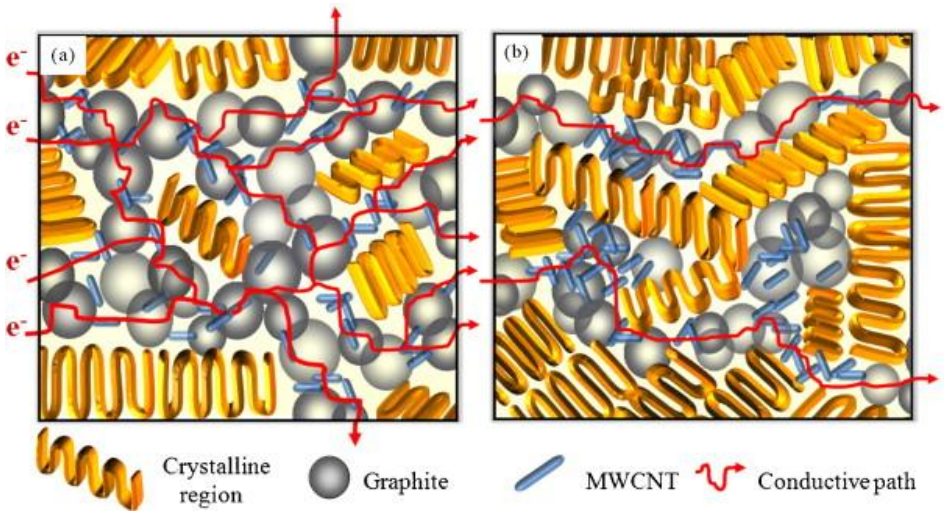

Figure 5.8 The model of conductive paths in the nanocomposite bipolar plates with (a) better dispersion of MWNTs in a low crystalline PP matrix (b) MWNTs aggregation in a high crystalline PP matrix [36].

Grossiord et al. [23] and Xu et al. [38] also pointed out that due to the increasing number of complete conductive paths, good dispersion can bring high composite conductivity. However, it has been also reported that agglomeration of CNTs to a certain extent helps enhancing the composite conductivity. Martin *et al.* [39], Du *et al.* [40] and Hu *et al.* [41] considered that electrical conductivities or low percolation thresholds can be achieved by heterogeneous distributions of SWNT in polymer matrices. Gojny *et al.* [24] showed that the stable dispersion can be detrimental for the overall conductivity because it lead to the formation of an isolating epoxy layer around the nanotubes. Delozier *et al.* [42] thought that a more uniform distribution of SWNT bundles would result in a reduced possibility of CNT bundle contacts to form a conductive network. It should be noted that while partially agglomerated systems may benefit from enhanced composite conductivity; it may be technically challenging to produce them in a highly controlled manner.

There are also some contradicting results regarding the effect of CNT alignment on electrical conductivity. Haggenmueller *et al.* [43] reported poly(methyl methacrylate) (PMMA)/SWNT composites with enhanced electrical properties along the fibre direction by aligning nanotubes in the matrix. Choi *et al.* [44] also observed that nanotube alignment contributed to the enhancement of electrical conductivity in epoxy/SWNT composites. This effect was explained by the formation of a more efficient percolation path in the parallel direction. On the other hand, the results of Du *et al.* [45] indicated that the alignment of nanotubes significantly lowered the electrical conductivity (6 orders of magnitude) compared to isotropic composites at the same nanotube concentration. Li *et al.* [46] studied the effect of nanotube alignment on the electrical conductivity of composites by using Monte Carlo simulations and taking into

account the nanotube waviness. It was found that both an increase and a decrease in electrical conductivity by nanotube alignment are actually possible, depending on the overall degree of alignment. The conductivity seems to be of the highest value when the alignment angle is around 20^{o}. This conclusion is consistent with the experimental observation of Du *et al.* [45]. The anisotropy of conductivity is strongly affected by nanotube alignment especially when the nanotube contents are small. But the effect of alignment becomes weaker at larger nanotube contents.

5.4 Carbon nanotube-based composite sensors

Polymer/CNT composites have been considered to replace conventional sensors in certain applications due to their flexibility and ease of manufacturing. The common feature among many reports on sensors is that a change in volume or deformation due to chemical, thermal or mechanical loading results directly in a change in resistance.

Nanotube-based composites were reported to be used as vapour sensors. As shown in Figure 5.9, when the polymer matrix is exposed to some external stimuli, the physical distance change between nanotubes due to polymer swelling is considered as one of the most common responses. Even if this distance change is a few angstroms, it will lead to a significant transition of electrical junctions from direct contact to tunneling in between CNTs. As a result, the electrical property change of the nanocomposite is very high. The number of sensing molecules and the interaction parameter with the matrix determine the extent of matrix swelling and resistance variation [47]. Yoon *et al.* [48] found that the gas concentration affects the distance between CNTs through polymer swelling. Wei *et al.* [49] also demonstrated that the aligned nanotube composite arrays showed similar changes in electrical resistance when subjected to thermal or optical exposure. Again,

they suggested that the resistance changes are attributed to expansion of the matrix.

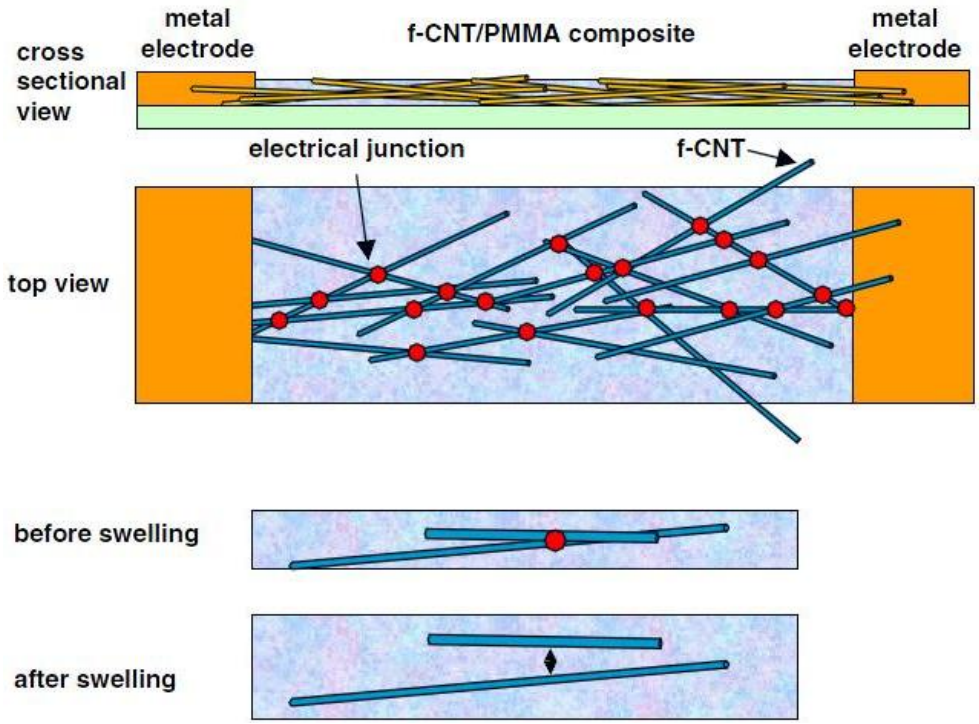

Figure 5.9 Schematic diagram of junction resistance change between two nanowires due to polymer matrix swelling [48].

Zhang *et al.* [50] reported that MWNT reinforced polycarbonate (PC) composites can be utilized as strain sensors. The sensitivity (electrical conductivity change to applied strain) of this nanocomposite was reported to be 3.5 times higher than traditional strain gages. They claimed that the instantaneous change in resistance with strain showed the potential for self-diagnostic and real-time health monitoring. Zhang *et al.* [51] also demonstrated a thermoplastic elastomer/MWNT composite capable of successfully sensing large strain deformations in the range of 0%-80%. The resistivity-strain relationship shows an exponential relationship with universal, nanotube content independent behaviour. They explained the controlling mechanism for changes in resistivity by fluctuation induced tunneling model when strain is greater than 5%, while

by conductive network deformation for strains below 5%.

Thostenson and Chou [52] demonstrated that conductive CNT networks formed in epoxy can be utilized as highly sensitive sensors for detecting the onset, nature, and evolution of damage in advanced polymer composites. Figure 5.10 shows the resistance response of a five-ply unidirectional composite during tensile loading. At low strain there is a linear increase in the resistance with deformation. A sharp increase in resistance occurs when ply delamination is initiated. As the delamination grows with increasing stress there is a large increase in resistance marked by increases in the slope of the resistance curve. The CNT network formed in these fibre reinforced polymer composites is less than 0.15 vol.%. More importantly, incorporation of *in situ* CNT-based sensing capability is non-invasive to the structural properties of the laminate.

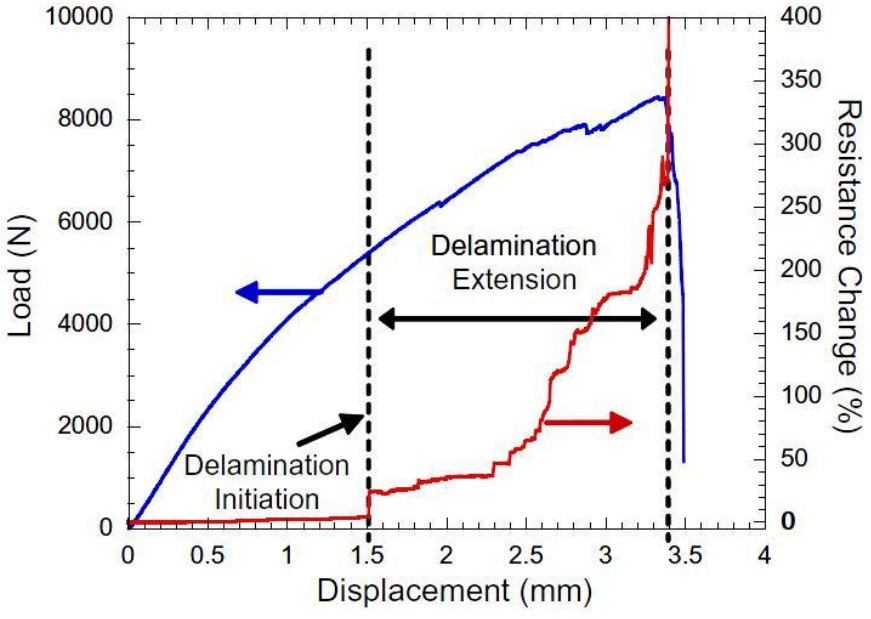

Figure 5.10 Load/displacement and resistance response of a five-ply unidirectional composite with the centre ply cut to initiate delamination [52].

In summary, carbon nanotubes are considered to be ideal candidates for multifunctional materials due to their unique properties. Effective processing to realize the full potential of CNTs is however still a great challenge. For development of CNT-based composites and their potential use as macroscopic sensors, a fundamental knowledge of their structure/property relations is necessary from the nanoscale to macroscopic scale.

5.5 References

1. K. Y. Lee, J. J. Blaker, and A. Bismarck, *Surface functionalisation of bacterial cellulose as the route to produce green polylactide nanocomposites with improved properties.* Composites Science and Technology, 2009. **69**(15): p. 2724-2733.
2. A. R. McLauchlin, and N. L. Thomas, *Preparation and thermal characterisation of poly (lactic acid) nanocomposites prepared from organoclays based on an amphoteric surfactant.* Polymer Degradation and Stability, 2009. **94**(5): p. 868-872.
3. M. Murariu, A. Doumbia, L. Bonnaud, A. L. Dechief, Y. Paint, M. Ferreira, C. Campagne, E. Devaux, and P. Dubois, *High-performance polylactide/ZnO nanocomposites designed for films and fibres with special end-use properties.* Biomacromolecules, 2011. **12**(5): p. 1762-1771.
4. E. T. Thostenson, Z. Ren, and T. W. Chou, *Advances in the science and technology of carbon nanotubes and their composites: a review.* Composites Science and Technology, 2001. **61**(13): p. 1899-1912.
5. T. W. Chou, L. Gao, E. T. Thostenson, Z. Zhang, and J. H. Byun, *An assessment of the science and technology of carbon nanotube-based fibres and composites.* Composites Science and Technology, 2010. **70**(1): p. 1-19.
6. O. Breuer, and U. Sundararaj, *Big returns from small fibres: a review of polymer/carbon nanotube composites.* Polymer Composites, 2004. **25**(6): p. 630-645.
7. C, Li, E.T. Thostenson, and T. W. Chou, *Sensors and actuators based on carbon nanotubes and their composites: a review.* Composites Science and Technology, 2008. **68**(6): p. 1227-1249.
8. R. F. Gibson, E. O. Ayorinde, and Y. F. Wen, *Vibrations of carbon nanotubes and their composites: a review.* Composites Science and Technology, 2007. **67**(1): p. 1-28.
9. B. Wei, R. Vajtai, and P. Ajayan, *Reliability and current carrying capacity of carbon nanotubes.* Applied Physics Letters, 2001. **79**(8): p. 1172-1174.
10. G. Maruccio, R. Cingolani, and R. Rinaldi, *Projecting the nanoworld: Concepts, results and perspectives of molecular electronics.* Journal of Materials Chemistry, 2004. **14**(4): p. 542-554.
11. B. I. Yakobson, C. Brabec, and J. Bernholc, *Nanomechanics of carbon tubes: instabilities beyond linear response.* Physical Review Letters, 1996. **76**(14): p. 2511.
12. B. Yakobson, G. Samsonidze, and G. Samsonidze, *Atomistic theory of mechanical relaxation in fullerene nanotubes.* Carbon, 2000. **38**(11): p. 1675-1680.
13. S. Cui, I. A. Kinloch, R. J. Young, L. Noé, and M. Monthioux, *The effect of stress transfer*

within double-walled carbon nanotubes upon their ability to reinforce composites. Advanced Materials, 2009. **21**(35): p. 3591-3595.

14. E. T. Thostenson, and T. W. Chou, *On the elastic properties of carbon nanotube-based composites: modelling and characterization.* Journal of Physics D: Applied Physics, 2003. **36**(5): p. 573.
15. P. C. Ma, N. A. Siddiqui, G. Marom, and J. K. Kim, *Dispersion and functionalization of carbon nanotubes for polymer-based nanocomposites: a review.* Composites Part A: Applied Science and Manufacturing, 2010. **41**(10): p. 1345-1367.
16. E. W. Wong, P.E. Sheehan, and C.M. Lieber, *Nanobeam mechanics: elasticity, strength, and toughness of nanorods and nanotubes.* Science, 1997. **277**(5334): p. 1971-1975.
17. J. P. Salvetat, A. J. Kulik, J. M. Bonard, G. A. D. Briggs, T. Stöckli, K. Metenier, S. Bonnamy, F. Béguin, N. A. Burnham, and L. Forró, *Elastic modulus of ordered and disordered multiwalled carbon nanotubes.* Advanced Materials, 1999. **11**(2): p. 161-165.
18. M. F. Yu, O. Lourie, M. J. Dyer, K. Moloni, T. F. Kelly, and R. S. Ruoff, *Strength and breaking mechanism of multiwalled carbon nanotubes under tensile load.* Science, 2000. **287**(5453): p. 637-640.
19. J. P. Salvetat, G. A. D. Briggs, J. M. Bonard, R. R. Bacsa, A. J. Kulik, T. Stöckli, N. A. Burnham, and L. Forró, *Elastic and shear moduli of single-walled carbon nanotube ropes.* Physical Review Letters, 1999. **82**(5): p. 944.
20. M. F. Yu, B. S. Files, S. Arepalli, and R. S. Ruoff, *Tensile loading of ropes of single wall carbon nanotubes and their mechanical properties.* Physical Review Letters, 2000. **84**(24): p. 5552.
21. S. Xie, W. Li, Z. Pan, B. Chang, and L. Sun, *Mechanical and physical properties on carbon nanotube.* Journal of Physics and Chemistry of Solids, 2000. **61**(7): p. 1153-1158.
22. P. Ciselli, *The potential of carbon nanotubes in polymer composites*, 2007, PhD thesis, Eindhoven Univeristy of Technology.
23. N. Grossiord, J. Loos, O. Regev, and C. E. Koning, *Toolbox for dispersing carbon nanotubes into polymers to get conductive nanocomposites.* Chemistry of Materials, 2006. **18**(5): p. 1089-1099.
24. F. H. Gojny, M. H. G. Wichmann, B. Fiedler, I. A. Kinloch, W. Bauhofer, A. H. Windle, and K. Schulte, *Evaluation and identification of electrical and thermal conduction mechanisms in carbon nanotube/epoxy composites.* Polymer, 2006. **47**(6): p. 2036-2045.
25. E. T. Thostenson, C. Li, and T.W. Chou, *Nanocomposites in context.* Composites Science and Technology, 2005. **65**(3): p. 491-516.
26. H. Fischer, *Polymer nanocomposites: from fundamental research to specific applications.* Materials Science and Engineering: C, 2003. **23**(6): p. 763-772.
27. van Es, M.A., *Polymer-clay Nanocomposites: The Importance of Particle Dimensions*. 2001.
28. M. Cadek, J. Coleman, V. Barron, K. Hedicke, and W. Blau, *Morphological and mechanical properties of carbon-nanotube-reinforced semicrystalline and amorphous polymer composites.* Applied Physics Letters, 2002. **81**(27): p. 5123-5125.
29. C. Velasco-Santos, A. Martinez-Hernandez, F. Fisher, R. Ruoff, and V. Castano, *Dynamical–mechanical and thermal analysis of carbon nanotube–methyl-ethyl methacrylate nanocomposites.* Journal of Physics D: Applied Physics, 2003. **36**(12): p. 1423.
30. T. Liu, I. Y. Phang, L. Shen, S. Y. Chow, and W. D. Zhang, *Morphology and mechanical*

properties of multiwalled carbon nanotubes reinforced nylon-6 composites. Macromolecules, 2004. **37**(19): p. 7214-7222.

31. W. D. Zhang, L. Shen, I. Y. Phang, and T. Liu, *Carbon nanotubes reinforced nylon-6 composite prepared by simple melt-compounding.* Macromolecules, 2004. **37**(2): p. 256-259.

32. J. C. Kearns, and R.L. Shambaugh, *Polypropylene fibres reinforced with carbon nanotubes.* Journal of Applied Polymer Science, 2002. **86**(8): p. 2079-2084.

33. J. N. Coleman, U. Khan, and Y. K. Gun'ko, *Mechanical reinforcement of polymers using carbon nanotubes.* Advanced Materials, 2006. **18**(6): p. 689-706.

34. J. Sandler, J. Kirk, I. Kinloch, M. Shaffer, and A. Windle, *Ultra-low electrical percolation threshold in carbon-nanotube-epoxy composites.* Polymer, 2003. **44**(19): p. 5893-5899.

35. M. B. Bryning, M. F. Islam, J. M. Kikkawa, and A. G. Yodh, *Very low conductivity threshold in bulk isotropic single‐walled carbon nanotube–epoxy composites.* Advanced Materials, 2005. **17**(9): p. 1186-1191.

36. S-H. Liao, C-Y. Yen, C-C. Weng, Y-F. Lin, C-C. M. Ma, C-H. Yang, M-C. Tsai, M-Y. Yen, M-C. Hsiao, S-J. Lee, X-F. Xie, and Y-H. Hsiao, *Preparation and properties of carbon nanotube/polypropylene nanocomposite bipolar plates for polymer electrolyte membrane fuel cells.* Journal of Power Sources, 2008. **185**(2): p. 1225-1232.

37. C-F. Kuan, H-C. Kuan, C-C. M. Ma, and C-H. Chen, *Mechanical and electrical properties of multi-wall carbon nanotube/poly (lactic acid) composites.* Journal of Physics and Chemistry of Solids, 2008. **69**(5): p. 1395-1398.

38. Y. Xu, B. Higgins, and W. J. Brittain, *Bottom-up synthesis of PS–CNF nanocomposites.* Polymer, 2005. **46**(3): p. 799-810.

39. C. A. Martin, J. K. W. Sandler, M. S. P. Shaffer, M-K. Schwarz, W. Bauhofer, K. Schulte, and A. H. Windle, *Formation of percolating networks in multi-wall carbon-nanotube–epoxy composites.* Composites Science and Technology, 2004. **64**(15): p. 2309-2316.

40. F. Du, C. Guthy, T. Kashiwagi, J. E. Fischer, and K. I. Winey, *An infiltration method for preparing single‐wall nanotube/epoxy composites with improved thermal conductivity.* Journal of Polymer Science Part B: Polymer Physics, 2006. **44**(10): p. 1513-1519.

41. G. Hu, C. Zhao, S. Zhang, M. Yang, and Z. Wang, *Low percolation thresholds of electrical conductivity and rheology in poly (ethylene terephthalate) through the networks of multi-walled carbon nanotubes.* Polymer, 2006. **47**(1): p. 480-488.

42. D. M. Delozier, K. A. Watson, J. G. Smith, T. C. Clancy, and J. W. Connell, *Investigation of aromatic/aliphatic polyimides as dispersants for single wall carbon nanotubes.* Macromolecules, 2006. **39**(5): p. 1731-1739.

43. R. Haggenmueller, H. Gommans, A. Rinzler, J. E. Fischer, and K. Winey, *Aligned single-wall carbon nanotubes in composites by melt processing methods.* Chemical Physics Letters, 2000. **330**(3): p. 219-225.

44. E. S. Choi, J. S. Brooks, D. L. Eaton, M. S. Al-Haik, M. Y. Hussaini, H. Garmestani, D. Li, and K. Dahmen, *Enhancement of thermal and electrical properties of carbon nanotube polymer composites by magnetic field processing.* Journal of Applied Physics, 2003. **94**(9): p. 6034-6039.

45. F. Du, J. E. Fischer, and K. I. Winey, *Coagulation method for preparing single‐walled carbon nanotube/poly (methyl methacrylate) composites and their modulus, electrical conductivity, and thermal stability.* Journal of Polymer Science Part B: Polymer Physics, 2003. **41**(24): p. 3333-3338.

46. C. Li, E. T. Thostenson, and T. W. Chou, *Effect of nanotube waviness on the electrical*

conductivity of carbon nanotube-based composites. Composites Science and Technology, 2008. **68**(6): p. 1445-1452.

47. T. Graves-Abe, F. Pschenitzka, H. Jin, B. Bollman, J. Sturm, and R. Register, *Solvent-enhanced dye diffusion in polymer thin films for polymer light-emitting diode application.* Journal of Applied Physics, 2004. **96**(12): p. 7154-7163.

48. H. Yoon, J. Xie, J. K. Abraham, V. K. Varadan, and P. B. Ruffin, *Passive wireless sensors using electrical transition of carbon nanotube junctions in polymer matrix.* Smart Materials and Structures, 2006. **15**(1): p. S14.

49. C. Wei, L. Dai, A. Roy, and T. B. Tolle, *Multifunctional chemical vapor sensors of aligned carbon nanotube and polymer composites.* Journal of the American Chemical Society, 2006. **128**(5): p. 1412-1413.

50. W. Zhang, J. Suhr, and N. Koratkar, *Carbon nanotube/polycarbonate composites as multifunctional strain sensors.* Journal of Nanoscience and Nanotechnology, 2006. **6**(4): p. 960-964.

51. R. Zhang, M. Baxendale, and T. Peijs, *Universal resistivity–strain dependence of carbon nanotube/polymer composites.* Physical Review B, 2007. **76**(19): p. 195433.

52. E. T. Thostenson, and T.W. Chou, *Carbon nanotube networks: sensing of distributed strain and damage for life prediction and self healing.* Advanced Materials, 2006. **18**(21): p. 2837-2841.

Chapter 6.

Conductive poly(lactic acid) tape reinforced with carbon nanotubes

6.1 Introduction

As reviewed in Chapter 5, CNTs provide much more effective reinforcement when they are uniaxial aligned compared to randomly distributed in isotropic composites. However, the alignment of CNTs could significantly lower the electrical conductivity.

Adding more conductive filler is a natural route to achieve improved electrical and mechanical properties of nanocomposite fibres. Bin *et al.* [1] prepared ultra-high molecular weight polyethylene/multi-walled carbon nanotubes (UHMWPE/MWNTs) conductive tapes from solution. The drawn composites containing 15 wt.% MWNTs showed 10^{-1} S m^{-1} in electric conductivity and 58 GPa in Young's modulus at room temperature. Later the same group [2] confirmed that iodine doping for drawn UHMWPE/MWNT tapes is one of the techniques to develop high modulus conductive materials. The nanocomposite tape containing 4.16 vol.% MWNTs exhibited a modulus of 25 GPa, while the corresponding electrical conductivity was about 10 S m^{-1}.

Thermal annealing of highly oriented polymer/CNT fibres or tapes was also reported. Miaudet *et al.* [3] found that annealing near the glass transition temperature (T_g) can dramatically increase the electrical conductivity of poly(vinyl alcohol) (PVA)/MWNTs

fibres. They explained this increase in conductivity by the increased mobility of polymer chains, which can lead to mobility of CNTs and an increase in quality and number of nanotube contacts in the network. Although the effect of thermal annealing on the mechanical properties of the polymer fibre was not reported in this study, it is inevitable that the good mechanical properties of these fibres or tapes cannot be retain after annealing due to polymer relaxation.

Deng *et al.* [4, 5] developed a methodology that allows for a thermal annealing process on highly oriented polypropylene (PP) tapes to improve conductivity without sacrificing mechanical properties. In order to achieve this, a bicomponent tape structure was fabricated by coextrusion followed by solid-state drawing. Here the neat homopolymer PP core, possessing a higher melting temperature, provides high mechanical properties, while co-PP/MWNT skins, possessing a lower melting temperature, was annealed above the melting temperature of the skins without affecting polymer relaxation in the core. This method produced a conductive (275 S m^{-1}), high-strength (500 MPa) polymer tape at relatively low (5 wt.%) MWNT loading in the skins, with an overall MWNT content in the tape at around 0.5 wt.%.

To date, the effort toward producing conductive fibres or tapes with high strength and stiffness continues. Up to now, few studies have reported on conductive PLA/MWNT fibres or tapes with high mechanical performance. McCullen *et al.* [6] reported a percolation threshold for PLA/MWNT electrospun fibre mats at about 0.3 wt.% and a tensile modulus of 55 MPa. Li *et al.* [7] fabricated oriented PLA and modified MWNT composites through solid-state drawing at 90 ^{o}C. High filler loading up to 15 wt.% MWNT was added into the polymer matrix to improve mechanical properties. Although

high values for both modulus (9.9 GPa) and strength (233 MPa) were reported for nanocomposite fibres of draw ratio 4.8 containing 5 wt.% MWNT, the nature of this increase in mechanical properties was more likely due to the a change in PLA morphology rather than MWNTs, as neat PLA fibres showed similar mechanical properties. Electrical properties were not reported in this work.

In this chapter, the influence of MWNTs and solid-state drawing on microstructure and resulting mechanical and electrical properties of PLA/MWNT nanocomposite tapes will be investigated. Various MWNT contents and drawing conditions will be studied in order to obtain the best compromise between high electrical conductivity and mechanical properties.

6.2 Experimental

6.2.1 Materials and sample preparation

Ingeo™ PLA 3051D was purchased from RESINEX, United Kingdom. Multiwall carbon nanotubes (MWNTs) (Nanocyl™ NC 7000) were kindly supplied by Nanocyl S.A. (Belgium). These MWNTs have an average diameter of 9.5 nm, length of 1.5 μm, and a surface area of 250–300 $m^2 g^{-1}$ according to the producer.

A masterbatch containing 15 wt.% MWNTs was prepared by melt blending in a DSM Xplore micro-compounder (The Netherlands) at 180 ^oC and 100 rpm for 3 min. 15 cm^3 materials can be mixed in a co-rotating, fully intermeshing, conical twin-screw compounder with a recirculation channel and a valve to vary the mixing time. This masterbatch was then diluted with pure PLA using the same processing conditions to produce nanocomposites with a desired MWNT concentration. Nitrogen gas flow was

used to minimize polymer degradation during the compounding process. The extruded strands were cut into pellets and then compression moulded into films at 180 ^{o}C for 3 min using a Collin hot press P300E (Germany). Samples of dimensions 40 mm $\times$ 4 mm were cut from these films and drawn at 80 ^{o}C at a cross head speed of 20 mm min^{-1} in a temperature controlled chamber attached to an Instron 5584 machine. The draw ratio (DR) of the tape is calculated by the following equation:

$$DR = \frac{Extension}{Original\ Length} \qquad Equation\ 6.1$$

In this chapter, samples are denoted as *x*MWNT DR=*y*, where *x* and *y* represents MWNTs weight percentage in PLA, and draw ratio of the oriented tapes, respectively. For example, 1MWNT DR=4 represents a sample containing 1 wt.% MWNTs and stretched to a draw ratio of four. Increasing MWNT content hampered the drawability of the nanocomposites. The maximum draw ratio for PLA nanocomposites with MWNT contents above 2 wt.% was only four.

6.2.2 Characterization

Morphological studies were carried out using scanning electron microscopy (SEM) (FEI Inspector-F, The Netherlands). A high acceleration voltage was applied for alignment observation. The samples were uncoated and directly observed on the surface along the drawing direction. For dispersion observations, samples were cold fractured in liquid nitrogen and then gold sputtered before analysis. SEM images were taken of each sample's cross-section perpendicular to the drawing direction.

Rheology was conducted on an AR 2000 Advanced Rheometer by TA Instruments

connected to an environmental chamber with a 25 mm parallel plate setup. The disc-shaped samples were tested at 180 ℃ over a frequency sweep range of 100 Hz to 0.01 Hz and strain of 0.1% which is within the linear elastic region of the material.

Mechanical tests were performed using an Instron 5586 at room temperature, equipped with a 1 kN load cell at a crosshead speed of 8 mm/min. The reported values were calculated as averages over six specimens.

Differential scanning calorimetry (DSC) (Mettler-Toledo 822e) was used to investigate the thermal properties. All samples were heated to 200 ^{o}C at 10 ^{o}C/min. Crystallinity was determined using the heat of fusion of 100% crystalline PLA, which is 93.6 J g^{-1} [8].

Wide angle X-ray scattering (WAXS) 2D patterns were recorded with the incident beam perpendicular to the tapes. The X-ray wavelength was 1.54 Å. The sample-to-detector distance was 50 mm. All images were corrected for background scattering. The details of the calculation method of Herman's factor were described in Chapter 3.

Specimens were also tested in tension mode using a Q800 dynamic mechanical analyser (DMA) from TA Instruments. The system was cooled to -10 ^{o}C, and then heated to 150 ^{o}C at a rate of 3 ^{o}C /min. A static force of 0.1 N was applied to ensure the tape was taut between the grips, while a strain of 0.1% was used throughout.

Bulk electrical conductivity was measured along the stretching direction with the two-point method. Silver paste was coated on both cross-sectional ends of the sample to ensure good contact with the electrodes of the electrometer. The resistance between two silver paste marks along the specimen length direction was measured using a Model

6517B Electrometer (Keithley Instrument Inc, USA) at room temperature. The voltage is scanned between 0 V and 30 V, at 0.5 V intervals. All current-voltage curves were linear in this study. The volume resistivity was calculated in relation to the specimen dimensions. For specimen with a resistance greater than $10^{10}\,\Omega$, electrical resistivity is not measurable and the tapes are considered as non-conductive. Three specimens for each composite were tested, and the average value was reported.

6.3 Results and discussion

6.3.1 Dispersion and alignment of MWNT

The homogeneous dispersion of MWNTs in polymer matrices is one of the most important requirements in achieving high mechanical reinforcement as inhomogeneities can lead to structural defects in the composite material. SEM images of fracture surfaces of isotropic films and tapes are shown in Figure 6.1. They show that MWNTs are well dispersed in the PLA matrix without showing noticeable aggregates for both isotropic films and tapes irrespective if the MWNT loading is 0.5 wt.% or 5 wt.%. It is well established that drawing can promote CNT dispersion in polymer matrices [9]. However, no differences in state of dispersion can be observed for the different draw ratios in this work.

As mentioned before, CNTs provide much greater effective reinforcement when they are uniaxial aligned rather than isotropically organized in bulk composites. The alignment of MWNTs in the PLA tapes was investigated with SEM, as shown in Figure 6.2. It is worth noting that SEM was used in a high accelerating voltage mode here, since Loos *et al.* [10] reported that SEM operated in charge contrast mode offers the potential to monitor the organization of CNTs networks in the polymer matrix of

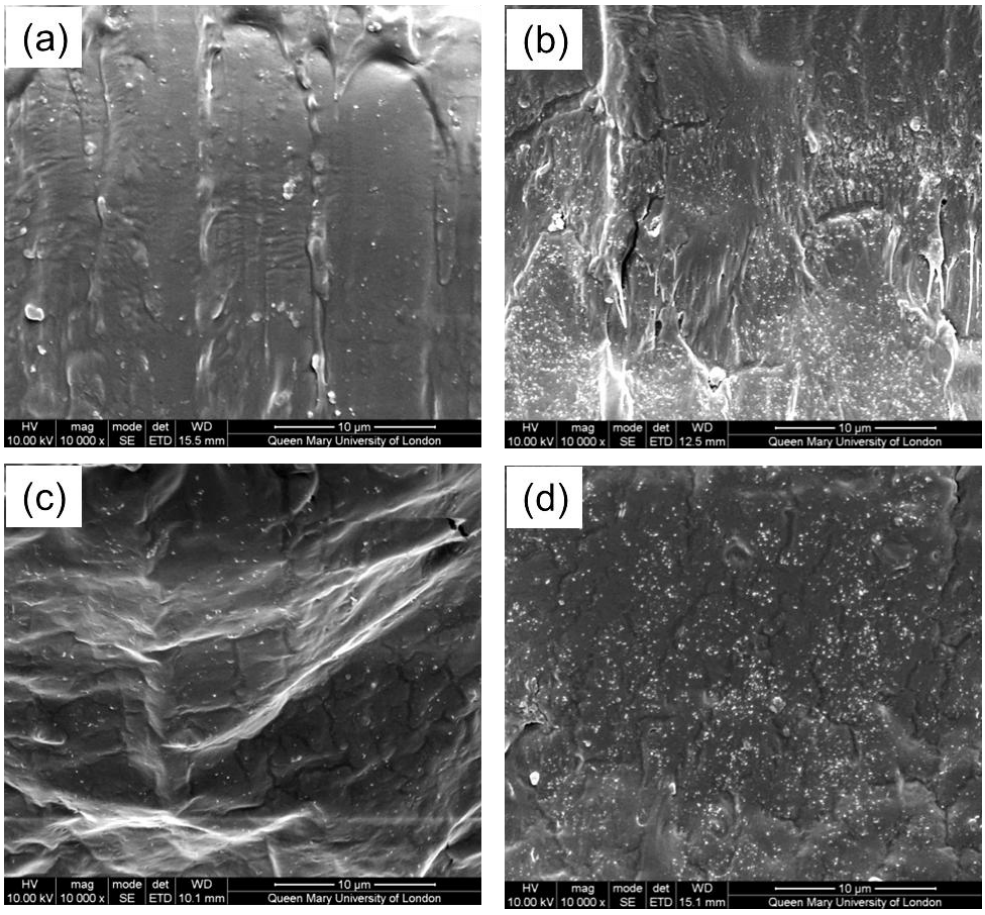

Figure 6.1 SEM images of cross-sectional areas of (a) 0.5MWNT DR=1; (b) 5MWNT DR=1; (c) 0.5MWNT DR=4; (d) 5MWNT DR=4.

conductive nanocomposite. The penetration depth of the primary electrons increases with increasing acceleration voltage. Therefore, using high acceleration voltage, the three-dimensional CNTs network underneath the polymer surface can be visualized. In Figure 6.2, the brightness variations in the images are related to the position of the CNTs in the sample. CNTs located at or near surface appear brighter, whereas CNTs located deeper in the nanocomposite appear darker. A filler network is observed in nanocomposites containing 5 wt.% MWNTs before drawing. Most of MWNTs are dispersed as entangled coils in isotropic film, while highly aligned MWNTs are seen after solid-state drawing, even at a relatively low draw ratio of 4.

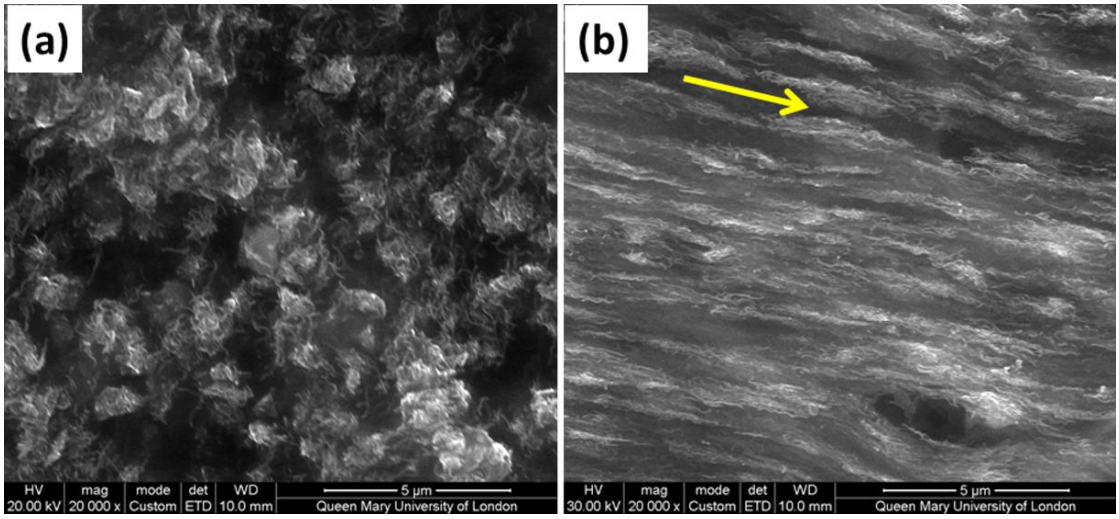

Figure 6.2 SEM images of (a) 5MWNT DR=1 and (b) 5MWNT DR=4 on the surface. Arrow indicates the drawing direction.

6.3.2 Rheological behaviour

Oscillatory rheology is a powerful tool to assess indirectly the dispersion state of the nanofiller in PLA matrix because the rheological responses are highly dependent on micro- and meso-structure and particle-particle interactions [10]. Figure 6.3(a) and (b) show the dependence of dynamic storage modulus (G') and complex viscosity ($|\eta^*|$) for the neat PLA and PLA/MWNT samples, respectively. At low frequencies, PLA chains are fully relaxed and present typical terminal behaviour with a scaling factor of about $G' \propto \omega^2$, which is consistent with Cox-Merz rule [11]. However, with the addition of MWNTs the dependence of low-frequency G' on ω weakens especially at high loading levels. The beginning of a plateau can be observed between a MWNT concentration of 0.7 wt.% and 1 wt.% where a sudden large jump in G' and $|\eta^*|$ occurs. This indicates that there is a sudden change in composite microstructure. As MWNT loadings increase, nanotube-nanotube interactions begin to dominate in the viscoelastic behaviour. As a result, the MWNTs form a rheological percolating network, which highly impede the

long range motion of polymer chains. Hence the Newtonian plateau of the viscosity curve disappears as seen in Figure 6.3(b). Wu *et al.* [12] also studied the viscoelasticity of PLA/CNT nanocomposites using the same PLA grade. They reported a higher rheological percolation threshold of about 2.7 wt.%. Since high aspect ratio nanotubes were used in both studies, the large increase seen here is believed to be caused by a better dispersion state in present system.

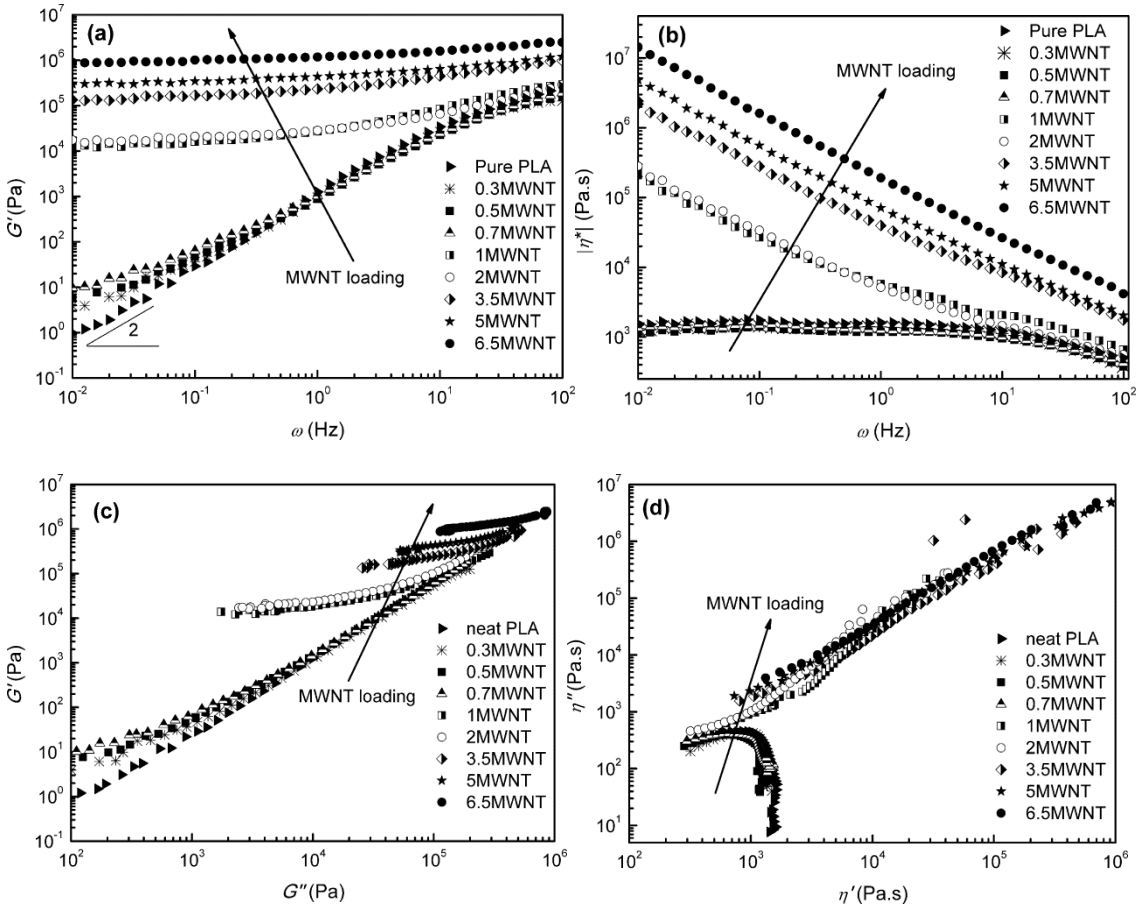

Figure 6.3 Variation in: (a) storage modulus (G'), (b) complex viscosity (|η|) , (c) Cole–Cole plots of dynamic storage modulus (G') vs. dynamic loss modulus (G") at various temperatures for neat PLA and PLA/MWNT samples and (d) imaginary viscosity (η") vs. real viscosity (η') for the neat PLA and PLA/MWNT samples.*

Further evidence to confirm rheological percolation can be extracted from plots of log G' versus log G'' (Cole-Cole plot). As can be clearly seen from Figure 6.3(c), the plots for both unfilled and filled compositions at 0.7 wt.% MWNTs follow the same path, with slight changes in slope. However, the slope in these plots decreases sharply, as nanofiller concentration exceeds 0.7 wt.%. This decrease in slope can be attributed to the formation of a physical network in the host matrix.

This strong restriction is further confirmed by the plots of imaginary viscosity (η'') vs. real viscosity (η') as shown in Figure 6.3(d), which is often used for the description of viscoelastic properties of polymers. The single arc of the neat PLA corresponds to the local dynamics of PLA. With the addition of MWNTs up to 0.7 wt.%, no changes are observed in the curves. As the loading level reaches 1 wt.%, the local relaxation arc of PLA disappears, and a rigid tail at high-viscosity region is observed. This indicates that the long-term relaxation of those restrained PLA chains becomes dominant in the whole relaxation behaviour of the nanocomposites. This also confirms that a percolation network is formed at present MWNT loadings and, that long-range motion of PLA chains is highly restrained as a result.

The cross-over point (G_c), being the point at which plots of G' and G'' intersect with frequency (ω) were also recorded in Figure 6.4. This point is representative of the transition from viscous to elastic behaviour. Neat PLA and nanocomposites with low MWNT loadings (< 0.7 wt.%) display a single cross-over point at higher frequencies, close to 100 Hz. With further addition of MWNTs, both G' and G'' increased, where G' increased significantly and G'' only slightly. Consequently, at intermediate MWNT loadings (1 wt.%) the curves of G' and G'' also intersected at lower frequencies (1 Hz).

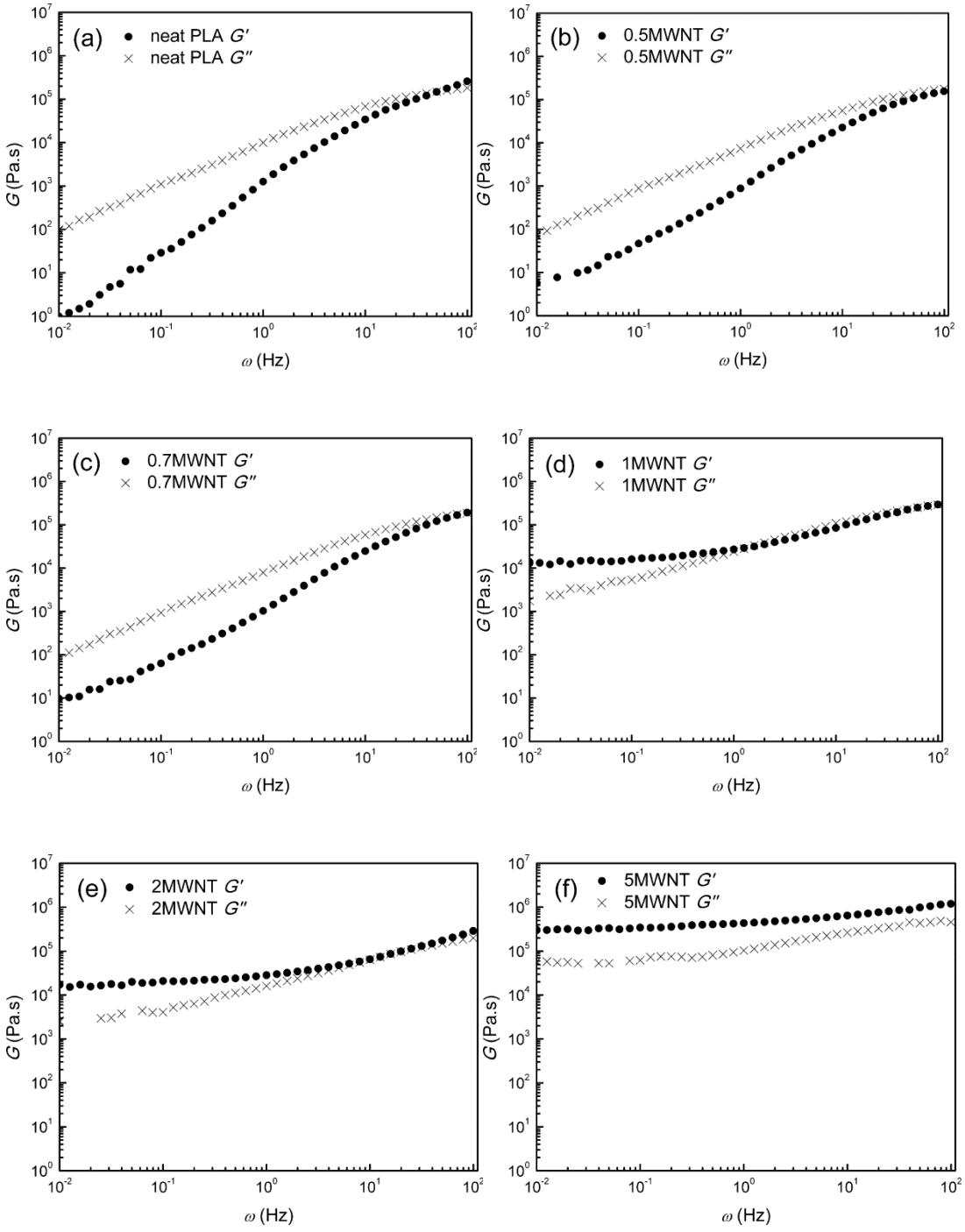

Figure 6.4 Cross-over points for curves of G' and G" as a function of frequency for (a) neat PLA and PLA/MWNT composites with (b) 0.5 wt.%, (c) 0.7 wt.%, (d) 1 wt.%, (e) 2 wt.% and (f) 5 wt.% MWNTs.

Interestingly, with further addition of MWNTs (> 2 wt.%), both curves merge and eventually for the composite with 5 wt.% MWNTs, G' is greater than G'' across the whole frequency range examined. These results confirm the onset of rheological percolation at MWNT loading of 0.7-1 wt.%. At higher filler concentrations an extensive interconnected nanotube network is formed and the composites display more solid-like behaviour.

6.3.3 Mechanical properties

The mechanical properties of MWNT reinforced nanocomposites are strongly dependent on several microstructural parameters such as the properties of the matrix, the properties of the MWNTs, the dispersion and alignment of the MWNTs, and the interfacial bonding. The Young's modulus and tensile strength of nanocomposites before and after drawing were plotted as a function of MWNT contents in Figure 6.5. For isotropic films, with the addition of MWNTs, both Young's modulus and tensile strength did not show significant improvements. For isotropic films containing 2 wt.% MWNTs, the Young's modulus increased from 1.9 GPa to 2.3 GPa, and tensile strength increased from 48 MPa to 53 MPa. On the other hand, for oriented tapes containing 2 wt.% MWNTs at draw-ratio (DR) 7.5, Young's modulus increased from 3.6 GPa to 5.5 GPa, while tensile strength was improved from 114 MPa to 156 MPa. As seen in Figure 6.5(a), the experimental data were fitted linearly for both nanocomposite films and tapes, and the analysis gave a slope dE_c/dV_f of 30 GPa, 92 GPa and 195 GPa for nanocomposites of draw ratio 1, 4 and 7.5, respectively. These results clearly demonstrate that solid-state drawing greatly improves the reinforcing efficiency of CNTs.

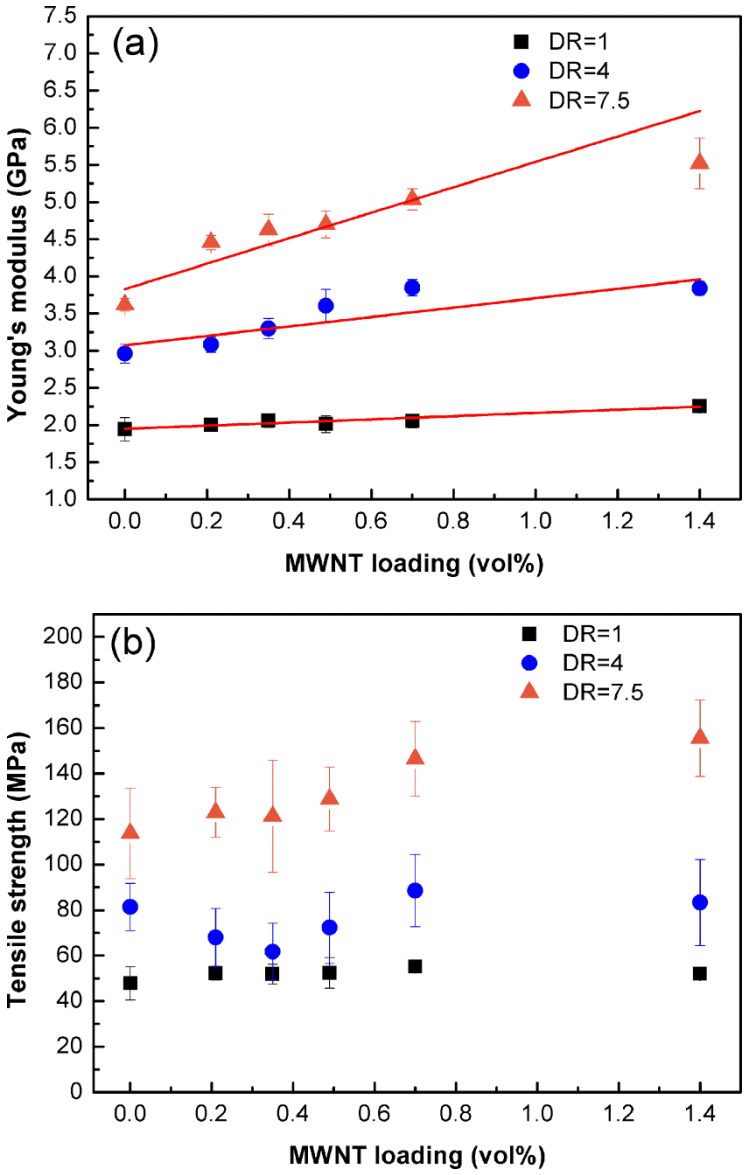

Figure 6.5 (a) Young's modulus and (b) tensile strength as a function of MWNT volume fraction in the composite isotropic films and oriented tapes, solid line in (a) represents the linear fit of the data.

Table 6.1 compares the effective reinforcement in terms of Young's modulus and tensile strength of CNTs in various PLA nanocomposites reported in literatures and this work. In order to compare different studies, we will use the rate of increase of Young's modulus with volume fraction dE_c/dV_f as a measure for reinforcement. The data

Table 6.1 Comparison of PLA/CNT nanocomposites fabricated by various methods and present work, where E_c is the composite Young's modulus, σ is the composite strength, and V_f is the nanotube volume fraction.

Type of CNT	**Max dE_c/dV_f [GPa]**	**Max σ [MPa]**
MWNTs [13]	62	-
MWNTs (DR=1) [7]	43	64
MWNTs (DR=2.8) [7]	54	138
MWNTs (DR=3.4) [7]	9	188
MWNTs (DR=4.8) [7]	7	230
Maleic anhydride grafted MWNTs [14]	-	76
PLA grafted MWNTs [15]	132	72
Oxidized MWNTs [16]	25	86
Functionalized MWNTs by DCA reaction [17]	109	57
PLA grafted MWNTs [18]	227	63
Acid-treated SWNTs grafted with 2-isocyanatopropyl triethoxysilane [19]	756	-
MWNTs (This work DR=1)	30	55
MWNTs (This work DR=4)	92	89
MWNTs (This work DR=7.5)	195	156

presented here are evaluated based on the values reported in the papers. It should be noted that as modulus does not always increase linearly with volume fraction, dE_c/dV_f is calculated at low volume fractions. The most obvious result here is that composites based on chemically modified nanotubes show the best results, as functionalization should significantly improve both dispersion and stress transfer. Moreover, it is shown that SWNTs demonstrate higher reinforcing efficiency than MWNTs. In case of

MWNTs, interlayer sliding (so-called 'sword and sheath' slippage) [20] and weak inter-tube coupling can limit their potential as structural reinforcement. Although the effective reinforcement of MWNTs in isotropic PLA films is rather low, this reinforcement efficiency is greatly enhanced after solid-state drawing and among the highest reported for MWNTs in PLA.

6.3.4 Micromechanical analysis

The Halpin-Tsai equations have been used successfully to predict the modulus of polymer/carbon nanotube composites [21, 22]. In case of a random distribution of nanotubes in the polymer matrix, the modified Halpin-Tsai equations are written as [23]:

$$E_c = \left[\frac{3}{8} \frac{1+2\left(\frac{l_{NT}}{D_{NT}}\right)\eta_L V_{NT}}{1-\eta_L V_{NT}} + \frac{5}{8} \frac{1+2\eta_T V_{NT}}{1-\eta_T V_{NT}} \right] E_m \qquad \textit{Equation 6.2}$$

$$\eta_L = \frac{\left(\frac{E_{NT}}{E_m}\right)-1}{\left(\frac{E_{NT}}{E_m}\right)+2\left(\frac{l_{NT}}{D_{NT}}\right)} \qquad \textit{Equation 6.3}$$

$$\eta_T = \frac{\left(\frac{E_{NT}}{E_m}\right)-1}{\left(\frac{E_{NT}}{E_m}\right)+2} \qquad \textit{Equation 6.4}$$

where E_c, E_{NT}, and E_m are the modulus of composite, nanotube, and polymer matrix, and l_{NT}, D_{NT}, and V_{NT} are the length, diameter, and volume fraction of nanotubes in the composite, respectively. It is worth noting that the modulus of carbon nanotubes E_{NT} is known to be a strong function of nanotube diameter or number of layers [20, 24-27].

Reported moduli range from 0.2 to 1 TPa. In this work, we have chosen to use the modulus reported in the paper [28] of 500 GPa since these nanotubes are similar to those studied here (~ 10 nm).

In case of aligned carbon nanotubes along the tape direction, the Halpin-Tsai equations are written as:

$$E_{\parallel} = [\frac{1+2(l_{NT}/D_{NT})\eta_{\parallel}V_{NT}}{1-\eta_{\parallel}V_{NT}}]E_m \qquad \textit{Equation 6.5}$$

$$\eta_{\parallel} = [\frac{(E_{NT}/E_m)-1}{(E_{NT}/E_m)+2(l_{NT}/D_{NT})}] \qquad \textit{Equation 6.6}$$

where $E_{\parallel}$ is the modulus of the composite tape with MWNTs aligned along the tape's axial direction. Since a high degree of MWNT alignment in PLA matrix was already observed at DR=4 (Figure 6.2), equation 6.5 and 6.6 were used for the calculations of nanocomposite tapes with DR of 4 and 7.5.

Using the nanotube's aspect ratio (l_{NT}/D_{NT}) as an adjustable parameter for fitting, the model shows a good agreement with the experimental data. Using l_{NT}/D_{NT} ~19, a good correlation is achieved for composites containing < 2 wt.% MWNTs. The low effective aspect ratio of MWNTs in the nanocomposite films is because of the random distribution of MWNTs in three dimensions in the matrix as seen in Figure 6.2(a); hence, their true aspect ratio is not fully exploited for optimal reinforcement. The calculated effective aspect ratio of the MWNTs increases to ~56 in oriented tapes. It is rather surprising that even in the case of oriented tapes the effective aspect ratio of the MWNTs is far lower than their original geometrical aspect ratio (~158). Wu *et al.* [28] explained that the large difference also found in their study mainly comes from

structural changes in the CNTs themselves. For instance, CNTs may be bent, entangled, and even break up during melt mixing, which will highly reduce their aspect ratio values. Another reason might be that as the Halpin-Tsai equation assumes perfect stress transfer, it highly unlikely that this is the case and the differences in aspect ratios are most likely the result of imperfect stress transfer. This data also shows that the stress transfer is better for aligned CNTs in drawn tapes than for isotropic films. Since MWNTs are used as received without any modification, the values obtained seem reasonable.

Table 6.2 Summary of reinforcement of MWNT in nanocomposites drawn at various draw ratios, where E_c is the composite Young's modulus, V_f is the nanotube volume fraction, σ is the composite strength, and l_{NT}/D_{NT} is the aspect ratio of MWNT.

Draw Ratio	**Max dE_c/dV_f [GPa]**	**Max σ [MPa]**	**Effective l_{NT}/D_{NT}**	**Method**
1	30	55	19±1.5	Fitting using Eq. (6.2)-(6.4)
4	92	89	26±2.8	Fitting using Eq. (6.5)-(6.6)
7.5	195	156	56±12	Fitting using Eq. (6.5)-(6.6)

6.3.5 Morphology change

It is worth noting that many studies on the effect of the addition on CNTs on polymer morphology indicated that the enhanced mechanical properties were a mere result of an altered crystallinity of the polymer matrices [22]. CNTs were found to nucleate and template oriented crystallization of polymer. In the present work, as shown in Table 6.3,

the crystallinity of PLA increased after drawing, indicating stress-induced crystallization of PLA during drawing. However, at the same DR, polymer crystallinity in PLA/MWNT tape is roughly similar to that of neat PLA tape. Therefore it is believed that the increase in modulus and strength in the case of tapes containing CNTs is not attributed to changes in crystallinity. With increasing MWNT loading, no significant changes in melting peaks were observed.

Table 6.3 The glass transition temperature (T_g), melting temperature (T_m), and crystallinity (X_c) of neat PLA and PLA/MWNT composites.

Sample	**DR**	T_g [a)]	T_{m1} [b)]	T_{m2} [b)]	X_c [b)]
	[-]	**[°C]**	**[°C]**	**[°C]**	**[%]**
PLA	1	69	-	153	1
0.3MWNT	1	69	-	153	2
0.7MWNT	1	69	-	153	4
1MWNT	1	68	-	152	2
2MWNT	1	70	-	153	1
PLA	7.5	79	144	152	32
0.3MWNT	7.5	79	144	152	32
0.7MWNT	7.5	83	143	152	34
1MWNT	7.5	83	143	152	35
2MWNT	7.5	85	-	152	33

Data obtained from [a)] DMA; [b)] DSC

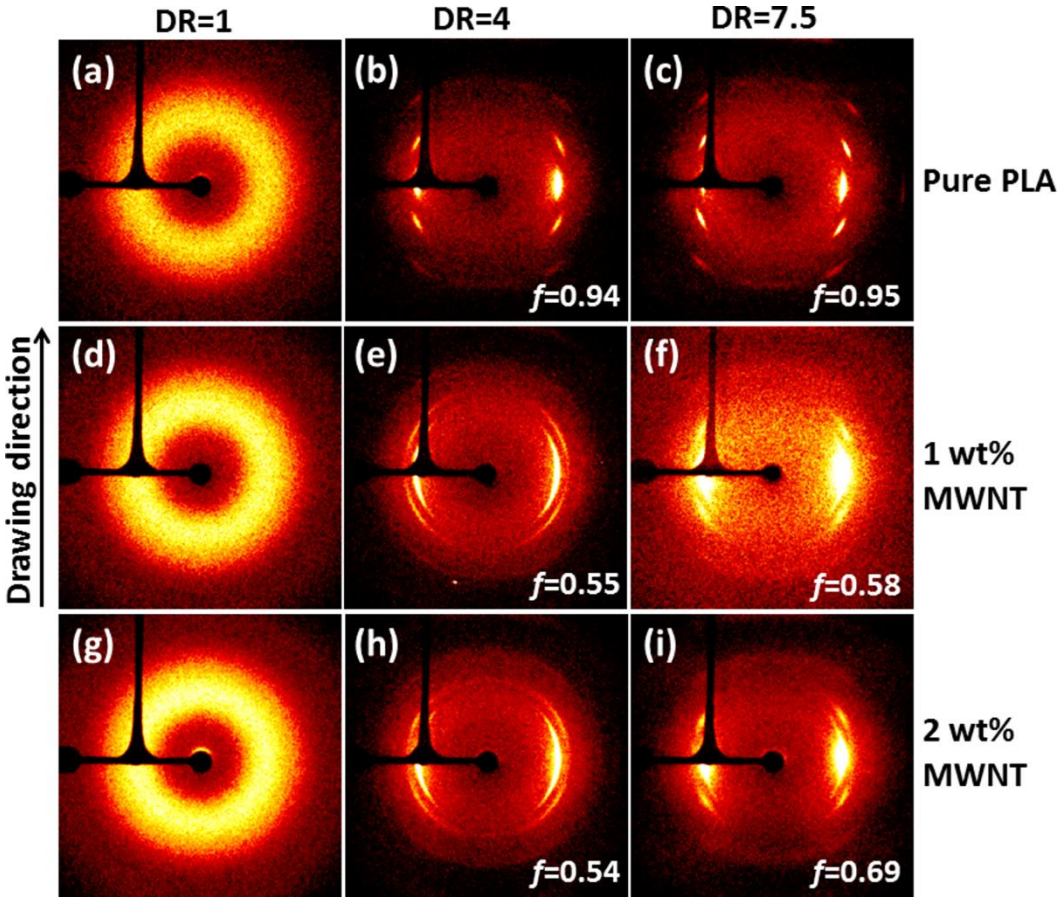

Figure 6.6 2D WAXS patterns of neat PLA and nanocomposites isotropic films and tapes. The Herman's orientation factor (f) is given by $f = \frac{3\cos^2\theta - 1}{2}$*, where θ is the angle between the chain axis and the tape axis.*

2D WAXS was performed to determine the influence of MWNT presence on PLA orientation after drawing. Figure 6.6 displays the 2D WAXS patterns of a series of neat PLA and nanocomposites with different draw-ratios (DR). Herman's orientation factor (*f*) calculated from Gaussian function is used to quantify the orientation of the PLA, and the corresponding values are listed in the corner of the graph. The neat PLA and nanocomposite films all show a diffuse isotropic scatter typical of an amorphous polymer. In case of uniaxially drawn PLA tape with DR=4, there is a rapid growth of

discrete equatorial reflection with a low azimuthal spread typical of a well-oriented crystalline phase. The Herman's orientation factors of neat PLA tapes are 0.94 and 0.95 for DR=4 and 7.5, respectively. However, with the addition of 1 wt.% MWNTs, Herman's orientation factor decreases to 0.55 and 0.58 for DR=4 and 7.5, suggesting crystals with lower degrees of orientation, which is quite unusual. In the present work, nanocomposite tapes were uniaxially drawn from isotropic amorphous films. A high degree of crystallinity and a highly ordered crystalline phase was established at low DR=4 for neat PLA tapes, but the presence of CNT in the PLA matrix seem to perturb the orientation of the polymer crystals rather than enhancing the orientation process.

Since no increase in crystallinity and polymer crystal orientation are observed in drawn tapes with the addition of MWNTs, DMA was performed to better understand the improved mechanical properties of the nanocomposite tapes. As seen in Table 6.3, T_g of neat PLA increases from 69 ℃ to 79 ℃ after drawing. Cicero *et al.* [29] reported the same trend in their two-step melt-spun drawn PLA fibres. Since T_g is associated with cooperative segmental motion of amorphous molecules, we can assume that the increased T_g can be attributed to strain-induced crystallization and enhanced orientation of the amorphous chains. Furthermore, for isotropic films there is only 1 ^oC increase in T_g with the addition of 2 wt.% MWNTs compared to neat PLA, while for drawn tapes the T_g of the nancomposites containing 2 wt.% MWNTs increases by 6 ^oC compared to neat PLA at the same DR. This indicates that solid-state drawing results in the retardation in the relaxation of amorphous regions due to physical interactions with the reinforcing phase. Therefore, the improved mechanical reinforcement efficiency in oriented nanocomposite tapes can also be contributed to the modification of the amorphous phase by an interplay between nanotube addition and solid-state drawing.

6.3.6 Electrical properties

Electrical properties of the PLA nanocomposites are also strongly depended on MWNT content and draw ratio. The electrical resistivity results of PLA/MWNT composites are plotted as a function of MWNT concentration in Figure 6.7(a). It can be seen that electrical resistivity increased with draw ratio. The significant decrease (up to several orders of magnitude) in electrical conductivity in drawn composite fibres as compared with isotropic nanocomposites was also reported for CNT loaded poly(methyl methacrylate) (PMMA) [30], PP [31] and polycarbonate (PC) [32]. This is attributed to the disruption of the CNT percolation network during drawing. However, nanocomposites with different MWNT loadings behave differently upon stretching. At low concentrations, the resistivity jumps rapidly with increasing draw ratio. For instance, the resistivity of a composite tape containing 1 wt.% MWNTs increased by a factor of 6 after drawing only four times, as compared to isotropic composites. The electrical resistivity of composite tapes containing 2 wt.% MWNTs increased from 4×10^{-2} to 5.7×10^{0} Ω m when draw ratio increased from 1 to 4, and it increased further to 3.5×10^{5} Ω m when draw ratio increased to 7.5. On the other hand, the resistivity for high MWNT loaded composites, such as 5 wt.% and 6.5 wt.%, remained nearly constant with draw ratio. Du *et al.* [33] reported that the percolation conductivity of a ‘stick’ type network depends on both the alignment and the concentration of the sticks. A higher CNT loading can improve tube-tube connections and compensate for tube displacement due to drawing.

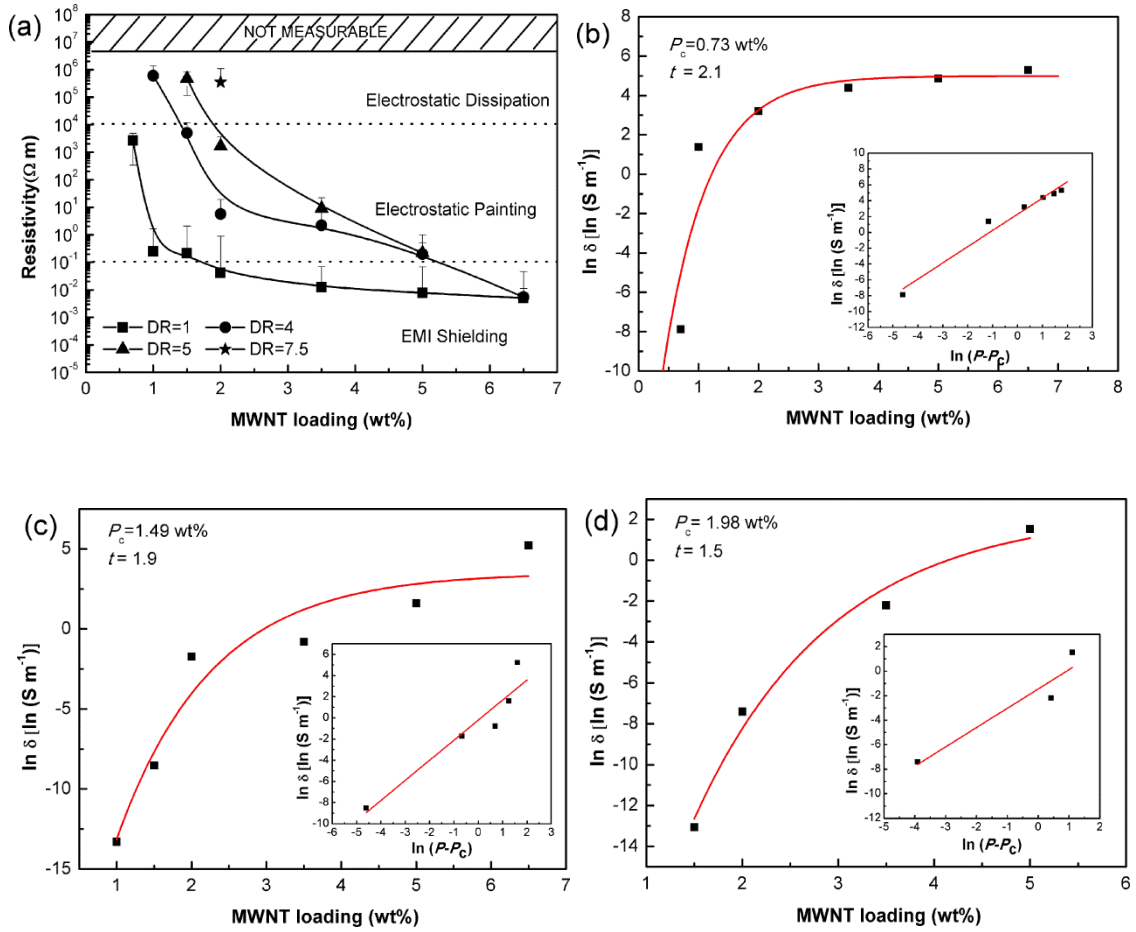

Figure 6.7 (a) Resistivity vs. nanotube loading of PLA/MWNT composites with various draw ratios; together with percolation equation fit to the experimental data of composites containing MWNTs at (b) DR=1, (c) DR=4, and (d) DR=5. Inset: a log-log plot of conductivity vs. reduced mass fraction determines the critical composition.

The electrical conductivities of isotropic and drawn PLA/MWNT composites all show typical percolation behaviour with increasing MWNT content (see Figure 6.7(b), (c) and (d)). To determine the percolation threshold P_c, the following scaling law is used:

$$\sigma = \sigma_0 (P - P_c)^t \qquad \textit{Equation 6.7}$$

where σ_0 is a scaling factor, σ is the conductivity of the nanocomposite and P is the filler content. The exponent t is an exponent which depends on the dimensionality of the

conductive network. A straight line with P_c = 0.73 wt.%, 1.49 wt.% and 1.98 wt.% gives a good fit for composite tapes of draw ratio 1, 4 and 5, respectively. Clearly, as expected the percolation threshold increases with draw ratio.

It is interesting to note that the conductivity of the composite tape with 2 wt.% MWNTs at draw ratio of 7.5 can still reach 10^{-6} S m^{-1} (3.5×10^5 Ω m), which is equivalent to conductivity levels of commercial conductive polymer fibres using carbon black as a conductive filler. For example, B31 conductive Terylene fibre of Japan Belltron and L602 conductive Terylene fibre of Japan Luana have both electrical resistivity of 10^6-10^8 Ω m [34].

Soroudi *et al.* [35] reported a conductive Panipol CXL (a polyaniline blend)/CNT modified PP fibre (7.5 wt.% CNTs) with resistivity of 6.25×10^{-2} Ω m. Li *et al.* [34] reported a poly(ethylene terephthalate) (PET) conductive fibre (0.6 wt.% CNTs) with a 'core-shell' structure, possessing a tensile strength of ~142 MPa and a bulk resistivity of 8×10^6 Ω m. Deng *et al.* [4] also produced a highly conductive (3.6×10^{-3} Ω m) and high-strength (500 MPa) PP tape (0.5 wt.% CNT) with a 'core-shell' structure,

Therefore, with the exception of 'core-shell' structures, the current PLA/MWNT tapes (2 wt.%, DR=7.5) are among the best compromises in terms of mechanical properties (5.5 GPa in Young's modulus, 156 MPa in strength) and electrical properties (3.5×10^5 Ω m in resistivity).

6.4 Conclusions

Conductive oriented PLA/MWNT tapes with enhanced mechanical properties were reported in this paper. Good dispersion of MWNTs in PLA matrix was observed by

SEM. With the addition of MWNTs, a percolating network was formed between 0.7 and 1 wt.%, and the long-range motion of PLA chains was highly restrained as a result. A high degree of MWNT alignment was already achieved at a draw ratio of 4. Both mechanical and electrical properties were strongly depended on the presence of MWNT and solid-state drawing. Micromechanical analysis showed that the reinforcing efficiency dE_c/dV_f increased from 30 GPa for isotropic composites to 195 GPa for oriented composite tapes, indicating that drawing greatly improved the effective reinforcement by MWNTs. A significant increase in electrical resistivity in drawn PLA/MWNT tapes as compared to isotropic films was observed. The electrical resistivity of oriented PLA/MWNT tapes ($\sim 3.5 \times 10^5\ \Omega$ m) was 7 orders of magnitude higher than that of isotropic composite films ($\sim 4 \times 10^{-2}\ \Omega$ m) at the same MWNT concentration (2 wt.%). Percolation threshold shifted from 0.73 wt.% to 1.98 wt.% after drawing 5 times. It is interesting to note that the nanocomposite tapes of 2 wt.% MWNTs and DR=7.5 have a volumetric electrical conductivity of 10^{-6} S m^{-1}, which similar to that of many commercial conductive fibres using carbon black as a conductive filler at much higher filler loadings.

6.5 References

1. Y. Bin, M. Kitanaka, D. Zhu, and M. Matsuo, *Development of highly oriented polyethylene filled with aligned carbon nanotubes by gelation/crystallization from solutions.* Macromolecules, 2003. **36**(16): p. 6213-6219.
2. Y. Bin, Q. Chen, K. Tashiro, and M. Matsuo, *Electrical and mechanical properties of iodine-doped highly elongated ultrahigh molecular weight polyethylene films filled with multiwalled carbon nanotubes.* Physical Review B, 2008. **77**(3): p. 035419.
3. P. Miaudet, C. Bartholome, A. Derre, M. Maugey, G. Sigaud, C. Zakri, and P. Poulin, *Thermo-electrical properties of PVA–nanotube composite fibres.* Polymer, 2007. **48**(14): p. 4068-4074.
4. H. Deng, T. Skipa, E. Bilotti, R. Zhang, D. Lellinger, L. Mezzo, Q. Fu, I. Alig, and T. Peijs, *Preparation of high-performance conductive polymer fibres through morphological control of networks formed by nanofillers.* Advanced Functional Materials, 2010. **20**(9): p.

1424-1432.

5. H. Deng, R. Zhang, C. T. Reynolds, E. Bilotti, and T. Peijs, *A novel concept for highly oriented carbon nanotube composite tapes or fibres with high strength and electrical conductivity.* Macromolecular Materials and Engineering, 2009. **294**(11): p. 749-755.

6. S. D. McCullen, K. L. Stano, D. R. Stevens, W. A. Roberts, N. A. Monteiro-Riviere, L. I. Clarke, and R. E. Gorga, *Development, optimization, and characterization of electrospun poly(lactic acid) nanofibres containing multi‐walled carbon nanotubes.* Journal of Applied Polymer Science, 2007. **105**(3): p. 1668-1678.

7. Z. Li, X. Zhao, L. Ye, P. Coates, F. Caton-Rose, and M. Martyn, *Structure and blood compatibility of highly oriented PLA/MWNTs composites produced by solid hot drawing.* Journal of Biomaterials Applications, 2013: p. 0885328213490047.

8. H. Li, and M.A. Huneault, *Effect of nucleation and plasticization on the crystallization of poly (lactic acid).* Polymer, 2007. **48**(23): p. 6855-6866.

9. F. Mai, K. Wang, M. Yao, H. Deng, F. Chen, and Q. Fu, *Superior reinforcement in melt-spun polyethylene/multiwalled carbon nanotube fibre through formation of a shish-kebab structure.* The Journal of Physical Chemistry B, 2010. **114**(33): p. 10693-10702.

10. R. G. Larson, *The structure and rheology of complex fluids*. Vol. 4. 1999: Oxford university press New York.

11. W. Cox, and E. Merz, *Correlation of dynamic and steady flow viscosities.* Journal of Polymer Science, 1958. **28**(118): p. 619-622.

12. D. Wu, L. Wu, M. Zhang, and Y. Zhao, *Viscoelasticity and thermal stability of polylactide composites with various functionalized carbon nanotubes.* Polymer Degradation and Stability, 2008. **93**(8): p. 1577-1584.

13. S. I. Moon, F. Jin, C. j. Lee, S. Tsutsumi, and S. H. Hyon, *Novel carbon nanotube/poly(L-lactic acid) nanocomposites; their modulus, thermal stability, and electrical conductivity*. in *Macromolecular Symposia*. 2005. Wiley Online Library.

14. C. F. Kuan, H. C. Kuan, C. C. M. Ma, and C. H. Chen, *Mechanical and electrical properties of multi-wall carbon nanotube/poly(lactic acid) composites.* Journal of Physics and Chemistry of Solids, 2008. **69**(5): p. 1395-1398.

15. J. T. Yoon, Y. G. Jeong, S. C. Lee, and B. G. Min, *Influences of poly(lactic acid)-grafted carbon nanotube on thermal, mechanical, and electrical properties of poly(lactic acid).* Polymers for Advanced Technologies, 2009. **20**(7): p. 631-638.

16. K. Chrissafis, K. Paraskevopoulos, A. Jannakoudakis, T. Beslikas, and D. Bikiaris, *Oxidized multiwalled carbon nanotubes as effective reinforcement and thermal stability agents of poly(lactic acid) ligaments.* Journal of Applied Polymer Science, 2010. **118**(5): p. 2712-2721.

17. R. M. Novais, F. Simon, P. Pötschke, T. Villmow, J. A. Covas, and M. C. Paiva, *Poly (lactic acid) composites with poly (lactic acid) ‐modified carbon nanotubes.* Journal of Polymer Science Part A: Polymer Chemistry, 2013. **51**(17): p. 3740-3750.

18. H. S. Kim, Y. S. Chae, B. H. Park, J. S. Yoon, M. Kang, and H. J. Jin, *Thermal and electrical conductivity of poly (l-lactide)/multiwalled carbon nanotube nanocomposites.* Current Applied Physics, 2008. **8**(6): p. 803-806.

19. W. M. Chiu, H. Y. Kuo, P. A. Tsai, and J. H. Wu, *Preparation and properties of poly (lactic acid) nanocomposites filled with functionalized single-walled carbon nanotubes.* Journal of Polymers and the Environment, 2013. **21**(2): p. 350-358.

20. M. F. Yu, O. Lourie, M. J. Dyer, K. Moloni, T. F. Kelly, and R. S. Ruoff, *Strength and breaking mechanism of multiwalled carbon nanotubes under tensile load.* Science, 2000.

287(5453): p. 637-640.

21. D. Qian, E. C. Dickey, R. Andrews, and T. Rantell, *Load transfer and deformation mechanisms in carbon nanotube-polystyrene composites.* Applied Physics Letters, 2000. **76**(20): p. 2868-2870.
22. M. Cadek, J. Coleman, V. Barron, K. Hedicke, and W. Blau, *Morphological and mechanical properties of carbon-nanotube-reinforced semicrystalline and amorphous polymer composites.* Applied Physics Letters, 2002. **81**(27): p. 5123-5125.
23. J. Gao, M. E. Itkis, A. Yu, E. Bekyarova, B. Zhao, and R. C. Haddon, *Continuous spinning of a single-walled carbon nanotube-nylon composite fibre.* Journal of the American Chemical Society, 2005. **127**(11): p. 3847-3854.
24. M. Treacy, T. Ebbesen, and J. Gibson, *Exceptionally high Young's modulus observed for individual carbon nanotubes.* Nature, 1996. **381**: p. 678 - 680.
25. E. W. Wong, P. E. Sheehan, and C. M. Lieber, *Nanobeam mechanics: elasticity, strength, and toughness of nanorods and nanotubes.* Science, 1997. **277**(5334): p. 1971-1975.
26. P. Poncharal, Z. Wang, D. Ugarte, and W. A. De Heer, *Electrostatic deflections and electromechanical resonances of carbon nanotubes.* Science, 1999. **283**(5407): p. 1513-1516.
27. Z. Pan, S. Xie, L. Lu, B. Chang, L. Sun, W. Zhou, G. Wang, and D. Zhang, *Tensile tests of ropes of very long aligned multiwall carbon nanotubes.* Applied Physics Letters, 1999. **74**(21): p. 3152-3154.
28. D. Wu, L. Wu, W. Zhou, Y. Sun, and M. Zhang, *Relations between the aspect ratio of carbon nanotubes and the formation of percolation networks in biodegradable polylactide/carbon nanotube composites.* Journal of Polymer Science Part B: Polymer Physics, 2010. **48**(4): p. 479-489.
29. J. A. Cicero, J. R. Dorgan, J. Janzen, J. Garrett, J. Runt, and J. S. Lin, *Supramolecular morphology of two-step, melt-spun poly(lactic acid) fibres.* Journal of Applied Polymer Science, 2002. **86**(11): p. 2828-2838.
30. F. Du, J. E. Fischer, and K. I. Winey, *Coagulation method for preparing single‐walled carbon nanotube/poly (methyl methacrylate) composites and their modulus, electrical conductivity, and thermal stability.* Journal of Polymer Science Part B: Polymer Physics, 2003. **41**(24): p. 3333-3338.
31. H. Deng, R. Zhang, E. Bilotti, J. Loos, amd T. Peijs, *Conductive polymer tape containing highly oriented carbon nanofillers.* Journal of Applied Polymer Science, 2009. **113**(2): p. 742-751.
32. P. Pötschke, H. Brünig, A. Janke, D. Fischer, and D. Jehnichen, *Orientation of multiwalled carbon nanotubes in composites with polycarbonate by melt spinning.* Polymer, 2005. **46**(23): p. 10355-10363.
33. F. Du, J. E. Fischer, and K. I. Winey, *Effect of nanotube alignment on percolation conductivity in carbon nanotube/polymer composites.* Physical Review B, 2005. **72**(12): p. 121404.
34. Z. Li, G. Luo, F. Wei, and Y. Huang, *Microstructure of carbon nanotubes/PET conductive composites fibres and their properties.* Composites Science and Technology, 2006. **66**(7): p. 1022-1029.
35. A. Soroudi, and M. Skrifvars, *Melt blending of carbon nanotubes/polyaniline/polypropylene compounds and their melt spinning to conductive fibres.* Synthetic Metals, 2010. **160**(11): p. 1143-1147.

Chapter 7.

Poly(lactic acid)/carbon nanotube nanocomposites with integrated degradation sensing

7.1 Introduction

Numerous hydrolytic degradation tests have been performed on PLA in order to simulate its process of degradation in the human body (T ~37 ^{o}C) [1-6] and in natural media such as soil or compost (25 ^{o}C < T < 58 ^{o}C) [7-9], all reporting that PLA can be hydrolysed to give low molecular weight water-soluble oligomers. It has been found that degradability can be modified significantly by changing the microstructure of the PLA [10], or by blending with other polymers, additives, plasticizers and often inorganic fillers [11, 12]. However, to the best of our knowledge, so far there is no report on the development of a degradation monitoring system, which would give on-line information regarding structural safety during the products lifetime, while at the same time reducing inspection and/or maintenance costs.

Chapter 5 reviewed some reports on polymer/carbon nanotube (CNT) composites as sensing materials for various stimuli, including temperature [13], gases [14], vapour [15], mechanical stress and strain [16, 17], pH [18], and liquids [19]. Generally, the underlying mechanism is that the introduced external stimuli results in a deformation of the CNT percolation network, thus leading to a change in electrical conductivity of the composites.

In this chapter, we pioneered the use of the evolution of electrical resistivity as a means to monitor poly(lactic acid) (PLA) degradation. As the morphology of the polymer changes during degradation, it results in a change of the filler network, thus leading to a change in electrical resistivity of the nanocomposites. Therefore, through the evolution of the electrical signal during PLA degradation, we will be able to correlate changes in electrical resistivity with degradation levels of the polymer.

Two different mediums were used to understand the degradation behaviour. Phosphate-buffered solution (PBS) is usually used to simulate *in vivo* conditions, while water is more related to environmental conditions. Various techniques were performed to study the hydrolytic degradation and morphological changes of PLA.

7.2 Experimental

7.2.1 Materials

Multi-walled carbon nanotubes (MWNTs) (NC7000®) were supplied by Nanocyl S. A., Belgium. MWNTs were used as received without purification. Ingeo® PLLA 3051D was purchased from RESINEX, United Kingdom. Phosphate buffered saline (PBS) powder was obtained from Sigma-Aldrich Chemical Co.

7.2.2 Sample preparation

MWNTs were melt-blended with PLA using a DSM X'plore 15 Mini-extruder (The Netherlands), at 180 ^{o}C and 100 rpm for 3 min to prepare masterbatch containing 15 wt.% MWNTs. This masterbatch was then diluted with neat PLA to the desired CNT concentration using the same processing conditions. Nitrogen gas flow was used to

minimize degradation of the polymer during the compounding process. The extruded strands were successively pelletized and compression moulded into films of 130 μm thickness using a hot press (Dr. Collin, P300E, Germany) at 180 ^{o}C for 3 min.

7.2.3 Hydrolytic degradation

Five rectangular samples of dimensions 60 mm × 4 mm × 0.15 mm were dried and immersed in glass vials (30 ml) of distilled water (25 ml) or PBS (25 ml) at pH 7.4 ± 0.2. The sealed vials were then placed in a hot water bath at the degradation temperature of 50 ^{o}C. Temperature plays a key role in the degradation rate of PLA. Zhang *et al.* [20] studied the hydrolytic degradation of PLA in water at temperatures close to T_g. They found that the weight loss speed of amorphous PLA at 60 ^{o}C was about 3 times faster than that at 50 ^{o}C. About 32% of the weight of amorphous PLA was lost after only 11 days at 60 ^{o}C. Hakkarainen *et al.* [21] reported similar results for PLA degradation in PBS. 33% of the molecular weight was lost after only 3 days when hydrolysis temperature was raised to 60 ^{o}C. In our preliminary tests, we found that PLA and its nanocomposites fractured into many pieces after 3 days at 75 ^{o}C. Therefore, in order to keep the samples intact for further tests, a lower temperature of 50 ^{o}C thus a slower degradation speed was chosen in present work. After selected immersion periods, specimens were removed from the vials, washed several times with distilled water and dried in desiccator until constant weight (see Figure 7.1). The weight losses of the samples were not applied to quantify the degradation here, since the very small amount of thin films gave big fluctuations when measuring using scales. Therefore, changes in molecular weight were used to measure the hydrolytic degradation.

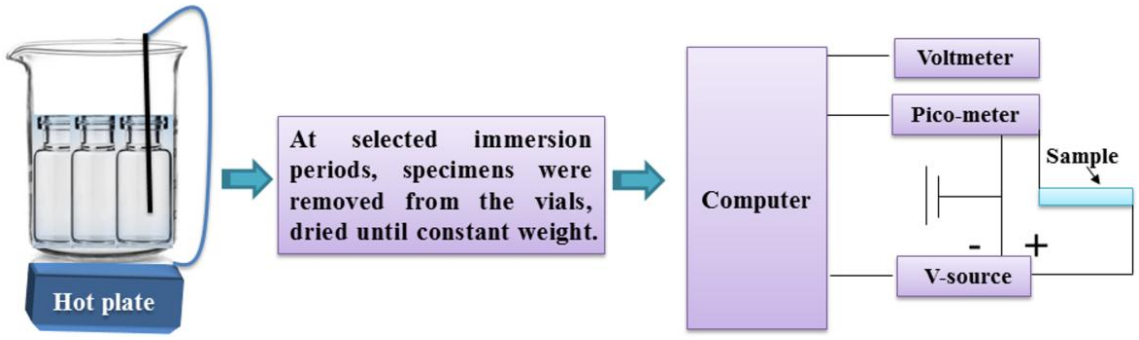

Figure 7.1 Sketch of hydrolytic degradation and electrical resistance measurement.

7.2.4 Characterization

Morphological studies were carried out on gold-coated samples using scanning electron microscopy (SEM) (FEI Inspector-F, The Netherlands).

Number average molecular weight (M_n) was determined by gel permeation chromatography (GPC). The same method and equipment were used as described in Chapter 3.

Differential scanning calorimetry (DSC) (Mettler-Toledo 822e) was used to investigate the thermal properties of the PLA films before and after degradation. All samples were heated to 200 ^oC at 10 ^oC min^{-1}. Crystallinity was determined using the heat of fusion of 100% crystalline PLA [22].

The morphological analysis by X-ray diffraction (XRD) was performed on a Siemens D5000 Diffractometer using Cu (K_α) radiation (wavelength: 1.54 Å) at room temperature in the range of $2\theta = 5^o$ to 40^o with a scanning rate of 2^o min^{-1}.

Infrared spectra (FT-IR) in the attenuated total reflection mode (ATR) were obtained on a Brüker Tensor 27 spectrometer. The samples were analysed in 4000 to 600 cm^{-1} range with a 4 cm^{-1} resolution.

The electrical conductivity of all films was measured by a simple two-point measurement using a picoammeter (Keithley 6485) and a DC voltage source (Agilent 6614C). Silver paste coating was used to ensure good contact with the electrodes of the electrometer. The volume resistivity was calculated in relation to the specimen dimensions. The measured volume resistance, R_V, was converted to volume resistivity, using the formula:

$$\rho = R_V \frac{A}{L} \qquad \textit{Equation 7.1}$$

where A is the effective area of the specimen and L is the specimen length. For specimens with a resistivity exceeding 10^{10} Ω, electrical resistivity is no longer measurable and the films are considered as 'non-conductive'. Three specimens for each composite were tested, and average value was reported.

7.3 Results and discussion

7.3.1 Hydrolytic degradation and morphological changes

Morphology changes of PLA during hydrolysis are investigated first. The appearance of neat PLA films changes after degradation. As shown in Figure 7.2, as degradation time increases, sample becomes relative opaque and brittle in both mediums. The opacity is probably attributed to light scattering due to the presence of water/degradation products/holes, or the evolution in crystallinity.

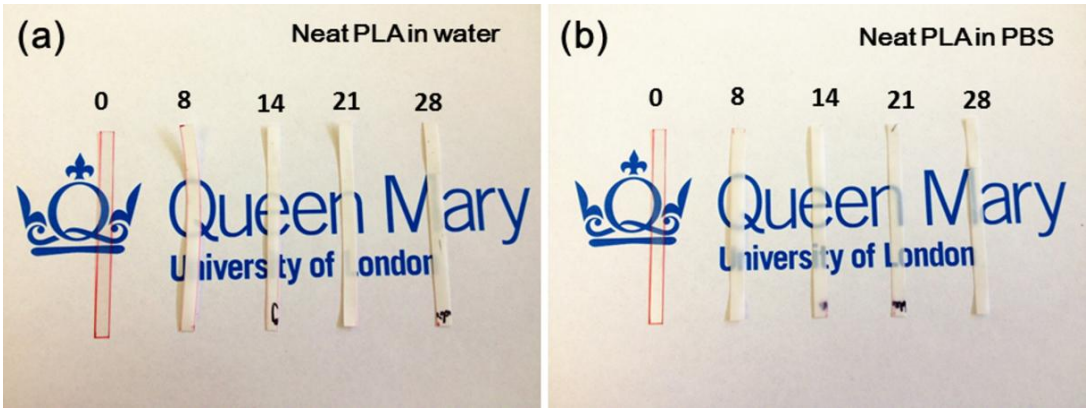

Figure 7.2 Optical images of the pure PLA samples degraded in (a) water and (b) PBS.

The morphology change on the sample surface is also observed using SEM (see Figure 7.3). Before degradation, the surface is smooth while after 28 days degradation in PBS several micro-holes are observed on the surface. This indicates that degradation occurs in present work.

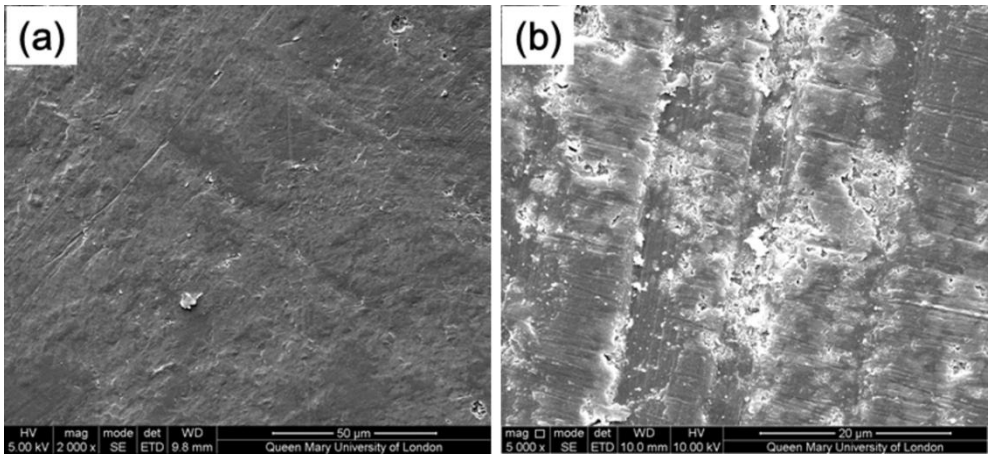

Figure 7.3 Surface morphology of pure PLA sample before (a) and after degradation in PBS for 28 days (b).

The M_n values of PLA films before and after hydrolysis are plotted in Figure 7.4 as a function of hydrolysis time. The M_n of the PLA films decreases linearly with hydrolysis time in both mediums, which means that the hydrolysis rates are constant corroborating

previous observations [20]. Accordingly, complete hydrolysis of PLA, in similar conditions, takes place at two stages. During the first stage, a rapid decrease in molecular weight was observed; while during the second stage, the decrease rate was much slower with increasing hydrolysis time. Therefore, the hydrolysis time range studied was most likely within the first stage of PLA degradation. After 28 days of degradation, M_n decreases by about 68% in water (from 72,633 g mol^{-1} to 22,991 g mol^{-1}), and by around 84% in PBS (from 72,633 g mol^{-1} to 11,593 g mol^{-1}). These results indicate that PBS leads to greater degradation than water because hydrolysed oligomers of PLA are swollen and solubilized more easily in PBS in the form of Na-salts as soon as they are produced. Consequently PLA chains undergo accelerated degradation before concomitant dissolution at extended hydrolysis time.

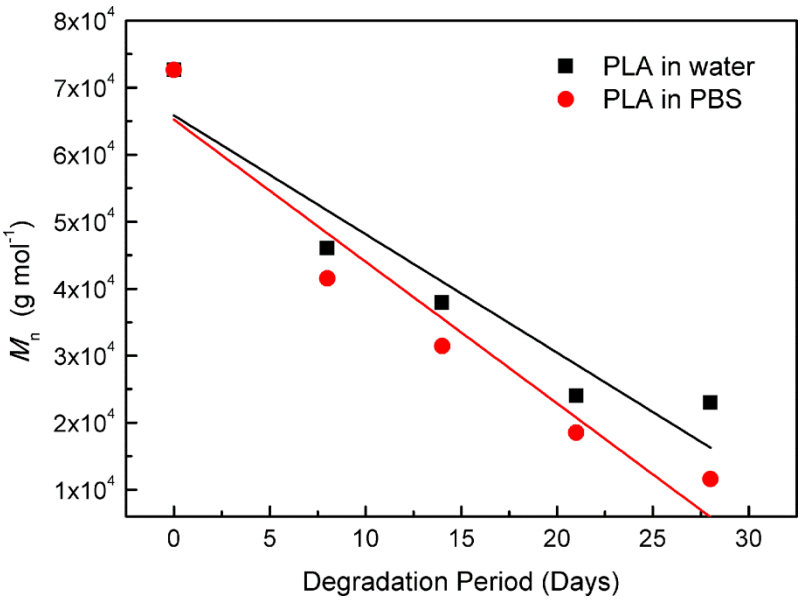

Figure 7.4 Residual molecular weights (M_n) of PLA films as a function of degradation time.

The morphology changes during hydrolysis appear clearly in the WAXD spectra of the samples (see Figure 7.5). It can be noticed that both neat PLA and PLA/1CNT

nanocomposites, which initially show only an amorphous halo, clearly exhibit crystalline peaks already after 8 days degradation in water. The main 2θ peak at 16.5^{o} is indexed as a (200)/(110) reflection of α-form homo-crystal structure. This stable α-form homo-crystal structure is found as the major component in PLA or PLA/CNT residues after degradation. The intensity of the peak at 16.5^{o} increases with degradation time, which means that crystallinity increases after hydrolysis.

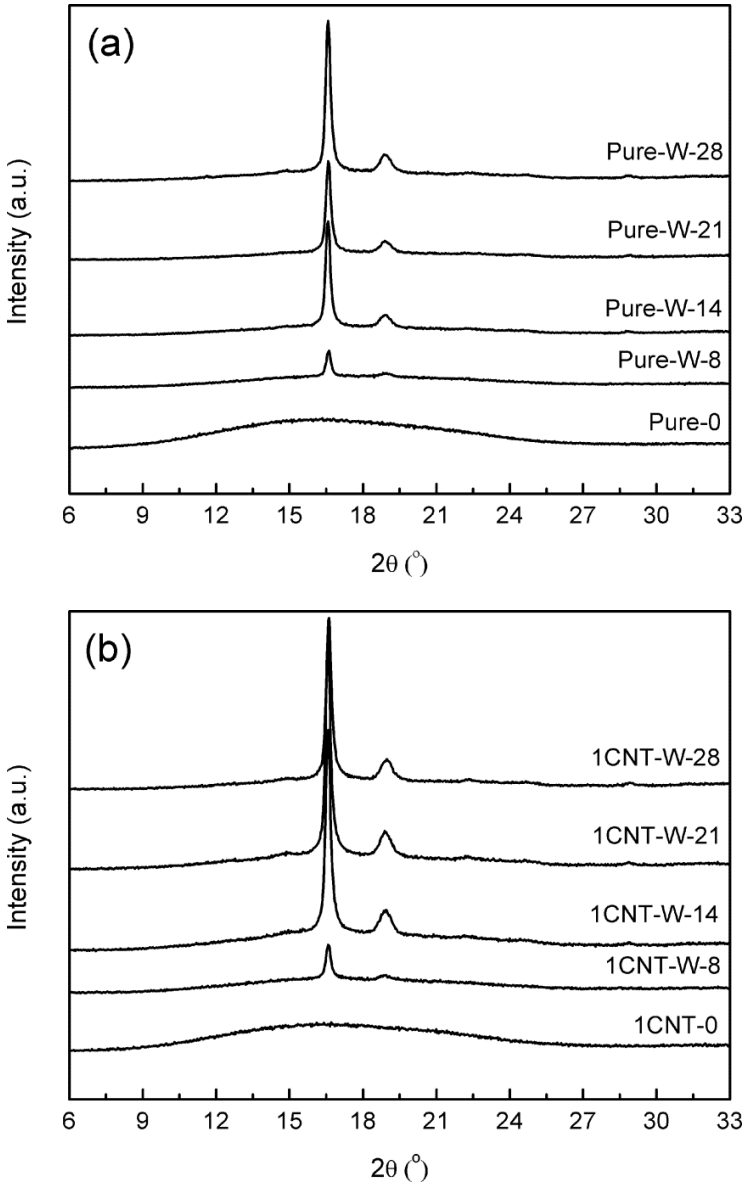

Figure 7.5 WAXD spectra of (a) neat PLA and (b) PLA/1CNT before and after selected times of hydrolysis.

This increase of crystallinity during hydrolysis can also be assessed by FT-IR, and the results are shown in Figure 7.6. It can be seen that the absorption band at 923 cm^{-1} (due to flexural C-H bond vibration), representative of the crystalline structure of PLA increases with hydrolysis time for samples degraded in both medium.

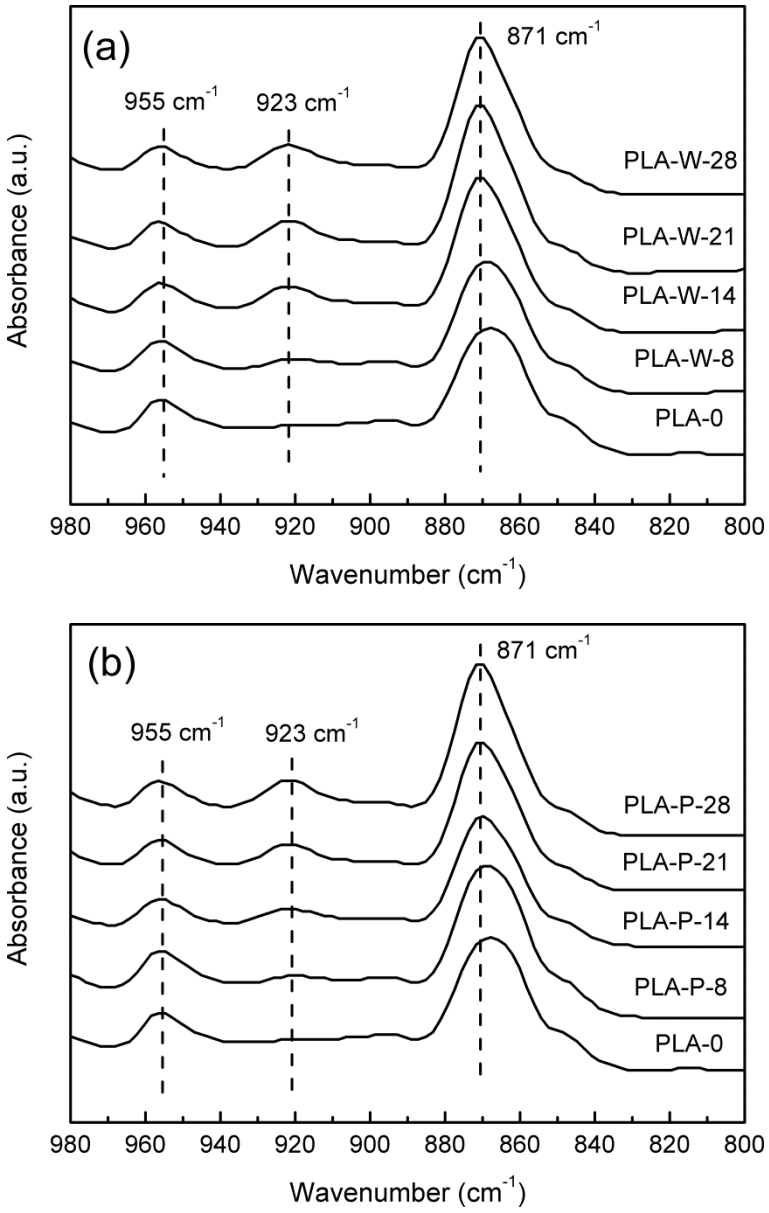

Figure 7.6 FT-IR spectra of neat PLA before and after selected times of hydrolysis in (a) water and (b) PBS.

Many studies have investigated the degradation behaviour of PLA. From these studies it is generally concluded that degradation proceeds through two main stages [21]. First, water diffuses into the amorphous regions as these phases allow water to penetrate more easily than the highly ordered and densely packed crystalline regions. The second stage starts in the crystalline regions when most or all of the amorphous regions have been removed. In order to better understand the effect of crystallinity on the degradation behaviour of PLA, DSC was performed.

Figure 7.7 shows the DSC scans of PLA films before and after hydrolysis for 28 days and Table 7.1 gathers the related values of glass transition temperature (T_g), melting temperature (T_m) and crystallinity (X_c). The glass transition endothermic peak at around 60 ^oC is supressed after the hydrolysis period. This confirms the preferential degradation of the amorphous phase. A small amount of amorphous chains is left in the residues as reported by Tsuji *et al.* [23]. On the other hand, a crystallization exothermic peak at around 134 ^oC is observed, which probably can be attributed to crystallites formed during DSC heating [24].

Table 7.1 Thermal properties obtained by DSC of PLA before and after degradation.

Sample	T_g [^oC]	T_m [^oC]	X_c [%]
PLA no degradation	62.8	149.1	1.6
PLA in water 28days	-	152.2	32.1
PLA in PBS 28days	-	151.8	36.5

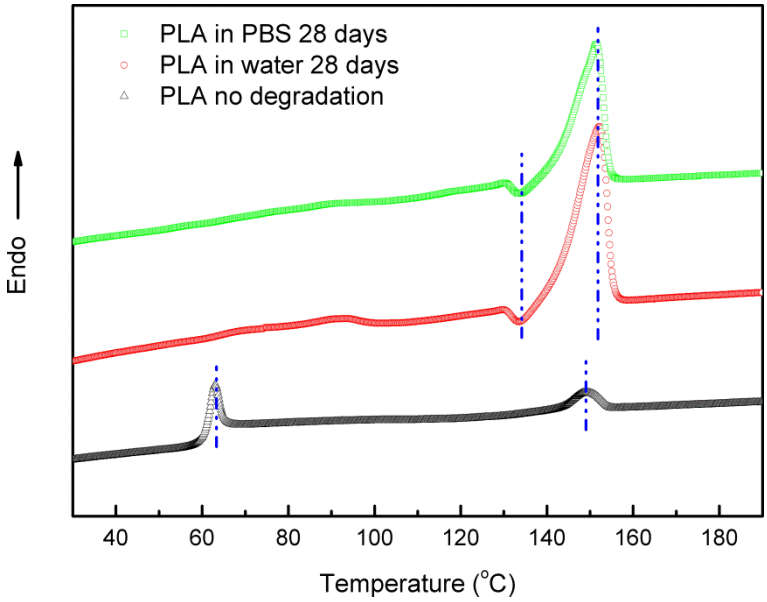

Figure 7.7 DSC scans of PLA films before and after degradation.

As seen in Figure 7.7 and Table 7.1, the T_m of PLA before hydrolysis shifted from 149.1 ^oC to 152.2 ^oC and 151.8 ^oC for PLA films degraded in water and PBS after 28 days, respectively. T_m for both degraded films show a 2 ^oC increase, which indicates that lamellae become thicker after degradation. On the other hand, the crystallinity values of both degraded PLA films in water and PBS increase after 28 days. This increase in crystallinity of PLA upon degradation is likely to be attributed to partial selective removal of PLA chains from free and restricted amorphous regions [20] and/or recrystallizaton from plastisticization effect due to the presence of tie-chain segments and water diffusion [25].

In conclusion, the reduced T_g and increased X_c of samples after degradation confirms that amorphous regions within the PLA have been partial removed.

7.3.2 Degradation sensing

As shown in Chapter 6, the percolation threshold for PLA/CNT isotropic films is around 0.7 wt.%. In this section, it will be demonstrated that the PLA/CNT films are not only electrically conductive but are also sensitive to degradation stimuli. Figure 7.8 shows the degradation of PLA/CNT films with different filler loadings in both mediums.

As seen in Figure 7.8a, typically resistivity decreases upon degradation in water. However, different nanotube concentrations lead to significant differences in sensitivity of the electrical signal. Resistivity remains almost constant for nanocomposites with 3 wt.% CNTs, while upon lowering the CNT content to 1 wt.%, a slight change in resistivity within one order of magnitude is observed. Similar behaviour is also observed for nanocomposites with 0.8 wt.% CNTs. Here, the change in resistivity is approximately two orders of magnitude, which indicates that a lower CNT concentration makes the system more sensitive as expected [15]. For composites with a CNT loading around the percolation threshold of 0.7 wt.% resistivity is dramatically reduced compared to higher concentrations. Here, the resistivity value changes about four orders of magnitude. Nanocomposites containing CNT concentrations below the percolation threshold (0.5 wt.%) were also investigated. The initial resistivity value for these composites is above 10^6 Ohm.m, which is outside the measurement range for the current experimental set-up. The results show that even after 14 days degradation in water resistivity is still not measurable. There is however a sudden drop in resistivity after 21 days of degradation, while it becomes constant quickly after that. In other words, the nanocomposites with 0.5 wt.% CNTs seem less sensitive over a wide

degradation time range than nanocomposites with 0.7 wt.% CNTs. However, the first sensory systems could still be of interest as they respond more in an on/off fashion rather than show a gradual change.

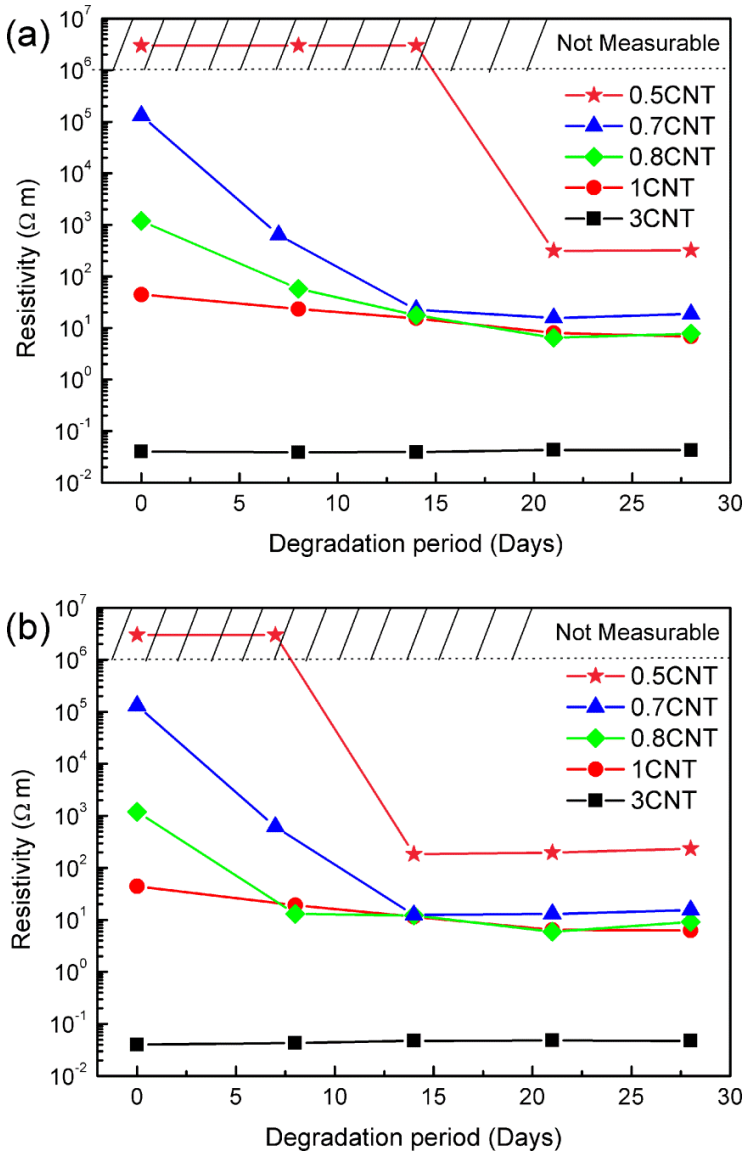

Figure 7.8 Evolution of resistivity during degradation for various composites degraded in (a) water and (b) PBS.

Changes in resistivity for composites degraded in PBS are fairly similar as in water (see Figure 7.8b). However, after 14 days of degradation in PBS the nanocomposites with

0.5 wt.% CNTs become conductive, while the sample degraded in water during the same period remains non-conductive. According to GPC results, this is due to the lower molecular weight attesting for a faster degradation in PBS. However, resistivity values of nanocomposites containing 0.5 wt.% CNTs degraded within 14 days are still not measurable. In short, these results indicate that composites with a CNT loading around the percolation threshold show greater sensitivity and the strongest signal change. These results can be explained from the well-established percolation theory [26], which states that conductive polymer composites (CPCs) with filler content close to the percolation threshold give sharper responses to changes in their environment. It is interesting to note that degradation sensing with CPCs results in a reduction in resistivity, i.e. and increase in conductivity due to an improved conductive network. Sensing of most other stimuli such as strain [27], damage [28], temperature [29], liquids and vapour [15] typically result in an increase in resistivity due to a break-down of the conductive network.

When CNTs are blended with semi-crystalline polymers, the nanotubes tend to be located in the amorphous phase, since chain folding expels the CNTs from the crystalline phase [30]. According to DSC results degradation partly removes amorphous PLA, which will directly result in a change in CNT network density within that phase.

In present study, the observed decrease in resistivity of the CPC, rather than the increase in resistivity as generally observed when sensing most other stimuli, can be explained on the basis of the volume exclusion theory. According to WAXD and DSC data, degradation partially removes the amorphous phase and induces re-crystallization of PLA. As CNTs are excluded from crystalline regions, an increased CNT network

density results in an increased effective CNT concentration in the amorphous phase (see Figure 7.9). The calculation of the effective CNT loading is based on assuming that CNTs are located in the amorphous phase. For instance, for nanocomposites containing 0.7 wt.% CNTs, if the total weight of the nanocomposites is 100 g, then the weight of CNTs in the nanocomposites is 0.7 g. Before degradation, the crystallinity is 1.6%, which means that the weight of the amorphous phase is (100-0.7) g × (1-1.6%) = 83.412 g. Therefore, the effective CNT loading in the nanocomposites is (0.7 g/83.412 g) × 100 ≈ 0.8 wt.%. However, after 28 days degradation in water, a part of the amorphous phase is removed, and the weight of the remaining amorphous phase is (100-0.7) g × (1-32%) = 67.524 g. Thus, the effective CNT loading now increases to (0.7 g/67.524 g) × 100 ≈ 1.0 %.

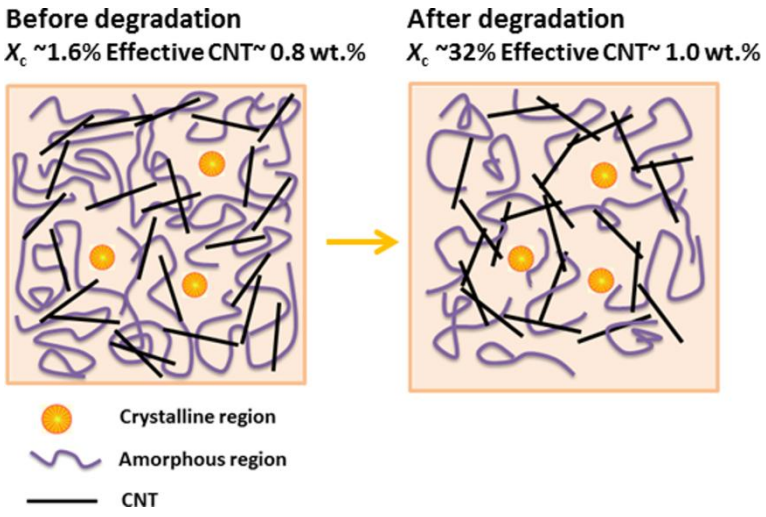

Figure 7.9 Schematic image of CNT network change after degradation. CNTs are presented in black and are not to scale. CNT network density increases due to the partial removal of amorphous phase.

The experimental data together with the theoretically predicted electrical conductivity using volume exclusion theory is plotted in Figure 7.10 as a function of CNT loading

for composites before and after 28 days degradation in water. Theoretical predictions fit the experimental data well. The volume exclusion effect in the formation of conductive paths due to the removal of amorphous phase is only operative at lower concentrations. At higher concentrations, the conductivity is almost undisturbed. This is probably due to the fact that composites containing 3 wt.% CNTs have already a very robust network and hence, polymer degradation does not lead to major changes in local nanotube densities.

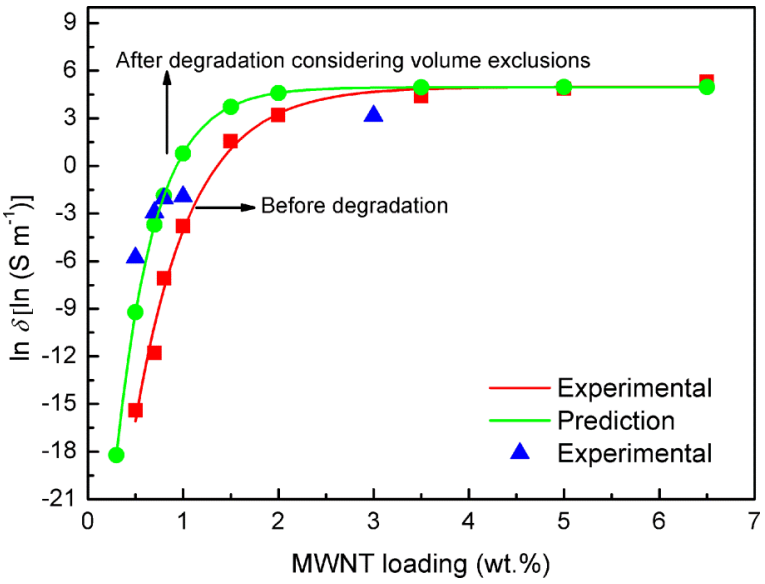

Figure 7.10 Experimental and predicted percolation threshold (P_c) based on volume exclusion theory of PLA/CNT composites before and after 28 days degradation in water. (Considering X_c = 32% for all degraded samples).

Figure 7.11 correlates the molecular weight of pure PLA with the corresponding electrical resistivity of the various nanocomposites. The curves show a similar trend as in Figure 7.8. Hence, by detecting an electrical signal change within this CPC film we are able to obtain on-line information of the degradation level of the PLA matrix without damaging the product. In summary, the developed PLA/CNT nanocomposites

demonstrated good degradation sensing capabilities at CNT concentrations around the percolation threshold, making them interesting candidates for applications in smart biocomposites.

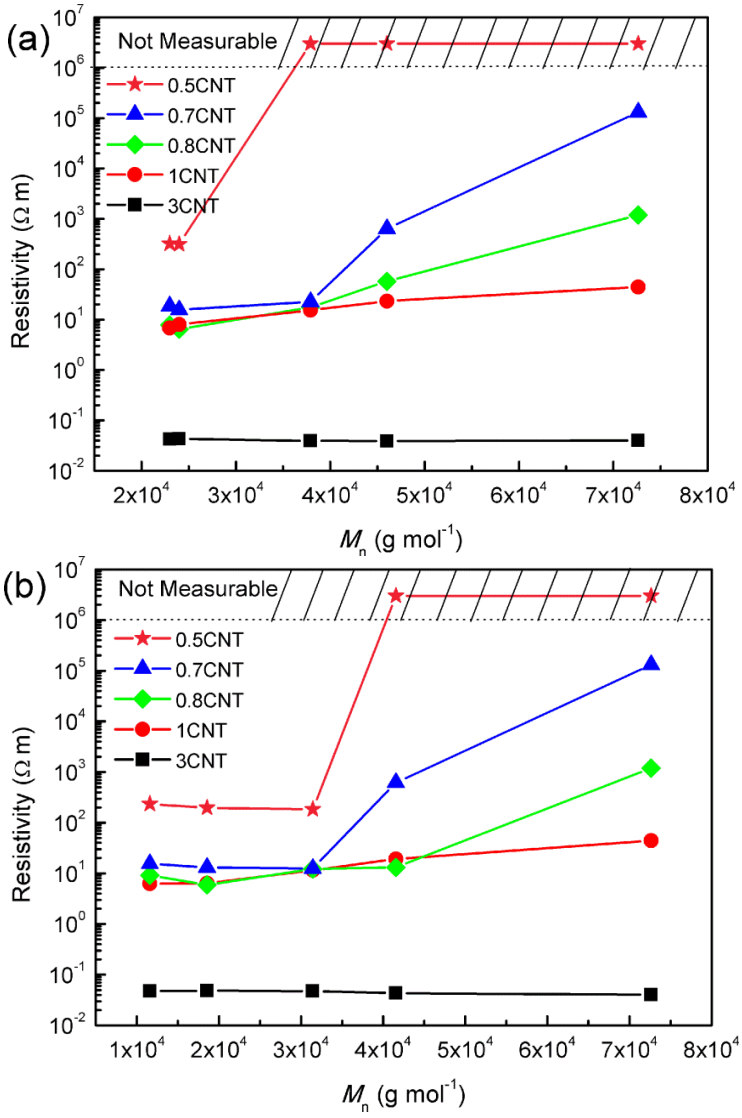

Figure 7.11 Correlation between residual molecular weight of pure PLA and corresponding electrical resistivity of nanocomposites degraded in (a) water and (b) PBS.

7.4 Conclusions

A degradation sensor based on PLA/CNTs has been successfully prepared. Nanocomposites with a CNT loading around the percolation threshold gave the highest sensitivity and strongest signal change. The observed increase in conductivity is due to an increased CNT network density after partial removal of the amorphous phase of the semi-crystalline polymer matrix. Such an in-situ degradation monitoring system would give on-line information regarding degradation level and makes it a good candidate for applications in smart biocomposite products. It should be noted that the degraded nanocomposites are too brittle to perform mechanical tests. The samples broke in the clamps during the test. Therefore, there is no correlation study between the mechanical properties and the electrical resistivity in this work.

In the current work non-oriented isotropic films were studied which can be used as stand-alone products but can also be applied to functionalise PLA products through the addition of a smart PLA surface coating or film. Such a degradation sensitive surface film could be very thin, thus reducing the overall quantity of CNTs needed in the final product. Moreover, the resulting overall reduction in CNTs required should have added benefits in terms of recyclability, biodegradability and compostability of these modified PLA products.

7.5 References

1. S. M. Li, I. Rashkov, J. L. Espartero, N. Manolova, and M. Vert, *Synthesis, characterization, and hydrolytic degradation of PLA/PEO/PLA triblock copolymers with long poly(L-lactic acid) blocks.* Macromolecules, 1996. **29**(1): p. 57-62.

2. S. K. Saha, and H. Tsuji, *Effects of molecular weight and small amounts of d-lactide units on hydrolytic degradation of poly(l-lactic acid)s.* Polymer Degradation and Stability, 2006. **91**(8): p. 1665-1673.

3. H. Tsuji, and C. A. Del Carpio, *In vitro hydrolysis of blends from enantiomeric poly(lactide)s. 3. Homocrystallized and amorphous blend films.* Biomacromolecules, 2003. **4**(1): p. 7-11.

4. H. Pistner, R. Gutwald, R. Ordung, J. Reuther, and J. Mühling, *Poly(l-lactide): a long-term degradation study in vivo: I. Biological results.* Biomaterials, 1993. **14**(9): p. 671-677.

5. H. Pistner, H. Stallforth, R. Gutwald, J. Mühling, J. Reuther, and C. Michel, *Poly(l-lactide): a long-term degradation study in vivo: II: physico-mechanical behaviour of implants.* Biomaterials, 1994. **15**(6): p. 439-450.

6. H. Pistner, D. R. Bendi, J. Mühling, and J. F. Reuther, *Poly(l-lactide): a long-term degradation study in vivo: III. Analytical characterization.* Biomaterials, 1993. **14**(4): p. 291-298.

7. M. A. Paul, C. Delcourt, M. Alexandre, P. Degée, F. Monteverde, and P. Dubois, *Polylactide/montmorillonite nanocomposites: study of the hydrolytic degradation.* Polymer Degradation and Stability, 2005. **87**(3): p. 535-542.

8. G. Ganjyal, R. Weber, and M. Hanna, *Laboratory composting of extruded starch acetate and poly(lactic acid) blended foams.* Bioresource Technology, 2007. **98**(16): p. 3176-3179.

9. R. Iovino, R. Zullo, M. Rao, L. Cassar, and L. Gianfreda, *Biodegradation of poly(lactic acid)/starch/coir biocomposites under controlled composting conditions.* Polymer Degradation and Stability, 2008. **93**(1): p. 147-157.

10. S. Iannace, A. Maffezzoli, G. Leo, and L. Nicolais, *Influence of crystal and amorphous phase morphology on hydrolytic degradation of PLLA subjected to different processing conditions.* Polymer, 2001. **42**(8): p. 3799-3807.

11. R. A. Miller, J. M. Brady, and D. E. Cutright, *Degradation rates of oral resorbable implants (polylactates and polyglycolates): rate modification with changes in PLA/PGA copolymer ratios.* Journal of Biomedical Materials Research, 2004. **11**(5): p. 711-719.

12. T. M. Wu, and C. Y. Wu, *Biodegradable poly(lactic acid)/chitosan-modified montmorillonite nanocomposites: Preparation and characterization.* Polymer Degradation and Stability, 2006. **91**(9): p. 2198-2204.

13. J. R. Wood, Q. Zhao, M. D. Frogley, E. R. Meurs, A. D. Prins, T. Peijs, D. J. Dunstan, and H. D. Wagner, *Carbon nanotubes: from molecular to macroscopic sensors.* Physical Review B, 2000. **62**(11): p. 7571-7575.

14. J. K. Abraham, B. Philip, A. Witchurch, V. K. Varadan, and C. C. Reddy, *A compact wireless gas sensor using a carbon nanotube/PMMA thin film chemiresistor.* Smart Materials and Structures, 2004. **13**(5): p. 1045-1049.

15. B. Kumar, M. Castro, and J-F. Feller, *Poly(lactic acid)–multi-wall carbon nanotube conductive biopolymer nanocomposite vapour sensors.* Sensors and Actuators B: Chemical, 2012. **161**(1): p. 621-628.

16. R. Zhang, M. Baxendale, and T. Peijs, *Universal resistivity-strain dependence of carbon nanotube/polymer composites.* Physical Review B, 2007. **76**(19): p. 195433.

17. E. Bilotti, R. Zhang, H. Deng, M. Baxendale, and T. Peijs, *Fabrication and property prediction of conductive and strain sensing TPU/CNT nanocomposite fibres.* Journal of Materials Chemistry, 2010. **20**(42): p. 9449-9455.

18. N. Ferrer-Anglada, M. Kaempgen, and S. Roth, *Transparent and flexible carbon nanotube/polypyrrole and carbon nanotube/polyaniline pH sensors.* Physica Status Solidi (b), 2006. **243**(13): p. 3519-3523.

19. P. Pötschke, T. Andres, T. Villmow, S. Pegel, H. Brünig, K. Kobashi, D. Fischer, and L. Häußler, *Liquid sensing properties of fibres prepared by melt spinning from poly(lactic acid)*

containing multi-walled carbon nanotubes. Composites Science and Technology, 2010. **70**(2): p. 343-349.

20. X. Zhang, M. Espiritu, A. Bilyk, and L. Kurniawan, *Morphological behaviour of poly(lactic acid) during hydrolytic degradation.* Polymer Degradation and Stability, 2008. **93**(10): p. 1964-1970.
21. M. Hakkarainen, A-C. Albertsson, and S. Karlsson, *Weight losses and molecular weight changes correlated with the evolution of hydroxyacids in simulated in vivo degradation of homo-and copolymers of PLA and PGA.* Polymer Degradation and Stability, 1996. **52**(3): p. 283-291.
22. D. Rangari, and N. Vasanthan, *Study of strain-induced crystallization and enzymatic degradation of drawn poly(l-lactic acid)(PLLA) Films.* Macromolecules, 2012. **45**(18): p. 7397-7403.
23. H. Tsuji, and K. Ikarashi, *In vitro hydrolysis of poly(l-lactide) crystalline residues as extended-chain crystallites: III. Effects of pH and enzyme.* Polymer Degradation and Stability, 2004. **85**(1): p. 647-656.
24. H. Tsuji, and K. Ikarashi, *In vitro hydrolysis of poly(l-lactide) crystalline residues as extended-chain crystallites: II. Effects of hydrolysis temperature.* Biomacromolecules, 2004. **5**(3): p. 1021-1028.
25. J. W. Leenslag, A. J. Pennings, R. R. Bos, F. R. Rozema, and G. Boering, *Resorbable materials of poly(l-lactide): VII. In vivo and in vitro degradation.* Biomaterials, 1987. **8**(4): p. 311-314.
26. S. R. Broadbent, and J. M. Hammersley. *Percolation processes I. Crystals and mazes*. in *Proc. Cambridge Philos. Soc*. 1957.
27. R. Zhang, H. Deng, R. Valenca, J. Jin, Q. Fu, E. Bilotti, and T. Peijs, *Carbon nanotube polymer coatings for textile yarns with good strain sensing capability.* Sensors and Actuators A: Physical, 2012. **179**: p. 83-91.
28. E. T. Thostenson, and T. W. Chou, *Carbon nanotube networks: sensing of distributed strain and damage for life prediction and self healing.* Advanced Materials, 2006. **18**(21): p. 2837-2841.
29. K. L. Lasater, and E. T. Thostenson, *In situ thermoresistive characterization of multifunctional composites of carbon nanotubes.* Polymer, 2012. **53**(23): p. 5367-5374.
30. C-C.Teng, C-C. M. Ma, Y-W. Huang, S-M.Yuen, C-C. Weng, C-H. Chen, and S-F. Su, *Effect of MWCNT content on rheological and dynamic mechanical properties of multiwalled carbon nanotube/polypropylene composites.* Composites Part A: Applied Science and Manufacturing, 2008. **39**(12): p. 1869-1875.

Chapter 8.

Marketing potential exploitation, summary and future work

Trials for fabricating the self-reinforced poly(lactic acid) (SR-PLA) composites and embedding smartness in PLA via the addition of carbon nanotubes (CNTs) were a learning experience. In this chapter, evidence is gathered to investigate the potential exploitation of the achieved work and remaining challenges, through a combination of desk research and telephone interviews conducted by Elucidare Limited. Even though SR-PLA have properties that are inferior to the mechanical properties of SR-PP composites, our research provided invaluable lessons on which conclusions could be drawn and discussed. Suggestions for future work are also provided at the end of this chapter.

8.1 Marketing research

The purpose of this section is to determine whether commercial exploitation opportunities exist for SR-PLA technology. Which hurdles are faced in order to commercialize the technology? The strengths, weaknesses, opportunities and threats involved are identified. For this two questions needs to be addressed. First of all, how do SR-PLA composites compare to alternatives such as natural fibre reinforced PLA composites in terms of performance, and what are the potential applications? Secondly, are SR-PLA composites potential substitutes for SR-PP composites, and is their

biodegradability and bio-base character valuable for the market?

8.3.1 Technology assessment

Is PLA more environmentally friendly?

Whenever someone hears that PLA is made from renewable resources, there is an immediate expectation that it must be better for the environment. However, one needs to ask the question if these products are really more environmentally friendly than petro-based polymers such as PP and PET. The mass of PLA originates from carbon dioxide (CO_2) in the atmosphere. However, like all manufacturing processes, the production of PLA requires additional energy. Then the relevant questions are: does the energy required for processing cause more CO_2 emissions than the amount of CO_2 embedded in PLA? And is the overall amount of fossil fuels required for processing of PLA less that the total needed for petro-based products? Moreover, how do biomass-based material producers compete with energy producers as well as food and feed?

Cargill Dow LLC [1] claimed that PLA uses fewer fossil resources and emits less CO_2 in its manufacturing than the petro-based products it replaces. These differences are measurable and significant according to the standard methodology for life-cycle inventory (LCI). Nova-Institut GmbH [2] contributed to the discussion about whether food crops should be used for other industrial uses. They suggested a differentiated approach to find the most suitable biomass for industrial uses based on scientific facts and logical arguments. They claimed that all kinds of biomass should be accepted for industrial uses depending on the sustainability and resource efficiency. Today, European policy only provides support for energy uses. However, the higher added value and

employment, as well as the greater land and resource efficiency speak in favour of supporting the material use of biomass.

While it is true that PLA has interesting environmental benefits, these benefits alone do not drive investment in manufacturing. The materials need to work well and need to be competitively priced. With large-scale production, prices are expected to drop. However, lactic acid-based bioplastics are expected to remain more expensive than commodity polymers in the near future. In other words, the cost, availability and physical properties of these bioplastics needs to be better than whatever it is they are to replace. Mazda's biofabric technology, which contains 100% plant-derived PLA and is being used in the seat covers and door trims, is a firm support for the use of bioplastics in the future. The fibre strength, durability, abrasion resistance, as well as flame retardant properties of these fibres are improved by controlling the molecular architecture.

Figure 8.1 Potential applications of SR-PLA composites.

The current market for PLA is mainly packaging. SR-PLA technology shows opportunities for expanding new market. Based on the properties of SR-PLA shown in

Chapter 4, the first commercial applications of these materials are likely to be in impact critical applications, such as luggage, sports products, underbody shields or as an alternative to natural fibre reinforced PLA for inner-trim parts (see Figure 8.1).

Can SR-PLA compete with PLA/natural fibre composites?

An essential point for looking into potential markets for SR-PLA composite is whether they have the right level of performances at the lowest possible cost. Generally, in the selection process, specific stiffness, specific strength and performance/cost values are considered as important criteria to make a decision. Table 8.1 gives a direct comparison of different engineering materials. These results are not expected to be absolute but are considered as a quick snapshot comparing their relative performance. Unidirectional natural fibre reinforced PLA composites represent the best combination of specific strength and specific modulus of all listed composites. It is worth noting that both SR-PLA composites and green composites are problematic due to their decomposable nature. The biodegradability issue needs to be addressed, especially when dealing with structural parts of exterior panels for future vehicles.

Can SR-PLA composites compete with SR-PP composites?

The commercial success of a material on a large scale will depend on many factors in addition to technological and environmental aspects. In recent years a wide range of SRPs has been presented in the literature. However, not all of these concepts are suitable for commercialization. Numerous potential industrial applications have been reported, mostly for SR-PP composites, as the cost/performance ratio of PP is one of the best of all polymers. To date, the most successful technology is based on hot

Table 8.1 The evaluation of various materials.

Sample	**Price [GBP/kg]**	**Density [10^3 kg/m^3]**	**Tensile strength [MPa]**	**Young's modulus [GPa]**	**HDT 1.8 MPa [^oC]**	**Specific strength (SS)**	**Specific modulus (SM)**	**SS/ Cost**	**SM/ Cost**
Neat PLA 4032D	~1.6	1.24	53	1.8	57	42.7	1.45	26.7	0.9
PLA+10 wt.% glass fibre [3]	1.88-2.26	1.31-1.33	59.3-62.4	6.8-6.98	105-107	46.1	5.2	22.3	2.5
PLA+30 wt.% glass fibre [3]	1.82-2.32	1.47-1.49	82.6-86.8	10.1-10.3	147-151	57.2	6.9	27.6	3.3
PLA+10 wt.% mineral filler +20 wt.% impact modifier	1.88-2.13	1.25-1.28	20-37	2.85-4.14	59.9-86.5	22.5	5.5	11.3	2.8
[3]	1.57-1.76	1.39-1.41	24-25.3	4.04-4.24	69-71	17.6	3.0	10.6	1.8
PLA+30 wt.% mineral filler+10% impact modifier [3]	1.95-2.2	1.29-1.31	55.6-58.4	5.19-5.32	53-55	43.8	4.0	21.1	1.9
PLA+30 wt.% natural fibre (woodflour/cellulose) + 10% impact modifier [3]	-	1.26-1.5	53	8.3	-	40	6.2	-	-
PLA+30 wt.% short flax fibre [4]	-	1.2-1.53	100	9.5	-	77	7.3	-	-
PLA+ 30 vol.% flax fibre mats [5]	-	1.2-1.5	130	15	-	100	11.6	-	-
UD PLA+ 30 vol.% kenaf [6]	-	1.2-1.5	223	22	-	158	15.6	-	-
UD PLA+ 70 vol.% kenaf [6]	2.01-2.26	1.11-1.21	29-52	2.3-2.6	49.7-79	34.9	2.1	16.3	1.0
PLA high impact [3]	-	1.21	278	6.7	-	224	5.5	-	-
SR-PLA tape	-	1.22	102	4.4	83	83.6	3.6	-	-
UD SR-PLA composites									

compaction and marketed as Curv®, and coextrusionbased SRP commercialized under the name PURE.

When considering the bio-based SR-PLA composites developed in the present work, great attention should be paid to their competitiveness with other existing SR-PP composites. The prefix ‘bio’ can only be attractive if material costs are moderate and customer acceptance can be guaranteed. Therefore, material data of SR-PLA composites, which are in competition with PP equivalents, should be referenced to adequate values. However, our results in Chapter 4 showed that SR-PLA composites are mostly interior to SR-PP composites in terms of cost/performance ratio.

SR-PLA composites could become even less competitive in the market when bio-based PP’s are used for SR-PP. Companies such as Braskem and Dow Chemical Company have been investing heavily in developing technologies to manufacture bio-based PP using ethanol derived from sugarcane. Braskem (Brazil) is to start its first bio-based PP manufacturing site with an initial annual capacity to be at least 50 kilo tons [7]. Bio-based PP is expected to replace synthetic PP in a number of applications in the near future.

8.3.2 Feedbacks from interviews

Managing Director, Net Composites

‘Although self-reinforced plastics are a nice idea on paper, it is probably fair to say they have struggled to get real commercial traction beyond Samsonite. It is very difficult to point to commercial applications where they have successful sold in any volume.’ The reason might be that ‘they sit in the space beyond conventional bulk polymers like

ordinary PP with certain properties and an attached price, and as you progressively reinforce PP using SRP the properties go up but also the price goes up. This has always been the challenge. It has always been questionable whether they hit the sweet spot.'

When they are asked about how does SRP with glass reinforced materials, they said, 'why would you go for SRP over a conventional composite? You might for impact performance. This is the fit for Samsonite. Other areas looked at types of shields and car flooring where you are exploiting the impact properties. And it can be recycled if a customer wants a monomaterial to recycle. However, there will only be a limited number of applications where impact performance is the deal maker. Similarly increased recycling is interesting to people but they don't to pay any more for that.'

Engineering team leader, Cobham PLC

'The uses for SRP are expanding. One of its primary draws is its impact performance. This is why people like Samsonite are using it for suitcases. And I have seen research for it to be used for floors in bomb resistant vehicles for military, but also it is gaining traction in semi-structural applications like automotive. And now also its electrical properties, namely it is a dielectric. SR-PP is almost completely invisible to radar and other electrical signals; coupled with its semi-structural properties means you can make quite effective radomes and other coverings for aerospaces, trains, and satcoms to cover radar and communications equipment.

Towards the end of my time at NetComposites we wanted to start looking at SR-PLA but unfortunately all our funding applications were rejected by the UK government and by Brussels. But yes, I certainly think there are legs to this. Changing from PP to a bio-sourced and biodegradable alternative has a lot of appeal to users of this kind of

material. We first looked at automotive industry and they said they would not be the kind of people that would be looking for a degradable alternative, but we found a lot of users that are using these materials because of their green credentials and because of the marketing potential it gives them. The greener, the better. So this would appeal not only to those using SR-PP but also those using a flax or hemp reinforced PLA. So there are two avenues you can come from: people that are currently using SRP materials and those using non-SR bioplastics and composites. Certainly we had dealings with automotive companies on SR-PP, but when we tried to "sell" them the idea of biodegradable materials they did not seem too receptive due to the fact that, well, they will degrade. It is as simple as that.' Then we mentioned the degradation sensor technology developed. They said, 'This is very interesting. I think this would be one of the big things that would help get PLA into semi-structural applications in the automotive industry. This will give them confidence that actually they can monitor it and they do know how long it will be good for. When we were talking to the automotive industry this was one of their big concerns. They said 'we don't know how long it takes to degrade; we don't know how long it will last.' If you have a painted PLA component then you have no idea what it is like inside: it looks the same whether it is degraded or not. Normally in a car, the PLA would be coated. But if there is a chip then with this CNT monitoring you would be able to detect degradation due to the unknown nature of the environment'.

Managing Director, Composites Evolution Limited

'SR-PLA is certainly interesting from a technical point of view. But it is a very rare customer that will pay extra just for bio-derived or compostable. The material has to

offer something else as well. PLA is already expensive. SR-PLA will be more expensive so it has to have a significant advantage over SR-PP. Even SR-PP hasn't taken off to the extent that was originally thought, so the markets for SR-PLA are possibly very narrow. There is an interesting feature in that the impact performance of PLA is improved when self-reinforced. PLA isn't that good in impact, so this might allow the use of PLA where not previously possible, but again depending on cost as it's already an expensive polymer.'

Manager-Advanced Materials Engineering Europe, Visteon

'When I worked on self-reinforced polymers we found there was quite an amazing step change in properties when they were being reinforced with themselves. But within this program we lost sight of the cost of these materials. Being cynical, typically the driver in automotive is for a low-cost material, and if they are green as well, great, but always the driver seems to be for low-cost material.'

From the desk research and telephone interviews, we can conclude that it could be difficult to commercialize SR-PLA technology. However, recent environmental regulations, societal concerns and growing environmental understanding throughout the world could be a driving force. Still exploitation of the results to commercialize a product faces the following hurdles:

1. Virgin PLA market is not mature enough and is still considered a niche market.
2. The cost/performance ratio of SR-PLA composites is poor.
3. SR-PP composites perform better. PP could be bio-based in future and is also recyclable.
4. Targeted markets are quite difficult to identify either because of lack of

performances or too high costs even if PLA is bio-sourced and potentially recyclable. Sports equipment might, however, be an option.

8.2 Summary

PLA is nowadays considered as one of the most promising bioplastics but exhibits rather limiting heat stability and brittleness in its pristine state. While significant gains in impact toughness and heat resistance have been realized using plasticization and blending, maintaining a high tensile strength and modulus of PLA is difficult. Upgrading of PLA can be done by the introduction of mineral fillers such as $CaCO_3$ or glass- or natural fibres but the introduction of such 'foreign' fillers is also in conflict with the basic idea behind recycling and monomaterial products.

In this thesis, fully biobased and recyclable self-reinforced PLA (SR-PLA) composites were developed using a film-stacking technique. The multiple end-of-life options offered by SR-PLA composites, including recycling and composting, empowers them to reduce the environmental impact of materials, and gives the end-user maximum flexibility in selecting environmentally sound waste disposal schemes.

In order to obtain optimum performance of the SR-PLA composites, first a tape-manufacturing route was optimized to ensure superior mechanical properties of the reinforcement. In accordance with literature, it was found that the Young's modulus and tensile strength of the post drawn tapes increased with increasing draw ratio and drawing temperature. PLA tapes with a maximum Young's modulus and tensile strength of approximately 6.7 GPa and 280 MPa could be routinely obtained on a pilot production line. Compared to isotropic PLA, a 3.7, 5.2, 12.7 times increase in Young's modulus, tensile strength and tensile toughness was achieved after solid-state drawing.

The consolidation of these highly oriented PLA tapes in a unidirectional (UD) or bi-directional (BD) form can be achieved by welding the tapes together by heating under pressure. This bonding is achieved by using a PLA matrix with a lower melting temperature than the tapes, thus preserving the orientation of PLA tape. It has been shown that it is possible to tailor the mechanical properties of SR-PLA laminates by altering the hot-pressing conditions. Compaction at 160 ℃ produced a well bonded structure and SR-PLA composites with good levels of strength and stiffness to make them suitable candidates for semi-structural components. UD SR-PLA composites compacted at 160 ^{o}C exhibited enhanced modulus (2.5 times) and strength (2 times) compared to neat PLA resin. On the other hand, SR-PLA composites consolidated at a lower temperature of 150 ℃ showed optimal energy absorption, which may find applications that are aimed at protection from low velocity impacts. BD SR-PLA composites compacted at 150 ^{o}C absorbed 14 times more energy compare to PLA resin as measured in dart impact tests. Furthermore, the HDT of UD SR-PLA increased by about 26 ^{o}C compared to neat PLA resin, mainly as a result of an increase in modulus and crystallinity.

According to the marketing research, SR-PLA composites do not poses the best cost/performance ratio in comparison to SR-PP or natural fibre reinforced PLA composites, which is identified as the main disadvantage of SR-PLA composites. However, the excellent impact performance may prove to turn out the key property of SR-PLA. The first market introduction may be therefore in impact applications such as sports equipment.

Another big concern from industry that prevents PLA from getting into semi-structural

applications is the degradation of PLA. For PLA based product to be used in more demanding engineering applications, the important issue of degradation during the product's life time has therefore been addressed in the second part of this thesis. We pioneered the use of minute amount (0.7 wt.%) of carbon nanotube (CNT) into a PLA matrix as a means to monitor degradation. Nanocomposites with a CNT loading around the percolation threshold gave the highest sensitivity and strongest signal change. The observed increase in conductivity is due to an increased CNT network density after partial removal of the amorphous phase of the semi-crystalline polymer matrix. Such an in-situ degradation monitoring system would give real-time information regarding structural safety and makes it a good candidate for applications in smart biocomposite products.

Apart from degradation sensing, conductive oriented PLA/MWNT tapes with enhanced mechanical properties were prepared. These tapes showed significant morphological, mechanical and electrical property changes after drawing, with polymer crystallinity, nanotube dispersion and alignment all being improved. Interestingly, the presence of the MWNTs perturbed the orientation of the crystalline polymer chain domains. Drawing lowered the electrical conductivity and increased the percolation threshold of the nanocomposites, but micromechanical analysis showed that it greatly improved the reinforcing efficiency of the MWNTs. This resulted in an overall good balance of physical properties of the oriented PLA/MWNT tapes with one of the best compromises in terms of high mechanical properties (5.5 GPa in Young's modulus, 156 MPa in strength) and electrical properties (3.5×10^{5} Ω m in resistivity) for conductive polymer composite fibres or tapes.

8.3 Future work

Both theoretical analysis referred to in Chapter 5 and experimental data reported in Chapter 6, indicates that 1D fillers are more promising for unidirectional oriented (1D) nanocomposites, while 2D fillers are more effective in 2D structures. It seems therefore natural to focus future works on bidirectionally (2D) oriented films based on PLA/nanoplatelets. Graphene, an atomically thin 2D material made of sp^2-hybridized carbon atoms, has attracted great attention since its discovery in 2004. The elaboration of PLA/graphene nanocomposites and their compatibilization have scarcely been investigated at this stage except for a few reports. Kim and Jeong [8] investigated the morphology, structures, thermal stability, mechanical and electrical properties of PLA/exfoliated graphite (PLA/EG) nanocomposites obtained by melt-compounding. EG nanoplatelets with ~15 nm thickness and ~10 μm diameter were prepared by the acid-treatment and rapid thermal expansion. When melt-compounded with PLA matrix, SEM images and XRD patterns confirmed that EG nanoparticles were homogeneously dispersed in the PLA matrix. As a result, the thermal degradation temperatures $T_{5\%}$ and Young's moduli increased from 350 ^{o}C and 3 GPa for neat PLA to 364 ^{o}C and 4.1 GPa for PLA/EG nanocomposites at a EG content of 3 wt.%. However, the experimental Young's moduli of PLA/EG nanocomposites were still far lower than the moduli predicted by the Halpin-Tsai model. The electrical percolation threshold of PLA/EG (3-5 wt.%) was also shown to be much lower than that of graphite-based nanocomposites (10-15 wt.%) [8]. To further realize the reinforcement of these nanofillers, it would be interesting to investigate biaxially stretched PLA/graphene films.

In Chapter 7, only isotropic PLA/CNT films were investigated. It has been demonstrated in Chapter 3 that orientated PLA tapes degrade slower than isotropic PLA films. Therefore, very interesting results can be also expected from studying the degradation sensing behaviour of PLA/CNT oriented conductive tape. As stated earlier, of particular importance in the development of sensors and actuators based on carbon nanotube composites is their electrical conductivity. Conductive PLA/CNT tapes were successfully prepared in Chapter 6. These tapes are less conductive compared to isotropic films, and the percolation threshold increased with solid state drawing. Thus, it is expected that the oriented tapes should be more sensitive to degradation than isotropic films at the same concentration of CNTs. Moreover, the level of electrical conductivity can be set rather accurately by the solid-state drawing process, meaning that the sensitivity can be tailored by the drawing process.

Besides the search for applications of SR-PLA technology, some research still needs to be carried out and basic questions need to be answered. In order for a material technology to be commercially successful, it is necessary that it can be delivered in the required form. The choice of processing routes used to create a product depends on the characteristics of the material itself and the complexity of the final part. There are some processing related problems for SR-PLA composites as temperatures required to achieve sufficiently low viscosities of polymer matrices to allow good matrix impregnation would normally also melt the reinforcement phase. Figure 8.2 shows an overview of the main forming options for SR-PP composites. The main options are direct forming (i.e. directly consolidating the composites from precursor fibres or fabrics in the final form) and thermoforming of pre-consolidated laminates. However, apart from tape relaxation during subsequent thermoforming, further degradation might

happen in the case of PLA through thermal degradation, leading to deterioration in mechanical properties. Therefore, forming conditions, such as strain rate applied during thermoforming, temperatures applied, thermal stability of PLA, must be all well understood.

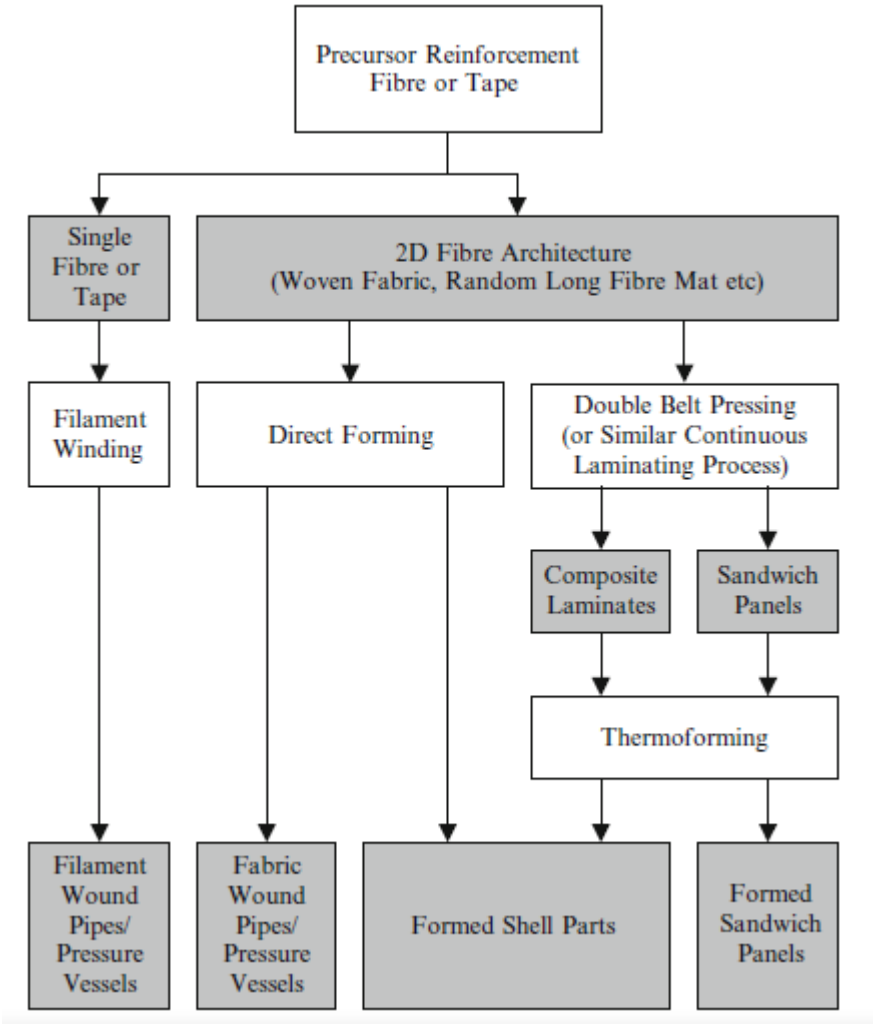

Figure 8.2 Some potential routes to manufacture SRP products [9].

In summary, we compared the economic, environmental and structural implications of SR-PLA composites with their alternatives: natural fibres reinforced PLA and SR-PP composites. Although SR-PLA composites have properties that are inferior to their direct competitors, the multiple end-of-life options offered by SR-PLA composites

empowers them to reduce the environmental impact of plastic products, and gives the end-user maximum flexibility in waste disposal schemes. Some research still needs to be carried out for scaling up this lab-proven technology; however our research provided invaluable lessons on which conclusions could be drawn and discussed. The inherent brittleness and poor thermal resistance of PLA, which are two main challenges towards its wider industrial application, has been overcome through the development of SR-PLA composites, while simultaneously improving the tensile strength and modulus of SR-PLA. Especially, the good impact properties of SR-PLA composites are impressive, which may find its use in applications such as luggage and sports equipment.

8.4 References

1. National Research Council Chemical Sciences Roundtable (US), *Commodity polymers from renewable resources: polylactic acid.* 2001. Available from: http://www.ncbi.nlm.nih.gov/books/NBK44131/
2. M. Carus, and L. Dammer, *Food or non-food: Which agricultural feedstocks are best for industrial uses?* Industrial Biotechnology, 2013. **9**(4): p. 171-176.
3. CES EduPack, *Granta Design Ltd*, in *Cambridge, UK* 2008.
4. K. Oksman, M. Skrifvars, and J-F. Selin, *Natural fibres as reinforcement in polylactic acid (PLA) composites.* Composites Science and Technology, 2003. **63**(9): p. 1317-1324.
5. E. Bodros, I. Pillin, N. Montrelay, and C. Baley, *Could biopolymers reinforced by randomly scattered flax fibre be used in structural applications?* Composites Science and Technology, 2007. **67**(3): p. 462-470.
6. S. Ochi, *Mechanical properties of kenaf fibres and kenaf/PLA composites.* Mechanics of Materials, 2008. **40**(4): p. 446-452.
7. *Bio-based polypropylene (PP) technology trends and market potential to 2020* 2014 Available from: http://www.grandviewresearch.com/industry-analysis/bio-based-polypropylene
8. I. H. Kim, and Y. G. Jeong, *Polylactide/exfoliated graphite nanocomposites with enhanced thermal stability, mechanical modulus, and electrical conductivity.* Journal of Polymer Science Part B: Polymer Physics, 2010. **48**(8): p. 850-858.
9. N. Cabrera N, B. Alcock, T, Schimanski, J. Loos, and T. Peijs, *Cost processing of recyclable single polymer thermoplastic composites*. in *ECCM10 - European Conference on Composite Materials*. 2002. Brugge, Belgium.

Publications

1. **Fang Mai**, Youssef Habibi, Philippe Dubois, Jean Francois Feller, Ton Peijs*, Emiliano Bilotti. *Smart poly(lactic acid)/carbon nanotube conductive biocomposites for degradation sensing,* ***Polymer.*** 2013, *54,* 6818-6823.

2. **Fang Mai**, Wei Tu, Emiliano Bilotti, Ton Peijs*. *Study of self-reinforced poly(lactic acid) composites with improved impact performance, tensile properties and heat resistance,* ***Composites Part A: Applied Science and Manufacturing.*** 2015, *76,* 145-153.

3. **Fang Mai**, Hua Deng, Sayamol Chankajorn, Qiang Fu, Emiliano Bilotti, Ton Peijs*. *Conductive poly(lactic acid) tape reinforced with carbon nanotube,* ***Macromolecular Materials and Engineering.*** DOI: 10.1002/mame.201500163.

4. **Fang Mai**, Wei Tu, Emiliano Bilotti, Ton Peijs*. *The influence of solid-state drawing on mechanical properties and hydrolytic degradation of melt-spun poly(lactic acid) (PLA) tapes,* ***Fibers***, Submitted.

5. **Fang Mai**, Kal Palatov, Emiliano Bilotti, Ton Peijs*. *Self-reinforced poly(lactid acid) (PLA) biocomposites with degradation sensing,* ***ECCM15***, Venice, Italy, June 24-28 2012.

6. **Fang Mai**, Emiliano Bilotti, Ton Peijs*. *High Performance self-reinforced poly(lactic acid) (PLA) biocomposites with degradation sensing,* ***ICCM19***, Montreal, Canada, July 28-August 2, 2013.

7. **Fang Mai**, Emiliano Bilotti, Ton Peijs*. *Self-reinforced poly(lactic acid) (PLA) composites with enhanced impact performance, tensile properties and heat resistance,* ***ICCM20***, Copenhagen, Denmark, July 19-24, 2015.

8. Max Munoz, Kasper Jørgensen, **Fang Mai**, Emiliano Bilotti, Hao Yang*. *Biodegradable materials for short term wireless implants,* ***2015 IEEE APS/URSI,*** Vancouver, Canada, July 19-25, 2015.